UNIVERSITÀ DEGLI STUDI DI PALERMO
Dottorato di ricerca in Ingegneria Civile e Ambientale
Dipartimento di Ingegneria Civile, Ambientale,
Aerospaziale, dei Materiali
Settore Scientifico-Disciplinare ICAR/01

DISCHARGE HYDROGRAPH ASSESSMENT THROUGH REVERSE ROUTING MODEL IN RIVERS WITH SIGNIFICANT LATERAL INFLOW

IL DOTTORE
ING. ELEONORA SPADA

IL COORDINATORE
PROF. ING. ORAZIO GIUFFRE'

TUTOR
ING. CARMELO NASELLO

CO TUTOR
PROF. ING. TULLIO TUCCIARELLI

CICLO XXVI
ANNO 2016

"...Ed è così che vediamo il mondo: lo vediamo come al di fuori di noi anche se è solo d'una rappresentazione mentale di esso che facciamo esperienza dentro di noi."

R. Magritte

DISCHARGE HYDROGRAPH ASSESSMENT THROUGH REVERSE ROUTING MODEL IN RIVERS WITH SIGNIFICANT LATERAL INFLOW

Tesi per il conseguimento del titolo di
Dottore di Ricerca

Eleonora SPADA

CONTENTS

CHAPTER II

Resistence flow formulas

CHAPTER III

Uniform flow formula for irregular sections of straight channels

(from E.Spada et al., Hydrol. Earth Syst. Sci., 19, 3857–3873, 2014)

CHAPTER IV

River flow assessment through reverse routing modeling with significant lateral inflow *(from E.Spada et al., 2015)*

LIST OF FIGURES

LIST OF TABLES

Acknowledgements

Firstly, I would like to thank my Professor Tullio Tucciarelli who introduced me to the hydraulic modeling and for all his help and guidance that he has given me over the past three years. A special thanks to my scientific tutor Ing. Carmelo Nasello and to my collegues for their never ending support, their patience and valuable advice.

I wish also to express my gratitude to the Administration de la gestion de l'eau of Grand-Duché de Luxembourg and the Centre de Recherche Public Gabriel Lippmann" for providing hydrometric and topographical data on Alzette River. I wish also yo thank Umbria Region, Department of Environment, Planning and Infrastructure, for providing Tiber River basin data.

SOMMARIO

L'attività di ricerca riportata nella presente tesi può collocarsi nel campo della modellazione delle correnti a superficie libera in alvei fluviali ed in particolare nella misura delle portate. La tesi è strutturata come segue. Nella prima parte viene riportato lo stato dell'arte delle diverse metodologie di stima delle portate in alveo mediante tecniche già validate; sia dirette (cioè basate sull'integrazione spaziale di misure di velocità) che principalmente indirette, cioè basate sull'analisi delle misure di livello in moto vario registrate in due diverse sezioni dell'alveo.

La misura diretta della portata in alvei fluviali può effettuarsi integrando nello spazio i valori di velocità misurati mediante sonde acustiche, meccaniche o elettromagnetiche. Questi strumenti posti a contatto con la corrente sono esposti a danneggiamenti e devono usualmente essere utilizzati da personale presente in loco. Ciò ne limita l'utilizzabilità in particolare durante gli eventi di piena significativi, quando tra l'altro è praticamente impossibile il campionamento dei punti di velocità nella porzione inferiore dell'area liquida usando sonde meccaniche. Questo implica la mancanza di misure di flusso dirette per tiranti idrici elevati, che sono invece indispensabili per la definizione di una scala di deflusso utile anche nel caso di piena. Inoltre l'utilizzo di una scala di deflusso implica una relazione one-to-one, che invece manca in presenza di effetti non stazionari legati ad eventi di piena.

Si è così incentrata l'attività di ricerca su una metodologia indiretta basata sulla stima della scabrezza media di un tratto di alveo attraverso la calibrazione di un modello numerico, utilizzando solo misure sincrone di

livello ottenute nelle due sezioni estreme del tratto stesso. Il modello idraulico è rappresentato dalle equazioni delle acque basse di Saint-Venant in forma diffusiva, avente come condizione al contorno di monte gli idrogrammi dei tiranti noti nella prima sezione strumentata, ed una condizione di diffusione nulla come condizione di valle. La semplicità delle condizioni al contorno richieste dalla modellazione diffusiva è una caratteristica di particolare pregio. Infatti, il modello diffusivo è assimilabile ad un particolare modello completo in cui l'accelerazione di gravità tenda all'infinito; ciò determina la presenza di una corrente sempre lenta su tutto il dominio, il cui stato idrodinamico dipende da una sola condizione al contorno per ogni punto appartenente alla frontiera del dominio di calcolo.

La metodologia è stata testata su un evento di piena verificatosi sul fiume Alzette in Lussemburgo, grazie alle informazioni di serie storiche di portate e tiranti forniti dal Centre de Recherche Public Gabriel Lippmann. La procedura di stima della portata, tuttavia è risultata essere fortemente influenzata dalla legge di resistenza utilizzata all'interno del modello di simulazione.

Nella seconda parte del presente lavoro di tesi, dopo un revisione critica delle diverse leggi di resistenza presenti in letteratura, si propongono due nuove leggi di resistenza per alvei fluviali, l'*INCM* e l'*LHRM*. La prima è una versione modificata della formula di Huthoff (*IDCM* method). L'*INCM*, così come l'*IDCM*, semplifica la legge di chiusura della turbolenza, con riferimento a sezioni di forma golenale composte da un numero limitato di sottosezioni, ed è basato sulla parametrizzazione degli stress di interfaccia attraverso un coefficiente avente l'unità di misura di una lunghezza e parametrizzato in funzione di

un coefficiente empirico adimensionale. La seconda legge di resistenza, più performante, è basata sulla definizione di un raggio idraulico "locale", calcolato in base alle caratteristiche idrauliche e geometriche di un tratto di sezione di ampiezza limitata e proporzionale al tirante idrico. L'estensione suddetta è pure proporzionale ad un coefficiente empirico. Il candidato ha dimostrato con alcuni esempi applicativi che la sensitività della portata rispetto ai coefficienti delle due diverse leggi di resistenza è minore di quella propria dei coefficienti "geometrici" presenti nei metodi analizzati in letteratura. Le due leggi sono stato dapprima testate sui risultati di esperimenti di larga scala eseguiti sul canale di Wallingford, UK, “Flood Channel Facility (FCF)” (Ackers 1993; Shiono and Knight 1991; Knight and Sellin 1987) ed in piccola scala sul canale Knight and Demetriou (1983) ed in seguito validate secondo tre diversi criteri. Il primo è il confronto con dati sperimentali dei canali in piccola e grande scala diversi da quelli utilizzati per la calibrazione. Il secondo criterio di validazione è consistito nel confronto tra i valori di scabrezza ottimale computati attraverso la modellazione monodimensionale per tre eventi storici registrati sul fiume Alzette settando all'interno del modello le due leggi proposte. La terza validazione è stata fatta attraverso il confronto con i risultati ottenuti con un solutore commerciale 3D (ANSYS CFX), che implementa al suo interno diversi modelli di turbolenza.

Il prodotto finale dell’attività di ricerca svolta dal candidato è infine rappresentato dallo sviluppo di una nuova metodologia per la stima della portata nell'ipotesi di afflussi laterali significativi, condizione nella quale la metodologia precedentemente citata non poteva essere applicata. La nuova metodologia presuppone che siano note la topografia delle sezioni di chiusura di ciascun tributario, prossime all'asta principale dell'alveo. La

portata laterale sarà funzione di un parametro di calibrazione k (tipico di ciascun tributario) che ingloba al suo interno il gradiente piezometrico ed il coefficiente di Manning di ciascun tributario. La metodologia è stata testata su due fiumi naturali, il Tevere e l'Alzette, grazie alla disponibilità di serie storiche di portata e tiranti forniti dal CNR-IRPI di Perugia. Nel caso studio dell'Alzette il tratto da modellare è stato esteso per tener conto di due canalizzazioni. I risultati stimati in termini di idrogrammi di portata e afflussi laterali sono molto soddisfacenti. L'errore computato al picco è infatti inferiore al 10% per tutti gli eventi analizzati e spesso inferiore all'errore che si commette mediante l'uso di misure dirette della portata per integrazione di valori di velocità.

THESIS OUTLINE

In recent years, the dramatic effects of floods has raised a public alert on floodplain management and hydraulic risk analysis. To provide an examples, the evaluation of floodprone areas and the assessment of dam safety rely both on the estimation of the maximum domain expected to be inundated within a given period of time. The design flood discharge hydrograph can be estimated, through statistical approaches, by analysing the available values of recorded discharge hydrographs.

However, several other techniques are also available, such as the design storm approach, the derived flood frequency and the continuous simulation method (Camici et al., 2010) based on the use of hydrological modelling. Regardless the adopted approach, the information on the observed discharge is fundamental for both the calibration and the validation of any model (McMillan et al., 2010). Moreover, the discharge hydrograph represents also the most commonly used upstream boundary condition in hydrodynamic modelling (Liu et al., 2007). Unfortunately, discharge cannot be directly sampled. Indeed, its value is derived from velocity measurements, carried out using several kinds of sensors.

The ideal gauged site is accessible for velocity measurements that are carried out for any desirable water level. In this condition, it is possible to build and update a steady rating curve (henceforth named rating curve) which represents the easiest way to convert water levels into discharge. In fact, the rating curve is a one-to-one algebraic relationship between stage and discharge. The relationship is developed on the basis of water level

and discharge pairs, derived from velocity measurements. Power or polynomial functions are usually applied to fit the measured data. The use of a one-to-one relationship is suitable to convert water levels into discharge, under steady flow conditions and also for unsteady flow situations with a kinematic behaviour (Dottori et al., 2009). This last condition corresponds to rivers with steep bed slope (> 1%). In all the other cases, unsteady phenomena can lead to hysteric effects and looped rating curves. These effects are mainly evident for high flow conditions and in large river sections. Nevertheless, steady rating curves are commonly used to convert water levels into discharge, also when unsteady effects are present. The related error has been estimated in literature by some numerical studies: by way of example, along the Po River (Di Baldassare and Montanari, 2009) an error estimate was found of about 10% at 95% confidence levels. However, discharge estimations at a river site are usually defined by recording water level data. Due to their characteristics of cheapness, easiness of installation and accuracy of measurements, stream gauges are the most widespread instruments along rivers. The time continuous series of water level data are commonly used to obtain a time continuous information on discharge. In this thesis, to compute the discharge along the rivers the author refers to the case of two hydrometric stations located faraway one from the other, where no discharge information is available at both river sites. In this case, only local stages are measured and, under the hypothesis of negligible lateral flow, a diffusive model is used. A diffusive model, or in other words a full dynamic model with zero inertia is used in the method proposed by Aricò et al. (2009). In particular, Aricò et al.'s hydraulic model (2009) allows the estimation of the discharge hydrograph at the upstream section,

by routing the observed upstream local stage hydrograph and using the observed downstream stages to calibrate several parameters as the Manning's roughness coefficient. This procedure is tested against field data coming from the Alzette River in Luxembourg, with negligible lateral inflow, in the first part of the thesis.

In the second part of this thesis, after a critical review of the different resistance laws, the author proposes two new resistance laws, named *INCM* and *LHRM*. The first is a modified version of the Huthoff formula (*IDCM* method). The *INCM*, as well as the *IDCM*, simplifies the closure problem of turbulence, with reference to the sections composed of a limited number of subsections, and is based on the parameterization of the shear stress interface through a length, parameterized as a function of a dimensionless empirical coefficient. The second resistance law, performing better, starts from the observation that, in the Manning formula, the mean velocity per unit energy gradient is proportional to a power of the hydraulic radius. It should then possible to get the total discharge as integral, along the lateral direction, of the elementary values computed around each vertical, using for each elementary value the same Manning formula, but also changing the original hydraulic radius with a 'local' one. This "local" hydraulic radius should take into account the effect of the surrounding section geometry, up to a maximum distance which is likely to be proportional to the local water depth, according to an empirical _ coefficient. The method gives up the idea of solving the Reynolds equations, due to the uncertainty of its parameters, but relies on the solid grounds of the historical experience of the Manning equation.

The two laws have been first tested on the experiments results carried out by a large scale channel in Wallingford, UK, "Flood Channel Facility

(FCF)" (Ackers 1993; Shiono and Knight 1991; Knight and Sellin 1987) and by a small scale channel in Birmingham (Knight and Demetriou, 1983) and later validated choosing three different criteria. The first is the comparison with the experimental data of small and large scale channels, different from those used for calibration. The second validation criterion is the comparison of optimal roughness coefficient computed by the hydraulic modeling for three events recorded on the River Alzette setting inside the model the two proposed laws. The third validation was made through a comparison with the results obtained with a commercial 3D solver (ANSYS CFX), implementing several different turbulence models.

Finally the discharge hydrograph estimation in rivers, based on reverse routing modeling and using only water level data at two gauged sections, is extended to the most general case of significant lateral flow contribution without needing to deploy rainfall-runoff procedures. The proposed methodology solves the Saint-Venant equations in diffusive form also involving the lateral contribution using an 'head driven' modeling approach where lateral inflow is assumed to be function of the water level at the tributary junction.

The method is characterized by few parameters to be assessed through calibration of the flow routing algorithm: the average Manning's roughness coefficient, n, of the main channel plus one parameter for each tributary related to its rating curve, estimated per unit roughness coefficient and per unit slope immediately upstream the confluence with the main river.

CHAPTER I

HYDRAULIC MODELLING FOR DISCHARGE ESTIMATION

1.1 Introduction

Hydraulic modeling provides water level and discharge estimation inside a river reach, whose structure is defined by geometry and roughness. In this thesis hydraulic modeling is used as a tool to turn one or two given water level hydrographs, that corresponds to the input model, into a discharge one.

The aim of this thesis is to address the issue related to discharge assessment at a gauged river site, in the hypothesis of velocity data completely missing or limited to mid-low water levels. In this context, a procedure that estimates the discharge hydrograph starting from the recorded water levels in the upstream section of a river reach and an auxiliary hydraulic quantity is proposed. With auxiliary hydraulic quantities we refer to an additional stage hydrograph or, in some instances, also to sporadic sets of velocity measurements (Corato et al., 2011). The procedure is based on the application of an hydraulic model, employed to route the recorded stages, while the auxiliary hydraulic quantity (e.g. stage hydrograph) is used for the Manning's roughness coefficient calibration in the hydraulic model itself. The observed upstream local stage hydrograph is routed along the computational domain representing the river reach, bounded by two sections (the upstream and downstream ones) located few miles from each other. The

observed downstream stage hydrograph can be used to calibrate the Manning's roughness coefficient, under the hypothesis of negligible lateral flow inside the modeled reach.

The mathematical model is given by the well-known De Saint Venant or shallow water equations (De Saint Venant, 1874) that describe the flood wave propagation in a channel.

1.2 Shallow Water Equations

Unsteady flow in natural channels can be described through the Saint-Venant equations (De Saint-Venant, 1871), also known as shallow water equations. Assuming that the flow varies gradually, the governing equations can be written in one-dimensional form as follows:

$$\frac{\partial A}{\partial t} + \frac{\partial q}{\partial x} = 0 \qquad (1.1\text{ a}),$$

$$\frac{\partial q}{\partial t} + \frac{\partial}{\partial x}\left(\frac{q^2}{A}\right) + gA\frac{\partial h}{\partial x} + gA(S_f - S_0) = 0 \qquad (1.1\text{ b}),$$

where A is the cross section, q is the discharge, h is the water depth, g is the gravity acceleration, S_f and S_0 are the energy and the channel slope, x is the flow direction, and t is the time. The sought after solution has to satisfy equations (1.1), along with the initial conditions of the unknowns h,q and the proper boundary conditions. The prope boundary conditions depend on the Froude number occurring at each end. Some of the possible ones are summarized in the following Table 1.1:

Table 1.1. Possible boundary conditions of Eqs. (1.1). Fr is the Froude number, subscript u or d stand for "upstream" or "downstream" section and the superscript star stands for "assigned value", H is the water level and S_0 the bed slope.

	Fr > 1	**Fr < 1**
Upstream	$H_u=H_u^*$ and ($\partial H_u/\partial x= - S_0$ or $q_u=q_u^*$)	$q_u=q_u^*$ *or* $H_u=H_u^*$
Downstream	None	$H_d=H_d^*$ or $\partial^2 H_d/\partial x_2= 0$ or $\partial H_d/\partial x= -S_0$

The complete model represented by equations (1.1 b) and (1.1 a) is used in the engineering practice quite rarely, especially for the simulation of the flood wave caused from the collapsing of a dam, around the section of the dam and in the time immediately following the event. In all other cases the first and the second term of equation (1.1 b) are negligible compared to the other ones. The local and convective inertia have different sign in both the rising and falling part of the hydrograph and their sum is often negligible, specially for high bed slope and/or small water depths. Even in the case of relatively small slope, of the order of a few units per thousand, the total inertia is extremely small compared to the other terms of the equation (1.1b). It is therefore a common practice to reduce equation (1.1b) in the following form:

$$\frac{\partial H}{\partial x} = \frac{\partial h}{\partial x} - S_0 = -S_f \qquad (1.2),$$

where H is the water level. S_f can be expressed as:

$$S_f = \frac{q^2}{Q^2(h)} \quad (1.3),$$

where $Q(h)$ is the specific discharge in the main river (also called conveyance), estimated according to uniform-flow condition and unit bottom slope.

According to this assumption, Eq. (1.1b) reduces to the following relationship:

$$\frac{\partial(h+z)}{\partial x} = -\frac{q^2}{Q^2(h)} \quad (1.4),$$

where derivative of z is the opposite of S_0 (i.e., $S_0 = -\partial z / \partial x$). The diffusive model requires the same b.c. of a complete model in the case of subcritical flow, i.e. one boundary condition at each end of the 1D domain. The boundary conditions usually given for the direct solution of the diffusive flow routing problem in the upstream and downstream sections are the first one of Table 1.1

The aforementioned simplification leads to a greater stability of the numerical model, especially in the case of complex geometry of the sections. This means that the errors in the estimation of the geometrical (slope and shape of the sections) and hydraulic (roughness coefficient) parameters produce, using the full dynamic momentum equation given by (1.1b), an error in the calculation of average speeds and water levels that is often greater than the error made by the solution of the simplified equation (1.4) calibrated with the same parameters. If the slope of the river bed is very high or water depth is very small, a further simplification can be done with the kinematic model and water depth derivatives can be

neglected in Eq. (1.4). According to Manning's formula, Eq. (1.4) can be written as:

$$S_f - S_0 = 0 \Leftrightarrow q = \frac{AR^{\frac{2}{3}}}{n}\sqrt{S_0}$$

(1.5).

In this case the continuity equation can be written as function of the wave celerity c [*Henderson*, 1966]:

$$c(q) = \frac{1}{L}\frac{dq}{dh} \qquad (1.6),$$

where L is the section top width. The same celerity, using the Manning's formula, can be expressed as function of the water depth, bed geometry and Manning coefficient, to get:

$$c(q) = \frac{S_0^{1/2}}{Ln}\left(\frac{2\sigma}{3\Re^{1/3}}\frac{d\Re}{dh} + L\Re^{2/3}\right) \qquad (1.7).$$

The kinematic model requires only one upstream b.c. that usually is the known entering discharge hydrograph. In the context of hydraulic model calibration and discharge estimation, kinematic (for large bed slope) and diffusive (for mild or small bed slope) models should be preferred to the dynamic one. There are several reason for that: the first (and minor) one is that a more complex model involves a larger computational cost, without any improvement in accuracy due to the parameter uncertainty. The second one is that, as previously pointed out, the boundary condition depends on the Froude number and, in case of supercritical flow, two conditions are required at the upstream end. In this case the assumption of an approximated kinematic boundary condition represents an additional error (Aricò et al., 2009). However, the third and

most important reason is that, as spreviously said, the introduction of the inertial terms (Aricò et al., 2011) provides a much larger sensitivity of the computed results to the topographic input data and a consequent much larger error in the computed variables.

For the numerical solution of Saint Venant Equations traditional finite difference such as the one of Preissman (Cunge, 1980), or finite lement schemes are usually applied. Implementation of b.c. different from the mentioned ones in these traditional schemes is not straigthtforward. In the following, the MAST numerical scheme is implemented for the solution of the diffusive flow routing problem. The MAST algorithm allows to easily incorporate nonlinear source terms (such as friction losses) and has a flexible structure that allows to easily set in the calibration problem boundary conditions different from the ones adopted for the solution of the direct flow routing problem.

1.3 MAST numerical scheme

Saint Venant equations (1) can be solved by many numerical techniques. In this thesis the diffusive hydraulic model is solved in space and time using the MAST technique. With a motivation that will be better explained in Chapter III, the assigned BC of the diffusive model solved for the estimation of the discharge hydrograph are the water levels at the upstream end and the zero diffusion condition at the downstream end.

The basic idea of the MAST algorithm is to apply a fractional time step procedure to compute the unknown surface level H at time level k+1, when the surface level is known at time level k. During the first half-step, the predicted level $H^{k+1/2}$ is estimated by integrating in time and space the following prediction equation,(where ∇_x is the spatial gradient operator along direction x):

$$\frac{\partial H^{k+1/2}}{\partial t} - \frac{1}{T^{k+1/2}}\left[\frac{(R^{K+1/2})^{\frac{2}{3}} A^{K+1/2}}{n}\frac{\nabla_x H^K}{\sqrt{\left|\nabla_X H^K\right|}}\right] = \frac{Q_L{}^{k+1}}{T^{K+1/2}} \qquad (1.8),$$

where T is the section width and Q_L is the lateral inflow, in m^2/s. In the second half-step the corrected level H^{k+1} is obtained by solving the fully implicit discretization of the following correction equation:

$$\frac{\partial H^{K+1}}{\partial t} - \frac{1}{\overline{T}}\left[\frac{\overline{R^{\frac{2}{3}}A}}{n}\left(\frac{\nabla_x H^{K+1} - \nabla_x H^K}{\sqrt{\left|\nabla_X H^K\right|}}\right)\right] = 0 \qquad (1.9),$$

where the top bar is the symbol of the mean (in time) operator, applied along the prediction step. The advantage of splitting the original problem

in a prediction plus a correction problem is that these problems are much easier to solve with respect to the original one.

By applying functional analysis, it can be shown that Eq. (1.8) is convective and its solution depends only on one upstream boundary condition only. Following spatial integration, Eq. (1.8) turns in a system of ordinary differential equations (ODEs).

Figure 1.1 illustrates the spatial discretization. The computational domain is divided into *m* elements, partitioned by *m*+1 sections. The cross-section in each element is assumed constant and the control volume (cell) of each internal section is given by the sum of the two adjacent element halves (see Fig. 1.1). Inside each cell the water level is assumed constant. For the *i*th control volume the convective sub problem can be written as:

$$\underbrace{q_{i-1}^{\overline{k+1/2}} + Q_{L,i}}_{qent} = \underbrace{S_i(H_i)\frac{dH_i}{dt}}_{Volume\ i\ Variation} + q_i \qquad (1.10),$$

where S_i is the horizontal area (see Fig. 1.1b), $q_{i-1}^{\overline{k+1/2}}$ is the flux leaving the $(i\text{-}1)^{\text{th}}$ cell at time k+1/2, q_i is the discharge leaving the i^{th} cell and Q_{Li} is the lateral inflow entering in the computationa cell control volume. Eq. (1.10) is the mass balance of the *i*th cell: the entering flux, *qent*, is balanced by the leaving flux *qi* and by the change of storage per unit time.

The mean entering flux $q_{i-1}^{\overline{k+1/2}}$ is known from the solution of the previous cell; therefore, Eq. (1.10) can be directly solved to compute the final H value at time k+1. The integration is carried on using a Runge-Kutta methodology with self adapting time sub-step (Press at al., 1988).

After integration, the average leaving flux $\overline{q_i^{k+1/2}}$ is provided by the time mass balance(Nasello and Tucciarelli, 2005):

$$\overline{q_i^{k+1/2}} = \overline{q_{i-1}^{k+1/2}} + Q_L - \frac{Vol_i^{k+1/2} - Vol_i^{k}}{\Delta t} \qquad (1.11),$$

where $Vol_i^{k+1/2}$ and Vol_i^{k} are the volumes of the *i*th cell, after and before the convective step, respectively. With reference to Fig. 1.1a, this volume is computed as

$$Vol_i = \frac{1}{2}(A_i \Delta x_i + A_{i-1} \Delta x_{i-1}) \qquad (1.12),$$

where A is the cross section area (the subscript indicates the section) and Δx_i is the distance between the *i*th and (*i+1*)th section. Finally, the entering flux of the next cell *i+1* is assumed equal to the average one leaving cell *i*th.

The corrective Eq. (1.9) is diffusive and its solution depends on both boundary conditions. After spatial discretization, a fully implicit time discretization is applied to the resulting system.

The advantage of solving Eq. (1.9) instead of Eq.(1.5) is that the unknown H^{k+1} can be replaced by the unknown $\eta = H^{k+1} - H^{k+1/2}$.The new variable is small with respect to H^{k+1}, and the same holds for its fluxes. This implies that also the error associated to the fully implicit numerical solution is small with respect to the error in the estimation of the original unknown H^{k+1}.

More details on the numerical solution computed using the MAST approach can be found in Nasello and Tucciarelli (2005).

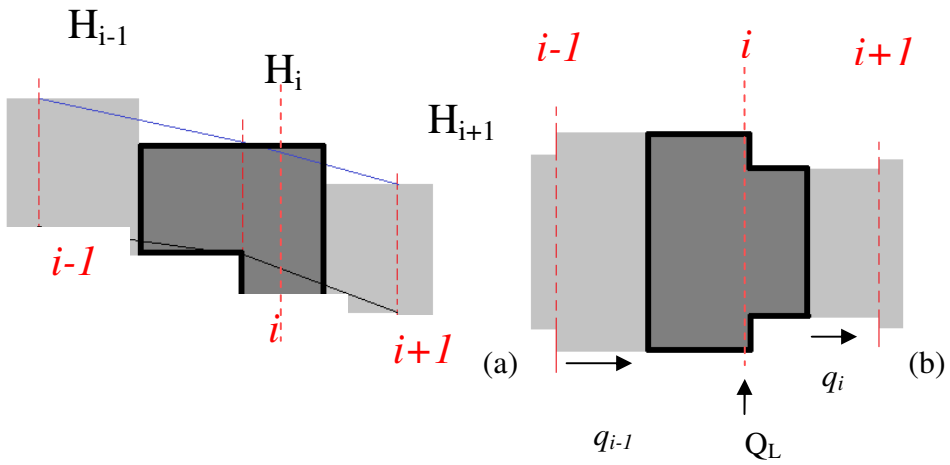

Figure 1.1. Spatial discretization (a) side view and (b) top view.

Observe that, if in the first upstream cell the water level time derivative is known from the assigned boundary condition, the entering discharge can be estimated from the l.h.s. of Eq. (1.10). Due to the order used in the solution of Eqs. (1.10) it would also be possible to estimate the lateral inflow in the following cells along the time step from k to k+1/2 as a known fraction of the computed upstream discharge.

1.4 Discharge estimation from double hydrograph

Hydraulic modelling is used as a tool to turn a given water level hydrograph, that corresponds to the input model, into a discharge one: the hydraulic model, simulating the flow routing along a river reach, is driven by an upstream water level hydrograph and its answer is afterwards evaluated in terms of discharge. In the context of discharge estimation in natural channels, this procedure can overcome several limitations of traditional techniques for discharge estimation, in particular during flood events. In fact, the calibration procedure allows estimating the Manning's roughness coefficient for each flood event, and this allows monitoring parameter variations, due for instance to the presence of vegetation or to local modifications of the channel morphology.

Discharge hydrograph estimation in natural channel is strictly dependent on resistance laws implemented inside the model. The aim of this chapter is to validate the procedure of Aricò et al. (2009) by means of field data information coming from the Alzette river (for three differents floods) with the restrictive hypothesis of negligible lateral inflows by changing the resistence law implemented inside the hydraulic model. The author chose *DCM* and *IDCM* formula (described in the next paragraph) to test the proceduce.

1.5 Divided channel method (*DCM*) and interactive divided channel method (*IDCM*)

In the *DCM* method the river section is divided into subsections with uniform velocities and roughness (Chow, 1959).

Division is made by vertical lines and no interaction between adjacent subsections is considered. Discharge is obtained by summing the contributions of each subsection, obtained by applying the Manning formula. In order to model the interaction between adjacent subsections of a compound section, Huthoff et al. (2008) proposed the so-called interactive divided channel method (*IDCM*). In this method the interface stress τ_{int} , associated with the lateral momentum transfer between the main channel and the floodplain(s) can be expressed as:

$$\tau_{\text{int}} = \frac{1}{2}\alpha\rho(U_{mc}{}^2 - U_{fp}{}^2) \qquad (1.13),$$

where $U_{mc}{}^2$ and $U_{fp}{}^2$ are the squared flow velocities of the main channel and floodplains and α is the dimensionless interface coefficient, estimated by Huthoff from different experiments.

1.6 Calibration criteria

Indirect method for discharge estimation in rivers relies on the evaluation of the Manning's roughness coefficient, *n*: this estimation is performed by calibrating the hydraulic model.

Strictly speaking, three gauged sections would be required to make always identifiable the corresponding calibration problem; two for the boundry conditions and one for the calibration of the manning coefficient. In spite of this, when both the known water level hydrographs are used as boundary conditions, with a Manning coefficient different from the real one, the resulting water level profiles displays artificial waves along the reach, that can be justified only if special perturbations occur downstream the final section. Aricò et al. (2008) used numerical simulations to show the generation of secondary anomalous waves at the downstream boundary section, in case an incorrect Manning coefficient is used in a 1D routing model. Based on this observation, Aricò et al. (2009) apply the following strategy: 1) an approximated downstream boundary condition (not involving water depth data) is adopted in a third section downstream the second gauged one, in order to avoid irregularities in the computed profiles, 2) the water depth data of the second gauged section are used to estimate the 'difference' between the measured and the computed water levels and 3) the Manning coefficient is calibrated by minimizing this difference.

The calibration procedure has been evaluated by minimizing two possible errors (Aricò et al., 2009) applied to the stage hydrographs in the second gauged section:

1) Root mean square error

$$RMSE = \left[\frac{\sum_{i=1,n} (h_i^{obs} - h_i^{sim})^2}{N} \right] \quad (1.14),$$

where h_i^{sim} is the water depth computed in the i^{t}h time level, h_i^{obs} is corresponding measured value and N is the number of observations in the downstream gauged section.

2) Relative time peak error

$$\Delta t_p = \left| t_p \Big|_{sim} - t_p \Big|_{obs} \right| \quad (1.15),$$

where $t_p\big|_{sim}$ is the peak time value of the computed stage hydrographs, while $t_p\big|_{obs}$ is the measured reference value.

The first error is a measure of the overall difference between the measured and the computed hydrograph and is, for this reason, more efficient in the general case, specially if small perturbations make unclear the location of the two hydrograph peaks. On the other hand, if a bias is given in the measure of the water levels (e.g. in the estimation of the zero reference level) this bias affects the first error much more than the second one.

1.7 Performance criteria

The performances of the discharge estimation procedure have been estimated in the evaluation tests by means of two possible criteria (Aricò et al., 2009) applied to the discharge hydrographs:

1. **Root mean square error:**

$$RMSE = \left[\frac{\sum_{i=1,n} (q_i^{obs} - q_i^{sim})^2}{N} \right] \quad (1.16),$$

where q_i^{sim} and q_i^{obs} are respectively the the simulated and the measured discharges at the ith time level.

2. Nash-Sutcliffe efficiency (Nash and Sutcliffe, 1970):

$$NS = \left[1 - \frac{\sum_{i=1,N} (q_i^{obs} - q_i^{sim})^2}{\sum_{i=1,N} (q_i^{obs} - \overline{q_i^{obs}})^2} \right] \quad (1.17),$$

where $\overline{q_i^{obs}}$ is the average value of the benchmark discharge hydrograph.

The Nash-Sutcliffe efficiency, *NS*, involves the whole hydrograph in its evolution in time. *NS* can range from $-\infty$ to 1: in this range of values, with increasing *NS* the fit between simulated discharge and observed data improves, with a perfect fit obtained for *NS* =1. Observe that, because the difference between simulated and observed data in Eq. (1.17) is calculated as sum of squared values, a major weight is given to the bigger errors that generally occur for higher values of the time series (Legates

and Mc Cabe, 1999). This leads to the fact that, generally, in Nash-Sutcliffe efficiency a major weight is given to the upper part of discharge hydrograph (Krause et al., 2005).

1.8 Study case: Alzette river

The investigated river is named Alzette. In Luxembourg the river meanders in a relative large and flat plain wide about 300 m and with a mean slope of ~ 0.08%. The modeled river reach is about 13 km long, with a mean channel width of ~ 30 m and an average depth of ~ 4m. The events of January 2003,January 2007 and January 2011 are investigated. The flood events have an estimated return period of 4 years (Montanry et al., 2008). For both these events, stage records are available along the Alzette river at four gauged stations (Pfaffenthal, Steinsel, Hunsdorf, Litgen) and in each section very reliable rating curves are available. The hydrometric data are recorded every 15 min. The whole procedure has been tested along the river reach, between Pfaffenthal and Hunsdorf gauged sections. The computational domain is extended to about half the distance between the two gauged sections (generally enough to minimize the effect of the approximation in the downstream b.c.).

It is worth to point out that the above-mentioned procedure allows discharge estimation only under the hypothesis of negligible lateral inflow. In practice, this is equivalent to the lack of tributary junctions between the two gauged sections.

1.8.1 Calibration results

The events calibrated with *DCM* and *IDCM* refer to dimensionless water stages hydrographs recorded in the gauged section of Hunsdorf. Suitable observation windows were chosen which include the peak hydrographs (See Figures 1.2). The falling limb is typically not included, since it has a lower slope and provides a lower sensitivity of the objective functions used for calibration with respect to the parameter *n*.

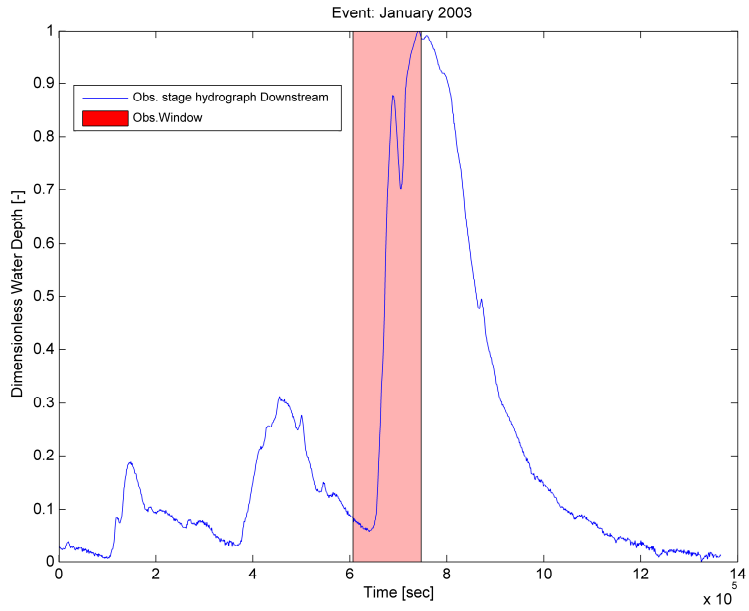

(a)

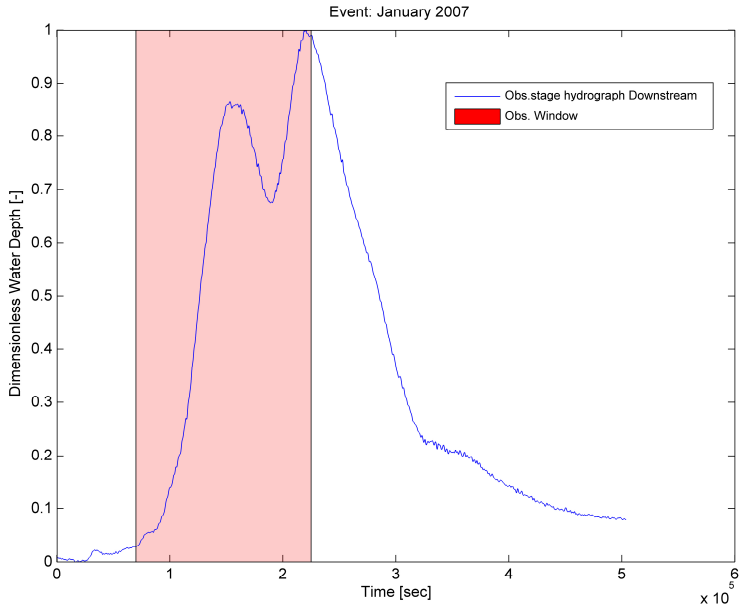

(b)

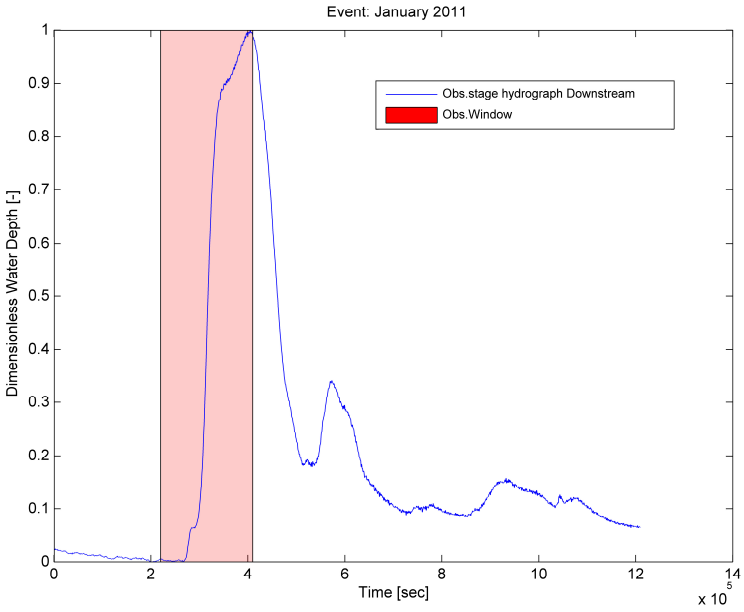

(c)

Figures 1.2. Calibration window for the events of: January 2003 (a), January 2007 (b), January 2011(c).

The *IDCM* calibration is carried out using three different α values:

Table 1.2. α values.

α values	
1°value	0.002
2°value (suggested by Huthoff)	0.02
3°value	0.2

DCM and *IDCM* calibrations made on water stages returns the following optimum Manning's roughness coefficients values (see Tables 1.3-1.5), obtained minimizing RMSE and Time Peak Error functions.

Table 1.3. The calibrated Manning's roughness coefficients returned by dimensionless water stages. Event 2003.

	Water stage calibration	
	$\mathbf{n_{opt}}$ **(RMSE)**	$\mathbf{n_{opt}}$ (ΔT_p)
DCM	0.054	0.054
IDCM (α= 0.002)	0.053	0.053
IDCM (α= 0.02)	0.047	0.047
IDCM (α= 0.2)	0.02	0.02

Table 1.4. The calibrated Manning's roughness coefficients returned by dimensionless water stages. Event 2007.

	Water stage calibration	
	$\mathbf{n_{opt}}$ **(RMSE)**	$\mathbf{n_{opt}}$ (ΔT_p)
DCM	0.051	0.051
IDCM (α= 0.002)	0.050	0.050
IDCM (α= 0.02)	0.044	0.044
IDCM (α= 0.2)	0.027	0.027

Table 1.5. The calibrated Manning's roughness coefficients returned by dimensionless water stage. Event 2011.

	Water stage calibration	
	n_{opt} (RMSE)	**n_{opt} (ΔT_p)**
DCM	0.051	0.051
IDCM (α= 0.002)	0.05	0.05
IDCM (α= 0.02)	0.046	0.046
IDCM (α= 0.2)	0.02	0.02

Figures 1.3 (a), (b), (c) show estimated and observed dimensionless stage hydrographs in Hunsdorf gauged site using nopt obtained by minimizing ΔTp and *RMSE* for the all analyzed events.

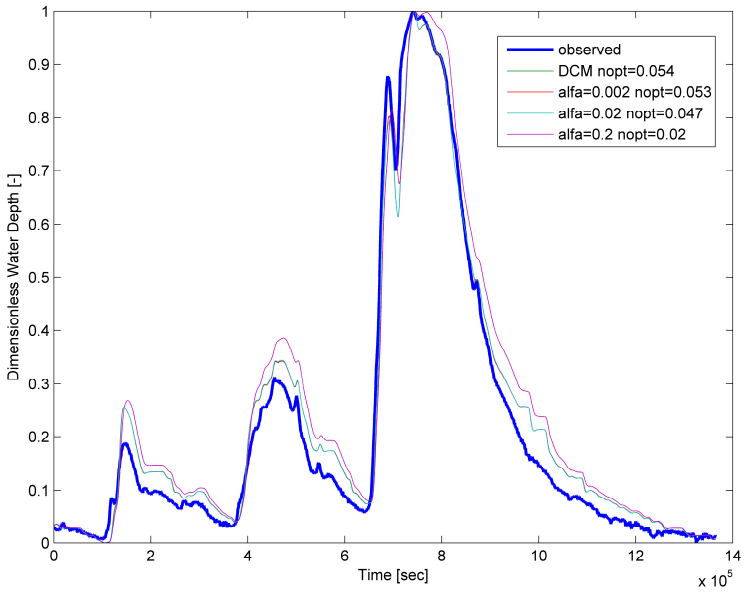

(a)

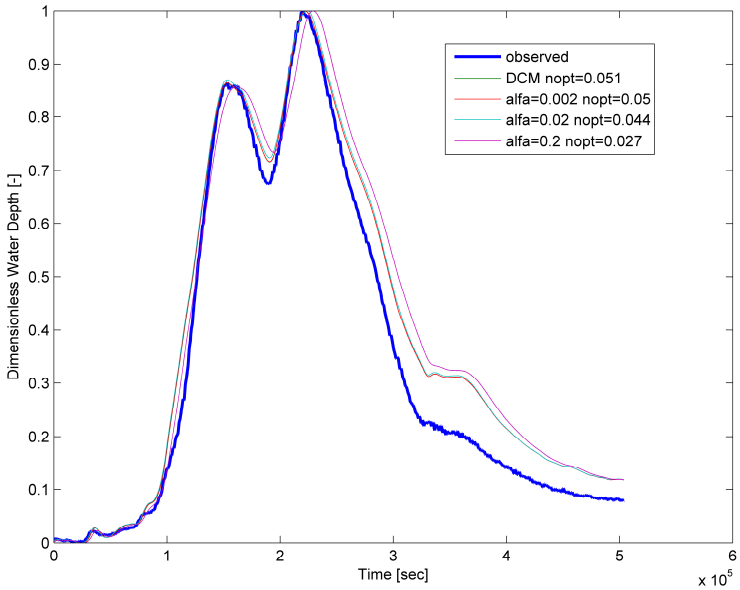

(b)

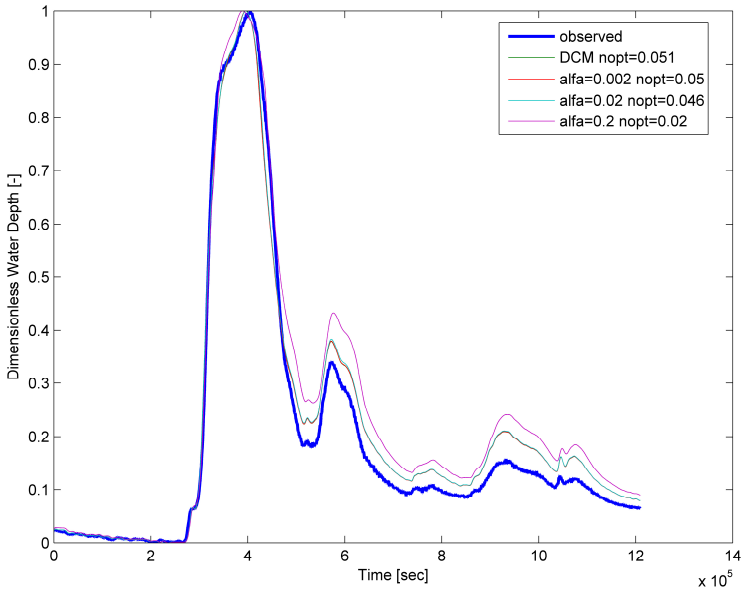

(c)

Figures 1.3. Measured and computed stage hydrograph in Hunsdorf section: event 2003 (a), event2007 (b), event2011 (c).

1.8.2 Permormance results

An overall good matching between recorded and simulated discharge hydrographs can be observed in the upstream gauged site for each event. Moreover for all the analyzed events the Nash Sutcliffe efficiency is greater than 0.90 and the *RMSE* is always close to one. Nevertheless when adopting *IDCM*, including lateral momentum exchange in the friction force formula, it is very difficult to appreciate the best value of the alfa coefficient and the optimal value 0.2 suggested by Huthoff is the one that provides worse results.

Table 1.6. Performance analysis in terms of Nash-Sutcliffe, *NSq*, and Root Mean Square Error, *RMSE* for the all investigated events at Pfaffenthal gauged site are showed. The Manning's roughness coefficients performed by water stages calibrations are also shown.

EVENT		**Hydraulic model calibration**		
		Dimensionless water stage calibration (rising limb)		
		n_{opt}	**NS**	**RMSE**
2003	**DCM**	0.054	0.9824	1.9683
	α=0.002	0.053	0.9866	1.7157
	α=0.02	0.047	0.9946	1.0914
	α=0.2	0.02	0.9701	2.5644
2007	**DCM**	0.051	0.9901	1.4434
	α=0.002	0.05	0.9932	1.1953
	α=0.02	0.044	0.9878	1.6036
	α=0.2	0.027	0.9161	4.2082
2011	**DCM**	0.051	0.9917	1.6631
	α=0.002	0.05	0.9908	1.7426
	α=0.02	0.046	0.994	1.4097
	α=0.2	0.02	0.9808	2.5212

Observe in Table 1.7 that most of the relative magnitude peak error are smaller than 10% .

Table 1.7. Performance analysis in terms of relative magnitude peak error for all the investigated events at Pfaffenthal gauged site. The calibrated Manning's roughness coefficients and discharge peaks values are also shown.

EVENT		**Discharge performance**		
		n_{opt}	**Discharge peak value [m^3/s]**	**ΔQp [%]**
2003	**DCM**	0.054	69.6416	-1.84
	α=0.002	0.053	70.4917	-0.61
	α=0.02	0.047	74.9998	5.43
	Alfa=0.2	0.02	70.452	-0.67
2007	**DCM**	0.051	52.0052	-3.22
	α=0.002	0.05	52.6971	-1.87
	α=0.02	0.044	56.1942	4.47
	α=0.2	0.027	45.229	-18.69
2011	**DCM**	0.051	86.5478	1.96
	α=0.002	0.05	86.0041	1.34
	α=0.02	0.046	88.325	3.94
	α=0.2	0.02	91.0076	6.77

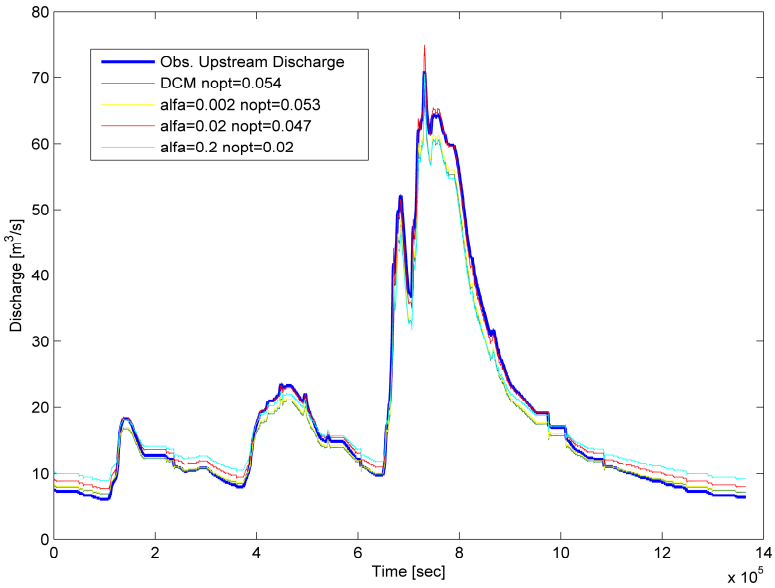
Obs. Upstream Discharge
DCM nopt=0.054
alfa=0.002 nopt=0.053
alfa=0.02 nopt=0.047
alfa=0.2 nopt=0.02
Discharge [m3/s]
Time [sec]
x 10^5

(a)

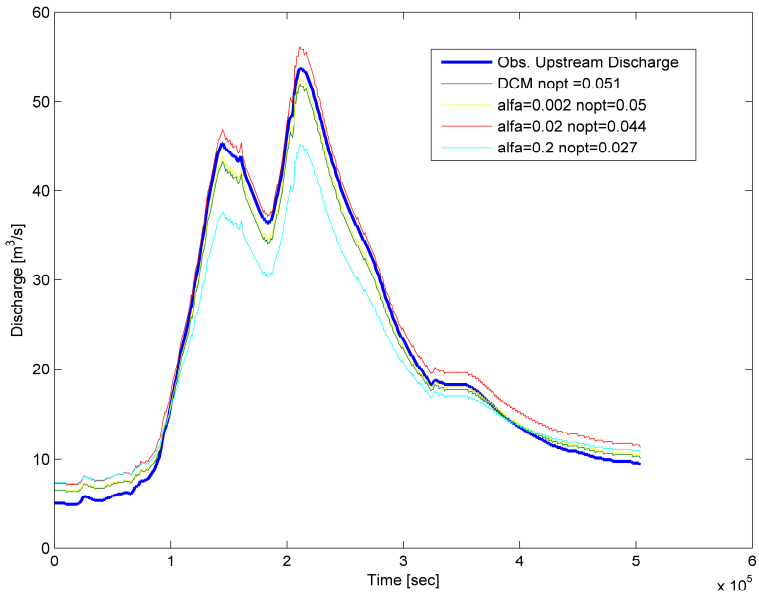
Obs. Upstream Discharge
DCM nopt =0.051
alfa=0.002 nopt=0.05
alfa=0.02 nopt=0.044
alfa=0.2 nopt=0.027
Discharge [m3/s]
Time [sec]
x 10^5

(b)

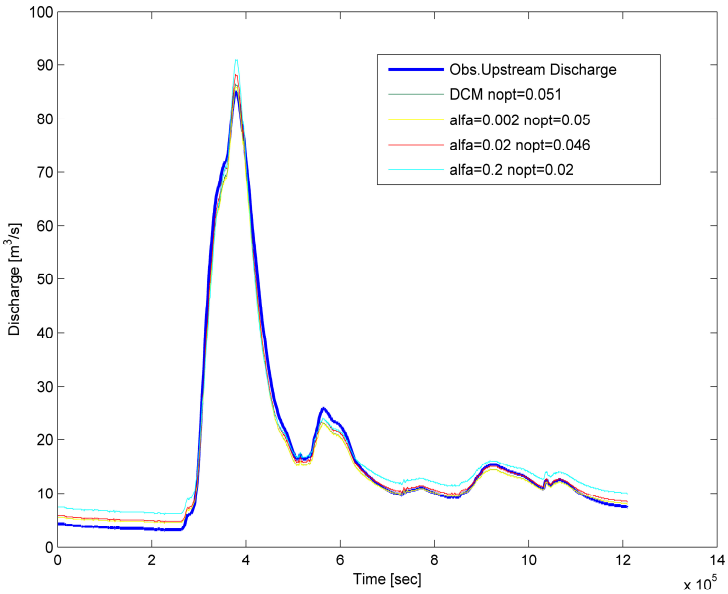

(c)

Figures 1.4. Measured and computed discharge hydrograph at Pfaffenthal gauged section: event 2003 (a), event2007 (b), event2011 (c)

It is also evident that optimal Manning's roughness coefficients decreases along with the inverse of alpha. A good estimation of the discharge hydrograph is obtained using the *IDCM* method within a large range of alfa, but the optimal value 0.02 suggested by Hutoff according to his laboratory experiments is out of this range. This result calls for an improvement of the resistance law formulas used for the hydrograph routing. The next chapter will explore the latest resistance laws available literature, starting from the well known Manning's formula. In the third chapter, a new version of the Huthoff's formula and a more efficient law, called *LHRM*, are proposed.

CHAPTER II

RESISTENCE FLOW FORMULAS

2.1 Introduction

Compound sections are a common configuration of artificial channels. The reason is that during floods the transportation capacity of rivers may not be enough to convey the total discharge and a compound channel configuration can occur. In these cases, the flow during floods submerges the surrounding fields, called floodplains, but allows their use for some type of human activity during the normal time. The difference in water depth between the main channel and the floodplains leads to a difference in the streamwise velocity between these subsections. The faster flow in the main channel interacts with the slower flow in the floodplains generating a mixing layer near the interface (van Prooijen et al. 2005). Due to exchange of momentus, this mixing region reduces the discharge capacity when compared with independent cross sections. In many cases the floodplains are covered by vegetation, increasing the bottom roughness and the overall resistance. This difference leads to a further increment of the velocity gradient between main channel and floodplain and the results is that strong lateral shear layers between these regions are observed (Tang and Knight 2009). Water depth - discharge uniform flow relationshiop in simple channels is accurately estimated since the method proposed by Antoine de Chézy (Myers 1978). This is not the case for compound channels, because of the mixing layer in the interface which creates a 3D flow structure (Shiono and Knight 1991). The traditional

method to estimate discharge during flood is based on an old approach that simply divides the total cross section along verticals at the interface between the main channel and the floodplains (Chow 1959). New 1D approaches can take into account the interaction occuring between the flows in each subsection. 2D and 3D methods allows a better estimation of the velocity field in the coumpound section but in practice, due to the amount of data required and the processing time, 1D methods are often preferred. Still, the momentum transfer should be taken into account in 1D modelling (Bousmar and Zech 1999). Since Sellin (1964) presented the first evidence of the flow characteristics in compound channels there have been several attempts to model it. Knight and Shiono (1996) referred the difficulty of the developed formulas to be applied universally as, in many cases, they had been set based on a reduced amount of data.

Modeling the flow in a compound channel by applying the simple Manning resistance formula does not take into account the sub-section velocity difference and leads to a clear underestimation of the normal discharge for given water level. Chow (1959) suggested the division of the channel in subsections where velocity and roughness could be considered as uniform. This method, called the Divided Channel Method, is still widely used in commercial models as HEC-RAS (Brunner 2008), ISIS (Knight 2001), SOBEK and Mike 11 (Huthoff et al. 2008). As pointed out in Knight (2001) this treatment of a compound channel assumes that there is no interaction between the subdivided areas despite the existence of mean velocity discontinuities at the assumed internal boundaries. Therefore, the simple division of the channel in subsections is not appropriate for modelling the discharge in compound channels (Knight and Shiono 1996) and leads, for a large number of subsections, to

a clear overestimation of the normal discharge for given water level. Different methods had been proposed with the attempt to model the interaction processes that occur in this type of flows, including the momentum transfer. According to Knight (2001), these methods can be divided into 5 groups: i) methods that change the sub-area wetted perimeters; ii) methods that make discharge adjustments (with experimental data, for example); iii) methods that include apparent shear stresses on the sub-area division lines; iv) methods where the lines are located at zero shear stress; v) methods that combine different divisions of the channel.

In this section, six methods were presented to model the flow in the compound channel.

2.2 Divided Channel Method (*DCM*)

This method assumes the division of the channle in several sub-sections, namely the main channel and the two lateral floodplains in the case of artificial compound sections. The typical division is through vertical lines, where the total flow is given by the sum of sub-section discharges:

$$Q = \sum_i Q_i = \sum_i K_i R_i^{\frac{2}{3}} A_i S_0^{\frac{1}{2}} \qquad (2.1),$$

in which Q stands for the total discharge, K for the subsection roughness coefficient, R for the hydraulic radius, A for the cross section area and S_0 for the slope of the channel. Index i indicates each subsection.

2.3 Coherence Method (*COHM*)

The Coherence Method was developed by Ackers (1993) and it improves the results of the *DCM*. This method uses two empirical coefficients for the adjustment of the sub-section discharges.

The coherence (*COH*) is the ratio between the discharge obtained by the Eq. (2.1) assuming only one section (Single Discharge Method - *SCM*, average roughness coefficient and velocity for the whole cross section) and the the discharge obtained by *DCM*:

$$COH = \frac{Q^{SCM}}{Q^{DCM}} \tag{2.2}.$$

The closest to 1 is this coefficient, the most appropriate is to treat the channel as a single one. When this ratio is significantly less than 1 it is necessary to apply a different correction, through a coefficient called *DISADF*. Figure 2.1 presents an example of one section with the division of the flow into 4 regions according to its relative depth (floodplain/main channel water depth ratio).

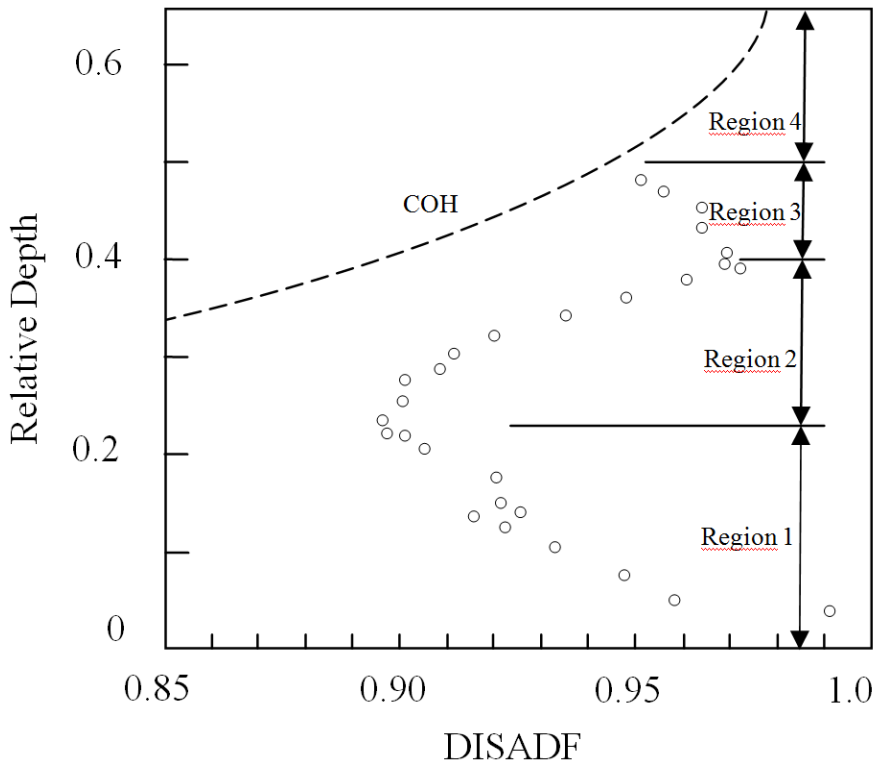

Figure 2.1. *DISADF* coefficient.

Ackers (1993) presented some empirical formulas to compute the DISADF in each flow region. The discharge is then obtained by the following equation:

$$Q = Q^{DCM} - DISDEF \quad \text{for flow region 1} \qquad (2.3),$$

$$Q = Q^{DCM} * DISADF \quad \text{for flow regions 2 to 4} \qquad (2.4),$$

in which *DISDEF* is a coefficient called discharge deficit, whose calculation procedure can be found, for example, in Wark et al. (1994).

According to Sahu et al. (2011) the error in the discharge estimation obtained in the region 1 is very large, because of the small amount of data available for the estimation of the *DISDEF* coefficient.

2.4 Debord Method (*DM*)

The Debord Method provides a correction of the *DCM* results based on laboratory experiments carried on with 16 different configurations (Nicollet and Uan 1979). In those tests, the uniform flow discharge measured in a channel with compound section was compared to that measured with the *DCM* method, where vertical separations were placed in the interface between sub-sections. The authors concluded that the most important parameter was the roughness ratio between subsections. According to *DM* the discharge can be computed with the following Eqs. (2.5) and (2.6).

$$Q_{mc} = \varphi k_{mc} R_{mc}^{\frac{2}{3}} A_{mc} S_0^{\frac{1}{2}} \qquad (2.5),$$

$$Q_{fp} = \sqrt{1 + \frac{A_{mc}}{A_{fp}}(1-\varphi^2)} k_{fp} R_{fp}^{\frac{2}{3}} A_{fp} S_0^{\frac{1}{2}} \qquad (2.6),$$

where the subscripts mc and fp stand for main channel and floodplain, respectively and φ stands for the experimental coefficient given by:

$$\varphi = \frac{1}{2}\left[(1-\varphi_0)\cos\left(\frac{\pi \frac{R_{fp}}{R_{mc}}}{0.3}\right)\right] + (1-\varphi_0) \qquad \text{for } 0<R_{fp}/R_{mc}\leq 0.3 \qquad (2.7),$$

$$\varphi = \varphi_0 0.9\left(\frac{k_{mc}}{k_{fp}}\right)^{\frac{1}{6}} \quad \text{for } R_{fp}/R_{mc}>0.3 \qquad (2.8).$$

2.5 Exchange Discharge Method (*EDM*)

This method takes into account the concept of apparent shear stress. The basis of this method is the transverse integration of the equation of momentum conservation. After some simplifications and algebric manipulation this equation could be written for the main channel and for the floodplains as showed in Eq. 2.9 and 2.10, respectively:

$$\rho g A_{mc} S_0 + (h_{\text{int},rig}\tau_{\text{int},rig} + h_{\text{int},lef}\tau_{\text{int},lef}) - \tau_0 P_{mc} = 0 \text{ for the main channel} \quad (2.9),$$

$$\rho g A_{fp} S_0 + h_{\text{int}}\tau_{\text{int}} - \tau_0 P_{mc} = 0 \qquad \text{for the floodplain} \qquad (2.10),$$

where ρ stands for the density of water, g for the acceleration due to gravity, h_{int} for the interface height; τ_{int} for the apparent shear stress in the main channel and floodplain interface; τ_0 for the bottom shear stress and P for the wet perimeter. Subscripts "rig" and "lef" stand for right and left, respectively. The mixing layer model by Smart (1992) is the base of *EDM* to model the momentum transfer due to turbulence. Therefore Eq. (2.10) is used for calculating the apparent shear stress (Bousmar and Zech 1999), as:

$$\tau_{\text{int}} = \frac{1}{2}\psi\rho(U_{mc} - U_{fp})^2 \qquad (2.11),$$

where ψ is an experimental parameter and U stands for the sub-section average velocity. *EDM* also models the momentum transfer associated with the geometry like converging main channels

2.6 Interacting Divided Channel Method (*IDCM*)

Huthoff et al. (2008) developed this method based on the apparent shear stress concept (Eq. 2.9 and 2.10). The authors used the formulation of van Prooijen et al. (2005) in order to model the momentum transfer in the interface, obtaining the following Eq. (2.12).

$$\tau_{\text{int}} = \frac{1}{2}\gamma\rho(U_{mc}{}^2 - U_{fp}{}^2) \qquad (2.12),$$

where γ is a coefficient, derived by the authors ccording to experimental results collected in the literature. Observe that in Eq. (2.12) the shear stress grows with floodplain and main channel velocity with exponent 2, while the exponent in Eqs. (2.11) is intermediate between 1 and 2. The first formulation (2.12) leads to a much more stable solution of the sught after velocities in the resulting equilibrium problem.

2.7 Weighted Divided Channel Method (*WDCM*)

The Weighted Divided Channel Method was developed by Lambert and Myers (1998) and it is based on the analysis of the velocity distributions in the main channel and in the floodplains. This method corrects the DCM results by weighting the velocities obtained with vertical and horizontal divisions between the subsections (Eqs. 2.13 and 2.14).

$$U_{mc} = \xi U_{mc}^{DCM-V} + (1-\xi) U_{mc}^{DCM-H} \quad (2.13),$$

$$U_{fp} = \xi U_{fp}^{DCM-V} + (1-\xi) U_{fp}^{DCM-H} \quad (2.14),$$

where superscripts *DCM-V* and *DCM-H* stand for the results of *DCM* with vertical and horizontal divisions, respectively and ξ for the weighting coefficient for the *WDCM* (see Lambert and Myers, 1998 for further details).

CHAPTER III

UNIFORM FLOW FORMULA FOR IRREGULAR SECTIONS OF STRAIGHT CHANNELS

3.1 Introduction

Computation of uniform flow formula (or vertically averaged velocities) is the first step of two major calculations in 1D shallow water modelling: 1) estimation of the discharge given the energy slope and the water stage and 2) estimation of the bottom shear stress for computing the bed load in a given river section.

Many popular software tools, like MIKE11 (MIKE11, 2009), compute the discharge Q, in each river section, as the sum of discharges computed in different sub-sections, assuming a single water stage for all of them. Similarly, HEC-RAS (HEC-RAS,2010) calculates the conveyance of the cross-section by the following form of Manning's equation:

$$Q = KS_f^{1/2} \tag{3.1},$$

where S_f is the energy slope and K is the conveyance, computed assuming the same hypothesis and solving each sub-section according to the traditional Manning equation.

The uniform flow formula almost universally applied in each sub-section is still the Chezy equation (Herschel, C., 1897). The advantage of

using the Chezy equation is that the associated Manning's coefficient has been calibrated worldwide for several types of bed surface and a single value is ready to use for each application. However, it is well known that the Chezy equation was derived from laboratory measurements taken in channels with a regular, convex cross-sectional shape. When the section results from the union of different parts, each with a strongly different average water depth, one of two options is usually selected. The first option, called Single Channel Method (*SCM*) is simply to ignore the problem. This leads to strong underestimation of the discharge, because the Chezy formula assumes a homogeneous vertically averaged velocity and this homogeneous value provides strong energy dissipation in the parts of the section with lower water depths. The second option, called Divided Channel Method (*DCM*) is to compute the total discharge as the sum of the discharges flowing in each convex part of the section (called subsection) , assuming a single water level for all parts (Chow 1959; Shiono et al. 1999; Myers and Brennan, 1990). In this approach, the wet perimeter of each subsection is restricted to the component of the original one pertaining to the subsection, but the new components shared by each couple of subsections are neglected. This is equivalent to neglecting the shear stresses coming from the vortices with vertical axes (if subsections are divided by vertical lines) and considering additional resistance for higher velocities, which results in overestimation of discharge capacity (Lyness et al. 2001).

Knight and Hamed (1984) compared the accuracy of several subdivision methods for compound straight channels by including or excluding the vertical division line in the computation of the wetted perimeters of the main channel and the floodplains. However, their results

show that conventional calculation methods result in larger errors. Wormleaton et al. (1982) and Wormleaton and Hadjipanos(1985) also discussed, in the case of compound sections, the horizontal division through the junction point between the main channel and the floodplains. Their studies show that these subdivision methods cannot well assess the discharge in compound channels.

The interaction phenomenon in compound channels has also extensively studied by many other researchers (e.g., Sellin 1964; Knight and Demetriou 1983; Stephenson and Kolovopoulos 1990; Rhodes and Knight 1994; Bousmar and Zech 1999; van Prooijen et al. 2005; Moreta and Martin-Vide 2010). These studies demonstrate that there is a large velocity difference between the main channel and the floodplain, especially at low relative depth, leading to a significant lateral momentum transfer. The studies by Knight and Hamed (1984), Wormleaton et al. (1982) indicate that vertical transfer of momentum between the upper and the lower main channels exists, causing significant horizontal shear able to dissipate a large part of the flow energy.

Furthermore, many authors have tried to quantify flow interaction among the subsections, at least in the case of compound, but regular channels. To this end turbulent stress was modelled through the Reynolds equations and coupled with the continuity equation (Shiono and Knight, 1991). This coupling leads to equations that can be analytically solved only under the assumption of negligible secondary flows. Approximated solutions can also be obtained, although they are based on some empirical parameters. Shiono and Knight developed the Shiono-Knight Method (*SKM*) for prediction of lateral distribution of depth-averaged velocities and boundary shear stress in prismatic compound channels (Shiono and

Knight, 1991; Knight and Shiono, 1996). The method can deal with all channel shapes that can be discretized into linear elements (Knight and Abril, 1996; Abril and Knight, 2004).

Other studies based on the Shiono and Knight method can be found in Liao and Knight (2007), Rameshwaran and Shiono (2007), Tang and Knight (2008) and Omran and Knight (2010). Apart from *SKM*, some other methods for analysing the conveyance capacity of compound channels have been proposed. For example, Ackers (1993) formulated the so called empirical coherence method. Lambert and Sellin(1996) suggested a mixing length approach at the interface, whereas more recently Cao et al. (2006) reformulated flow resistance through lateral integration using a simple and rational function of depth-averaged velocity. Bousmar and Zech (1999) considered the main channel/floodplain momentum transfer proportional to the product of the velocity gradient at the interface times the mass discharge exchanged through this interface due to turbulence. This method, called *EDM*, also requires a geometrical exchange correction factor and turbulent exchange model coefficient for evaluating discharge.

A simplified version of the *EDM*, called Interactive Divided Channel Method (*IDCM*), was proposed by Huthoff et al. (2008). In *IDCM* lateral momentum is considered negligible and turbulent stress at the interface is assumed to be proportional to the span wise kinetic energy gradient through a dimensionless empirical parameter α. *IDCM* has the strong advantage of using only two parameters, α and the friction factor, *f*. Nevertheless, as shown in the next section, α depends on the way the original section is divided.

An alternative approach could be to simulate the flow structure in its complexity by using a three-dimensional code for computational fluid dynamics (CFD). In these codes flow is represented both in terms of transport motion (mean flow) and turbulence by solving the Reynolds Averaged Navier Stokes (RANS) equations (Wilcox, 2006) coupled with turbulence models. These models allow closure of the mathematical problem by adding a certain number of additional partial differential transport equations equal to the order of the model. In the field of the simulation of industrial and environmental laws second order models (e.g. k-ε and k-ω models) are widely used. Nonetheless, CFD codes need a mesh fine enough to solve the boundary layer (Wilcox, 2006), resulting in a computational cost that can be prohibitive even for river of few km.

In this study two new methods, aimed to represent subsection interactions in a compound channel, are presented. The first method, named "INtegrated Channel Method" (*INCM*), derives from the previous Huthoff formula, which is shown to give results depending on the way the river cross section is discretized in sub-sections. The same dynamic balance adopted by Huthoff is written in differential form, but its diffusive term is weighted according to a ξ coefficient proportional to the local water depth.

The second one, named “local hydraulic radius method” (*LHRM*), derives from the observation that, in the Manning formula, the mean velocity per unit energy gradient is proportional to a power of the hydraulic radius. It should then be possible to get the vertically averaged velocity along each vertical by using the same Manning formula, where the original hydraulic radius is changed with a "local" one. This "local"

hydraulic radius should take into account the effect of the surrounding section geometry, up to a maximum distance which is likely to be proportional to the local water depth, according to an empirical β coefficient. The method gives up the idea of solving the Reynolds equations, due to the uncertainty of its parameters, but relies on the solid grounds of the historical experience of the Manning equation.

The the following paragraphs are organized as follows: Two of the most popular approaches adopted for computation of the vertically averaged velocities are explained in details, along with the proposed *INCM* and *LHRM* methods. The ξ and β parameters of respectively the *INCM* and *LHRM* methods are then calibrated from available discharge lab experimental data and a sensitivity analysis is carried out. The *INCM* and *LHRM* methods are finally validated according to three different criteria. The first criterion is comparison with other series of the previous laboratory data, not used for calibration. The second criterion is comparison with discharge data measured in one section of the Alzette river Basin (Luxembourg). Because the friction factor is not known a priori, *INCM* and *LHRM* formulas are applied in the context of the indirect discharge estimation method, which simultaneously estimates the friction factor and the discharge hydrograph from the unsteady state water level analysis of two water level hydrographs measured in two different river sections. The third validation criterion is comparison with the vertical velocity profiles obtained by the ANSYS CFX solver, in a cross section of the Alzette river. In the conclusions, it is finally shown that application of bed load formulas, carried out by integration of elementary solid fluxes computed as function of the vertically averaged velocities,

can lead to results that are strongly different from those obtained by using the simple mean velocity and water depth section values.

3.2 Divided Channel Method (*DCM*) and Interactive Divided Channel Method (*IDCM*)

In the *DCM* method the river section is divided into subsections with uniform velocities and roughness (Chow, 1959). Division is made by vertical lines and no interaction between adjacent subsections is considered. Discharge is obtained by summing the contributions of each subsection, obtained by applying the Manning formula:

$$q = \sum_i q_i = \sum_i \frac{R_i^{2/3} A_i}{n_i} \sqrt{S_f} \qquad (3.2),$$

where q is the total discharge, A_i , R_i and n_i are the area, the hydraulic radius and the Manning's roughness coefficient of each sub section i of a compound channel and S_f is the energy slope, assumed constant across the river section. *DCM* is extensively applied in most of the commercial codes, two of them cited in the introduction.

In order to model the interaction between adjacent subsections of a compound section, the Reynolds and the continuity equations can be coupled (Shiono and Knight, 1991), to get:

$$\rho \frac{\partial}{\partial y}\left(H\overline{U}_v\overline{V}_d\right) = \rho g H S_0 + \frac{\partial}{\partial y}\left(H\overline{\tau}_{xy}\right) - \tau_b\left(1+\frac{1}{s^2}\right)^{1/2} \qquad (3.3),$$

where ρ is the water density, g is the gravity acceleration, y is the abscissa according to the lateral direction, U and V are respectively the velocity components along the flow x direction and the lateral y direction,

H is the water depth, the sub-index d marks the vertically averaged quantities and the bar the time average along the turbulence period, S_0 is the bed slope, s is the section lateral slope, and τ_β is the bed shear stress. The $\bar{\tau}_{xy}$ turbulent stress is given by the eddy viscosity equation, that is:

$$\bar{\tau}_{xy} = \rho \bar{\varepsilon}_{xy} \frac{\partial U_d}{\partial y} \tag{3.4a}$$

$$\bar{\varepsilon}_{xy} = \lambda U_* H \tag{3.4b}$$

where the friction velocity U_* is set equal to:

$$U_* = \left(\frac{f}{8g} \right)^{1/2} U_d \tag{3.5}$$

and f is the friction factor, depending on the bed material. The analytical solution of Eqs. (3.3)-(3.5) can be found only if the left hand side of Eq. (3.3) is zero, which is equivalent to neglecting secondary flows. Other solutions can only be found by assuming a known Γ value for the lateral derivative. Moreover, λ is another experimental factor depending on the section geometry. The result is that solution of Eq. (3.3) strongly depends on the choice of two coefficients, λ and Γ, which are additional unknowns with respect to the friction factor *f*.

In order to reduce to one the number of empirical parameters (in addition to *f*) Huthoff et al. (2008) proposed the so-called Interactive Divided Channel Method (*IDCM*).

Integration of Eq. (3.3) over each i^{th} subsection, neglecting the averaged flow lateral momentum, leads to:

$$\rho g A_i S_0 = \rho f_i P_i U_i^2 + \tau_{i+1} H_{i+1} + \tau_i H_i \tag{3.6}$$

where the left-hand side of Eq.(3.6) is the gravitational force per unit length, proportional to the density of water ρ, to the gravity acceleration g, to the cross-sectional area A_i, and to the stream wise channel slope S_0. The terms at the right-hand side are the friction forces, proportional to the friction factor f and to the wet solid boundary P_i, as well as the turbulent lateral momentum on the left and right sides, proportional to the turbulent stress τ and to the water depth H.

Turbulent stresses are modelled quite simply as:

$$\tau_{i+1} = \frac{1}{2}\rho\alpha\left(U_{i+1}^2 - U_i^2\right) \tag{3.7},$$

where α is a dimensionless interface coefficient, U^2_i is the square of the vertically averaged velocity and τ_i is the turbulent stress along the plane between subsection *i-1* and *i*. If subsection *i* is the first (or the last) one, velocity U_{i-1} (or U_{i+1}) is set equal to zero.

Following a wall-resistance approach (Chow, 1959), the friction factor f_i is computed as:

$$f_i = \frac{g\, n_i^2}{R_i^{1/3}} \tag{3.8},$$

where n_i is the Manning's roughness coefficient and R_i (=A_i/P_i) is the hydraulic radius of subsection *i*.

Equations (3.6) forms a system with an order equal to the number m of subsections, which is linear in the U_i^2 unknowns. The results are affected by the choice of the α coefficient, which is recommended by Huthoff et al. (2008), on the basis of lab experiments, equal to 0.02. Computation of the velocities U_i makes it easy to estimate discharge q.

IDCM has the main advantage of using only two parameters, the *f* and α coefficients. On the other hand, it can be easily shown that α, although it is dimensionless, depends on the way the original section is divided. The reason is that the continuous form of Eq. (3.6) is given by:

$$\rho g\left(HS_0 - \frac{f\,U^2}{g\,cos\theta} \right) = \frac{\partial}{\partial y}\left(\tau H\right) \tag{3.9},$$

where θ is the bed slope in the lateral direction. Following the same approach as the *IDCM*, if we assume the turbulent stress τ to be proportional to both the velocity gradient in the lateral direction and to the velocity itself, we can write the right-hand side of Eq. (3.9) in the form:

$$\frac{\partial}{\partial y}\left(\tau H\right) = \frac{\partial}{\partial y}\left(\frac{\alpha_H}{2} \rho\, U \frac{\partial U}{\partial y} H \right) \tag{3.10},$$

and Eq. (3.9) becomes:

$$\rho\left(gHS_0 - \frac{f\,U^2}{g\,cos\theta} \right) = \frac{\partial}{\partial y}\left(H \frac{\partial}{\partial y}\left(\alpha_H \rho U^2\right) \right) \tag{3.11}.$$

In Eq. (3.10) α_H is no longer dimensionless, but is a length. To get the same Huthoff formula from numerical discretization of Eq. (3.10), the author should set:

$$\alpha_H = 0.02\,\Delta y \tag{3.12},$$

where Δy is the subsection width, i.e. the integration step size. This implies that the solution of Eq. (3.11), according to the Huthoff formula, depends on the way the equation is discretized and the turbulence stress term on the r.h.s. vanishes along with the integration step size.

3.3 The new methods

3.3.1 Integrated Channel Method (*INCM*)

INCM derives from the *IDCM* idea of evaluating the turbulent stresses as proportional to the gradient of the squared averaged velocities, leading to Eqs. (3.7) and (3.11). Observe that dimensionless coefficient α, in the stress computation given by Eq. (3.7), can be written as the ratio between α_H and the distance between verticals *i* and *i+1*. For this reason, coefficient α_H can be thought of as a sort of mixing length, related to the scale of the vortices with horizontal axes. *INCM* assumes the optimal α_H to be proportional to the local water depth, because water depth is at least an upper limit for this scale, and the following relationship is applied:

$$\alpha_H = \xi H \tag{3.13},$$

where ξ is an empirical coefficient to be further estimated.

3.3.2 Local hydraulic radius method (*LHRM*)

LHRM derives from the observation that, in the Manning equation, the average velocity is set equal to:

$$V = \frac{R^{2/3}}{n}\sqrt{S_0} \tag{3.14},$$

and has a one-to-one relationship with the hydraulic radius. In this context the hydraulic radius has the meaning of a global parameter, measuring the interactions of the particles along all the section as the ratio

between an area and a length. The inconvenience is that, according to Eq. (14), the vertically averaged velocities in points very far from each other remain linked anyway, because the infinitesimal area and the infinitesimal length around two verticals are summed to the numerator and to the denominator of the hydraulic radius independently from the distance between the two verticals. To avoid this, *LHRM* computes the discharge as an integral of the vertically averaged velocities, in the following form:

$$q = \int_0^L h(y)U(y)dy \tag{3.15},$$

where U is set equal to:

$$U = \frac{\Re_l^{2/3}}{n}\sqrt{S_0} \tag{3.16},$$

and $\Re_l$ is defined as local hydraulic radius, computed as:

$$\Re_l(y) = \frac{\int_a^b h(s)N(y,s)ds}{\int_a^b N(y,s)\sqrt{ds^2+dz^2}} \tag{3.17a},$$

$$a = \max(0,\ y-\beta h) \tag{3.17b},$$

$$b = \min(L,\ y+\beta h) \tag{3.17c},$$

where z is the topographic elevation (function of s), β is an empirical coefficient and L is the section top width. Moreover $N(y, s)$ is a shape function where:

$$N(y,s)=\begin{cases} -\dfrac{\left[y-\beta h(y)\right]-s}{\beta h(y)} & \text{if} \quad a<s<y \\ \dfrac{\left[y-\beta h(y)\right]-s}{\beta h(y)} & \text{if} \quad b>s>y \\ 0 & \text{otherwise} \end{cases} \qquad (3.18).$$

Equations (3.18) show how the influence of the section geometry, far from the abscissa *y*, continuously decreases up to a maximum distance, which is proportional to the water depth according to an empirical positive coefficient β. After numerical discretization, Eqs (3.15)-(3.17) can be solved to get the unknown q, as well as the vertically averaged velocities in each subsection. If β is close to zero and the size of each subsection is common for both formulas, *LHRM* is equivalent to *DCM*; if β is very large *LHRM* is equivalent to the traditional Manning formula. In the following, β is calibrated using experimental data available in the literature. A sensitivity analysis is also carried out, to show that the estimated discharge is only weakly dependent on the choice of the β coefficient, far from its possible extreme values.

3.4 Evaluation of the ξ and β parameters by means of lab experimental data

INCM and *LHRM* parameters were calibrated by using data selected from six series of experiments run at the large scale Flood Channel Facility (FCF) of HR Wallingford (UK), (Knight and Sellin, 1987; Shiono and Knight, 1991; Ackers, 1993), as well as from four series of experiments run in the small-scale experimental apparatus of the Civil Engineering

Department at the University of Birmingham (Knight and Demetriou, 1983). The FCF series were named F1, F2, F3, F6, F8 and F10; the Knight and Demetriou series were named K1, K2, K3 and K4. Series F1, F2, and F3 covered different floodplain widths, while series F2, F8, and F10 kept the floodplain widths constant, but covered different main channel side slopes. Series F2 and F6 provided a comparison between the symmetric case of two floodplains and the asymmetric case of a single floodplain. All the experiments of Knight and Demetriou (1983) were run with a vertical main channel wall, but with different B/b ratios. The series K1 has B/b = 1 and its section is simply rectangular. The B/b ratio, for Knight's experimental apparatus, was varied by adding an adjustable side wall to each of the floodplains either in pairs or singly to obtain a symmetrical or asymmetrical cross section. The geometric and hydraulic parameters are shown in Table 1; all notations of the parameters can be found in Fig. 3.1 and S_0 is the bed slope. The subscripts "mc" and "fp" of the side slope refer to the main channel and floodplain, respectively. Perspex was used for both main flume and floodplains in all tests. The related Manning roughness is 0.01 $m^{-1/3}s$.

The experiments were run with several channel configurations, differing mainly for floodplain geometry (widths and side slopes) and main channel side slopes (see Table 1). The K series were characterized by vertical main channel walls. More information concerning the experimental setup can be found in Table 3.1 (Knight and Demetriou, 1983; Knight and Sellin, 1987; Shiono and Knight, 1991).

Four series, named F1, F2, F3 and F6, were selected for calibration of the β coefficient, using the Nash Sutcliffe (NS) index of the measured and

the computed flow rates as a measure of the model's performance (Nash and Sutcliffe, 1970).

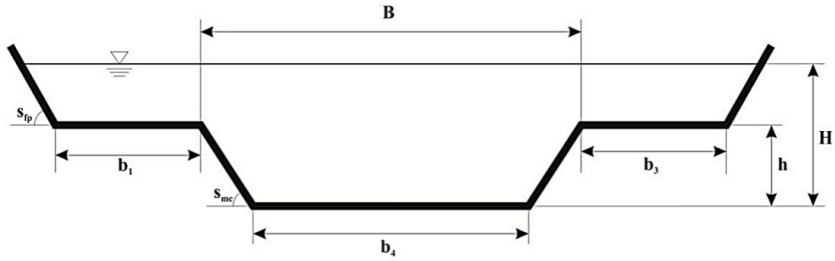

Figure 3.1. Compound channel geometric parameters.

Table 3.1. Geometric and Hydraulic Laboratory Parameters of the experiment series.

Series	S_0	h	B	b_4	b_1	b_3	s_{fp}	s_{mc}
	[‰]	[m]	[m]	[m]	[m]	[m]	[-]	[-]
F1	1.03	0.2	1.8	1.5	4.1	4.1	0	1
F2					2.25	2.25	1	1
F3					0.75	0.75	1	1
F6					2.25	0	1	1
F8					2.25	2.25	1	0
F10					2.25	2.25	1	2
K1	0.97	0.1	0.2	0.15	0.23	0.23	0	0
K2					0.15	0.15		
K3					0.08	0.08		
K4					-	-		

The remaining three series, named F2, F8 and F10, plus four series from Knight and Demetriou, named K1, K2, K3 and K4, were used for validation (no.) 1, as reported in the next section. NS is given by:

$$NS = \left[1 - \frac{\sum_{j=1,2} \sum_{i=1,N_J} \sum_{K=1,M_{N_J}} (q_{i,j,k}^{obs} - q_{i,j,k}^{sim})^2}{\sum_{j=1,2} \sum_{i=1,N_J} \sum_{K=1,M_{N_J}} (q_{i,j,k}^{obs} - \overline{q_{i,j,k}^{obs}})^2} \right] \quad (3.19),$$

where N_j is the number of series, M_{Nj} is the number of tests for each series, $q^{sim}{}_{i,j,k}$ and $q^{obs}{}_{i,j,k}$ are respectively the computed and the observed discharge (j = 1 for the FCF series and j = 2 for the Knight series; i is the series index and K is the water depth index). $\overline{q_{i,j,k}^{obs}}$ is the average value of the measured discharges.

Both ξ and β parameters were calibrated by maximizing the Nash Sutcliffe (NS) index, computed using all the data of the four series used for calibration. See the NS versus ξ and β curves in Figs. 3.2a and 3.2b.

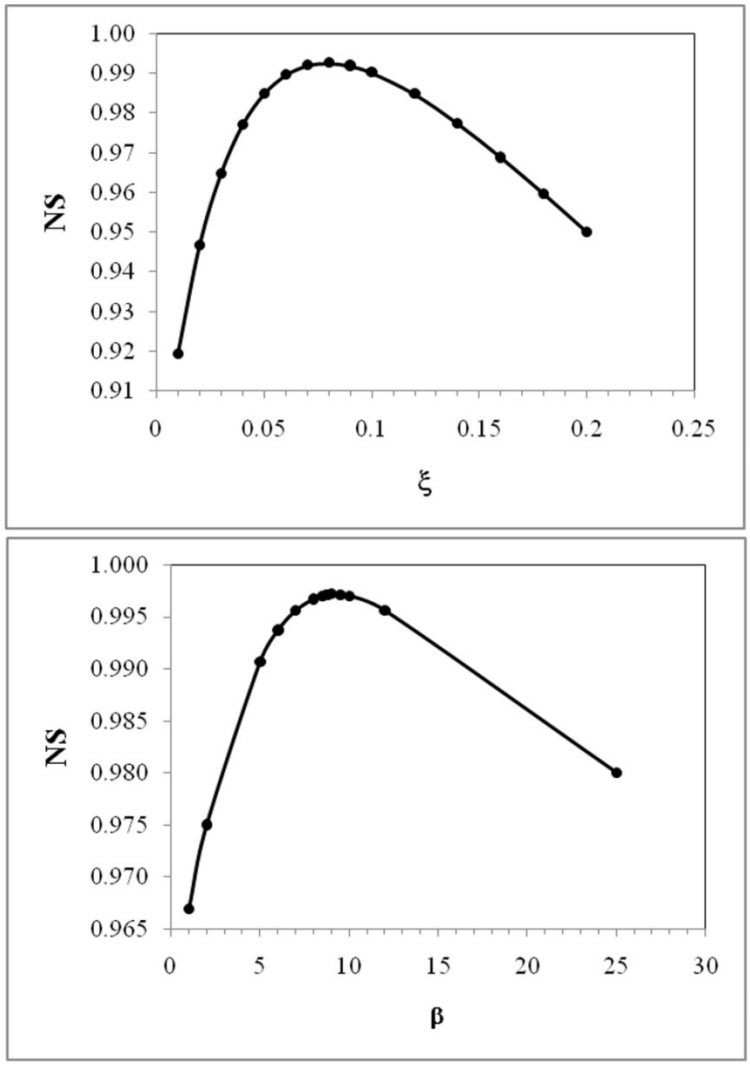

Figure 3.2. NS versus ξ and β curves respectively for *INCM* (a) and *LHRM* (b) methods.

Calibration provides optimal ξ and β coefficients respectively equal to 0.08 and 9. The authors will show in the next sensitivity analysis that even a one-digit approximation of the ξ and β coefficients provides a stable discharge estimation.

3.5 Sensitivity analysis

We carried out a discharge sensitivity analysis of both new methods using the computed $\xi = 0.08$ and $\beta=9$ optimal values and the data of the F2 and K4 series. Sensitivities were normalized in the following form:

$$I_s = \frac{1}{q_{INCM}} \frac{\Delta q}{\Delta \xi} \qquad (3.20),$$

$$L_s = \frac{1}{q_{LHRM}} \frac{\Delta q}{\Delta \beta} \qquad (3.21),$$

where Δq is the difference between the discharges computed using two different β and ξ values. The assumed perturbations"$\Delta\beta$" and "$\Delta\xi$" are respectively $\Delta\beta = 0.001\ \beta$, $\Delta\xi = 0.001\ \xi$.

The results of this analysis are shown in Table 3.2a for the F2 series, where H is the water depth and Q_{meas} the corresponding measured discharge. They show very low sensitivity of both the *INCM* and *LHRM* results, such that a one digit approximation of both model parameters (ξ and β) should guarantee a computed discharge variability of less than 2%.

The results of the sensitivity analysis, carried out for series K4 and shown in Table 3.2b, are similar to the previous ones computed for F2 series.

Table 3.2a. Sensitivities I_s and L_s computed in the F2 series for the optimal parameter values.

H [m]	$Q_{meas}[m^3s^{-1}]$	I_s	L_s
0.156	0.212	0.2209	0.2402
0.169	0.248	0.1817	0.2194
0.178	0.282	0.1651	0.2044
0.187	0.324	0.1506	0.1777
0.198	0.383	0.1441	0.1584
0.214	0.48	0.1305	0.1336
0.249	0.763	0.1267	0.132

Table 3.2b. Sensitivities I_s and L_s computed in the K4 series for the optimal parameter values.

H [m]	$Q_{meas}[m^3s^{-1}]$	I_s	L_s
0.085	0.005	0.3248	0.3282
0.096	0.008	0.2052	0.225
0.102	0.009	0.1600	0.1709
0.114	0.014	0.1354	0.1372
0.127	0.018	0.1174	0.1208
0.154	0.029	0.0851	0.0866

3.6 Validation criterion

3.6.1 Validation n.1 - Comparison with laboratory experimental data

A first validation of the two methods was carried out by using the calibrated parameter values, the same Nash-Sutcliffe performance measure and all the available experimental series. The results were also compared with results of *DCM* and *IDCM* methods, the latter applied using the suggested α = 0.02 value and five subsections, each one corresponding to a different bottom slope in the lateral *y* direction. The NS index for all data series is shown in Table 3.3.

Table 3.3. Nash-Sutcliffe Efficiency for all (calibration and validation) experimental series.

	Series	***DCM***	***IDCM***	***INCM***	***LHRM***
Calibration Set	*F1*	0.743	0.9807	0.9847	0.9999
	F2	0.618	0.9923	0.9955	0.9965
	F3	0.722	0.9744	0.9261	0.9915
	F6	0.737	0.9733	0.9888	0.9955
Validation Set	*F8*	-0.08	0.9881	0.9885	0.9964
	F10	-0.09	0.9965	0.9975	0.9978
	K1	-14.5	-0.701	-8.294	0.9968
	K2	-0.98	0.3452	-1.835	0.9619
	K3	0.176	0.6479	-0.394	0.979
	K4	0.288	0.888	0.3548	0.9958

The *DCM* results are always worse and are particularly bad for all the K series. The results of both the *IDCM* and *INCM* methods are very good for the two F series not used for calibration, but are both poor for the K series. The *LHRM* method is always the best and also performs very well in the K series. The reason is probably that the K series tests have very low discharges, and the constant $\alpha = 0.02$, the coefficient adopted in the *IDCM* method, does not fit the size of the subsections and Eq. (3.13) is not a good approximation of the mixing length α_H in Eq. (3.12) for low values of the water depth. In Figs. 3a and 3b the NS curves obtained by using *DCM*, *IDCM*, *INCM* and *LHRM*, for series F2 and K4, are shown.

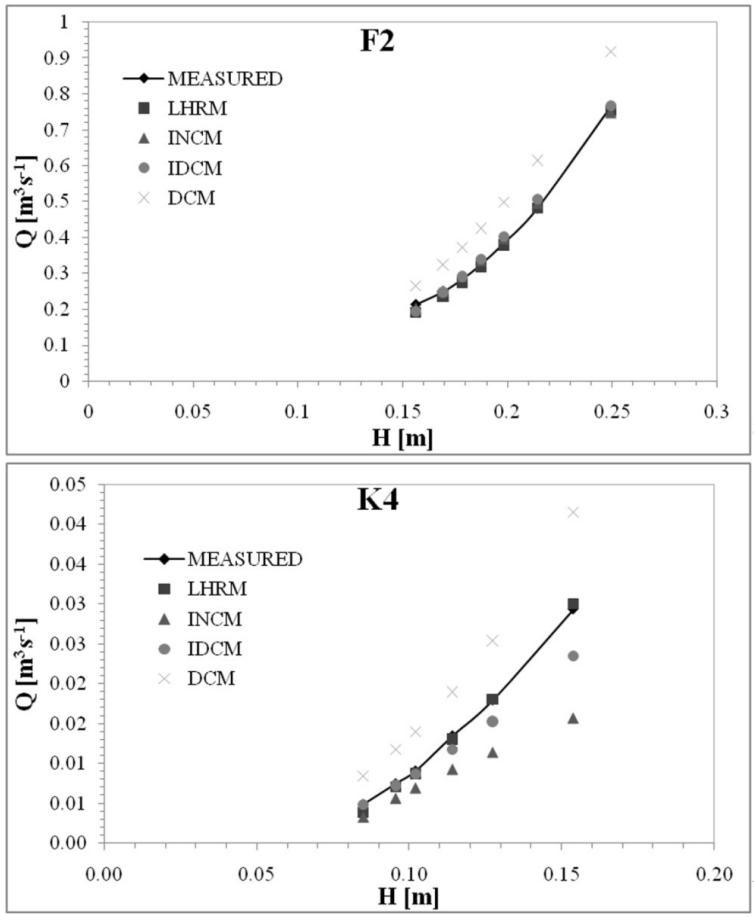

Figure 3.3. Estimated discharge values against HR Wallingford FCF measures for F2 (a) and K4 (b) series.

3.6.2 Validation n.2 - Comparison with field data

Although rating curves are available in different river sites around the world, field validation of the uniform flow formulas is not easy, for at least two reasons:

1) The average friction factor f and the related Manning's coefficient are not known as in the lab case and the results of all the formulas need to be scaled according to the Manning's coefficient to be compared with the actually measured discharges;

2) River bed roughness does change, along with the Manning's coefficient, from one water stage to another (it usually increases along with the water level).

A possible way to circumvent the problem is to apply the compared methods in the context of a calibration problem, where both the average Manning's coefficient and the discharge hydrograph are computed from the known level hydrographs measured in two different river cross sections (Perumal et al., 2007; Aricò et al., 2009). The authors solved the diffusive wave simulation problem using one known level hydrograph as the upstream boundary condition and the second one as the benchmark downstream hydrograph for the Manning's coefficient calibration.

It is well-known in the parameter estimation theory (Aster et al., 2012) that the uncertainty of the estimated parameters (in our case the roughness coefficient) grows quickly with the number of parameters, even if the matching between the measured and the estimated model variables (in our case the water stages in the downstream section) improves. The use of only one single parameter over all the computational domain is motivated

by the need of getting a robust estimation of the Manning's coefficient and of the corresponding discharge hydrograph.

Although the accuracy of the results is restricted by several modeling assumptions, a positive indication about the robustness of the simulation model (and the embedded relationship between the water depth and the uniform flow discharge) is given by: 1) the match between the computed and the measured discharges in the upstream section, 2) the compatibility of the estimated average Manning's coefficient with the site environment.

The area of interest is located in the Alzette River basin (Gran-Duchy of Luxembourg) between the gauged sections of Pfaffenthal and Lintgen (Fig. 3.4).

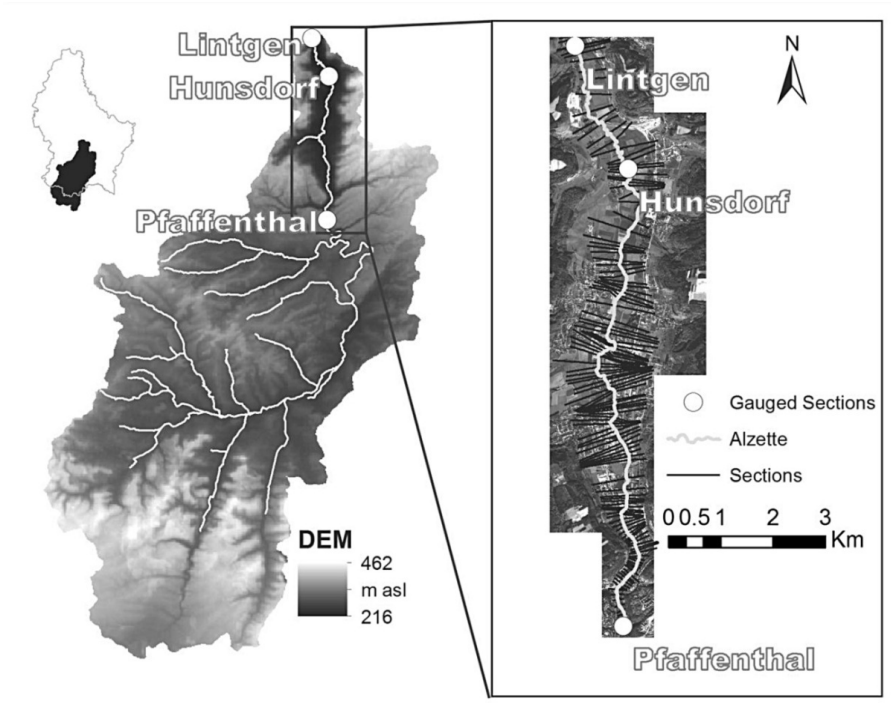

Figure 3.4. The Alzette Study Area.

The river reach length is about 19 km, with a mean channel width of ~30 m and an average depth of ~4 m. The river meanders in a relatively large and flat plain about 300 m, with a mean slope of ~0.08%.

The methodology was applied to a river reach 13 Km long, between two instrumented sections, Pfaffenthal (upstream section) and Hunsdorf (downstream section), in order to have no significant lateral inflow between the two sections.

Events of January 2003, January 2007 and January 2011 were analysed. For these events, stage records and reliable rating curves are available at the two gauging stations of Pfaffenthal and Hunsdorf. The main hydraulic characteristics of these events, that is duration (Δt), peak water depth (H_{peak}) and peak discharge (q_{peak}), are shown in Table 3.4.

Table 3.4. Main characteristics of the flood events at the Pfaffenthal and Hunsdorf gauged sites.

Event	Δt [h]	Pfaffenthal		Hunsdorf	
		H_{peak} [m]	q_{peak} [m^3s^{-1}]	H_{peak} [m]	Q_{peak} [m^3s^{-1}]
January 2003	380	3.42	70.98	4.52	67.8
January 2007	140	2.9	53.68	4.06	57.17
January 2011	336	3.81	84.85	4.84	75.1

In this area a topographical survey of 125 river cross sections was available. The hydrometric data were recorded every 15 min. The performances of the discharge estimation procedures were compared by means of the Nash Suctliffe criterion.

The results of the *INCM* and *LHRM* methods were also compared with those of the *DCM* and *IDCM* methods, the latter applied by using α =

0.02 and an average subsection width equal to 7 m. The computed average Manning's coefficients n_{opt}, reported in Table 3.5, are all consistent with the site environment, although they attain very large values, according to *DCM* an *IDCM*, in the 2011 event.

Table 3.5. Optimum roughness coefficient, n_{opt}, for the three flood events.

Event	***DCM*** n_{opt} [$sm^{-1/3}$]	***IDCM*** n_{opt} [$sm^{-1/3}$]	***INCM*** n_{opt} [$sm^{-1/3}$]	***LHRM*** n_{opt} [$sm^{-1/3}$]
January 2003	0.054	0.047	0.045	0.045
January 2007	0.051	0.047	0.046	0.045
January 2011	0.07	0.07	0.057	0.055

The estimated and observed dimensionless water stages in the Hunsdorf gauged site, for 2003, 2007 and 2011 events are shown in Figs. 3.5-3.7.

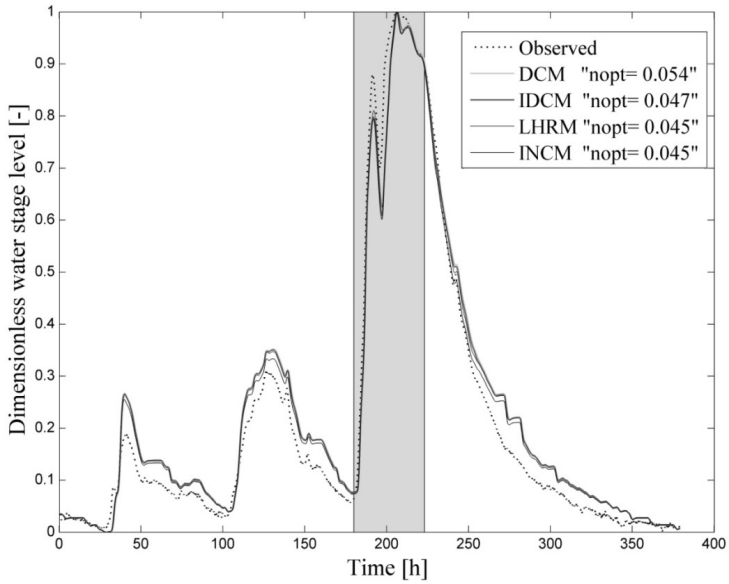

Figure 3.5. Observed and simulated stage hydrographs at Hunsdorf gauged site in the event of January 2003.

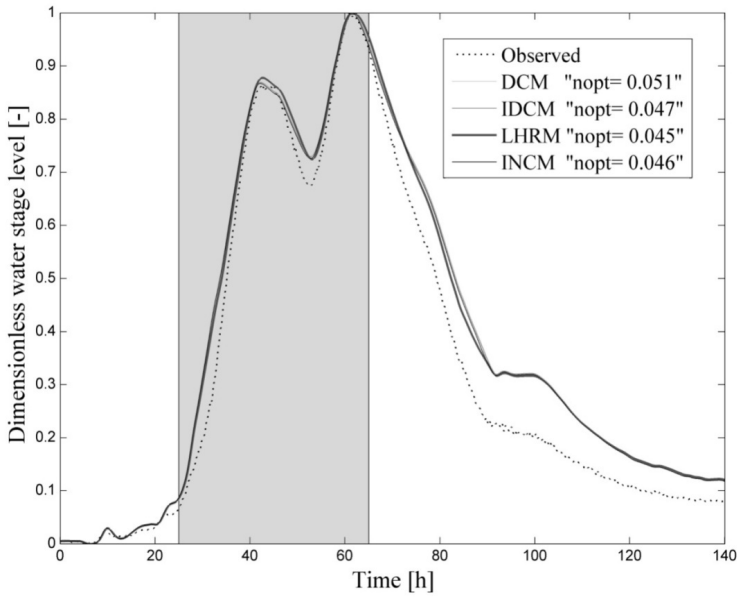

Figure 3.6. Observed and simulated stage hydrographs at Hunsdorf gauged site in the event of January 2007.

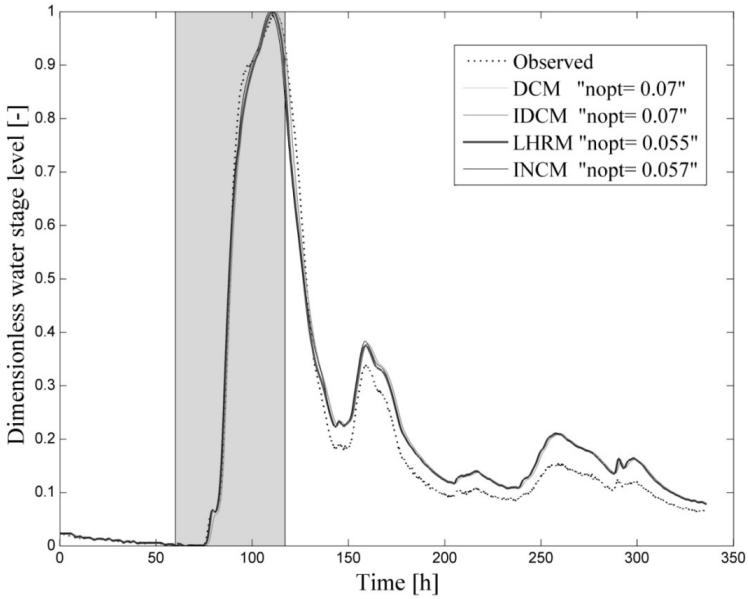

Figure 3.7. Observed and simulated stage hydrographs at Hunsdorf gauged site in the event of January 2011.

Only the steepest part of the rising limb, located inside the colored window of each Figure, was used for calibration. The falling limb is not included, since it has a lower slope and is less sensitive to the Manning's coefficient value.

A good match between recorded and simulated discharge hydrographs can be observed (Figs. 3.8-3.10) in the upstream gauged site for each event.

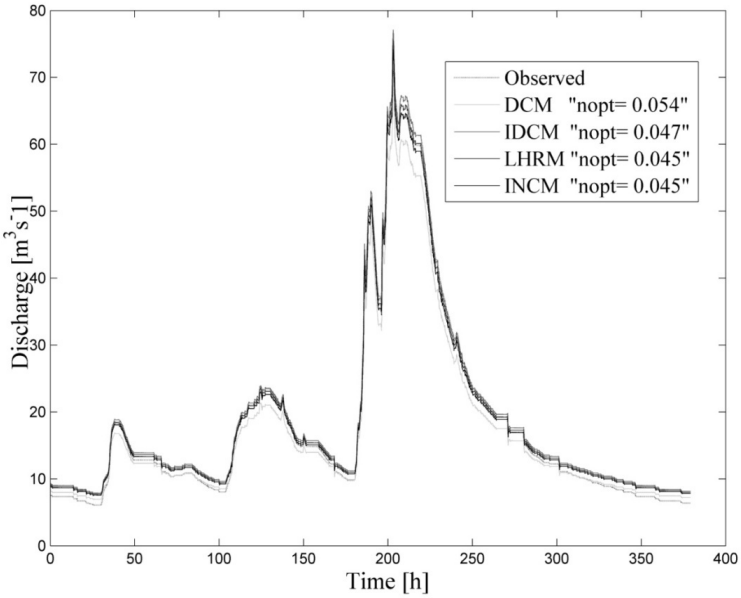

Figure 3.8. Observed and simulated discharge hydrographs at Pfaffenthal gauged site in the event of January 2003.

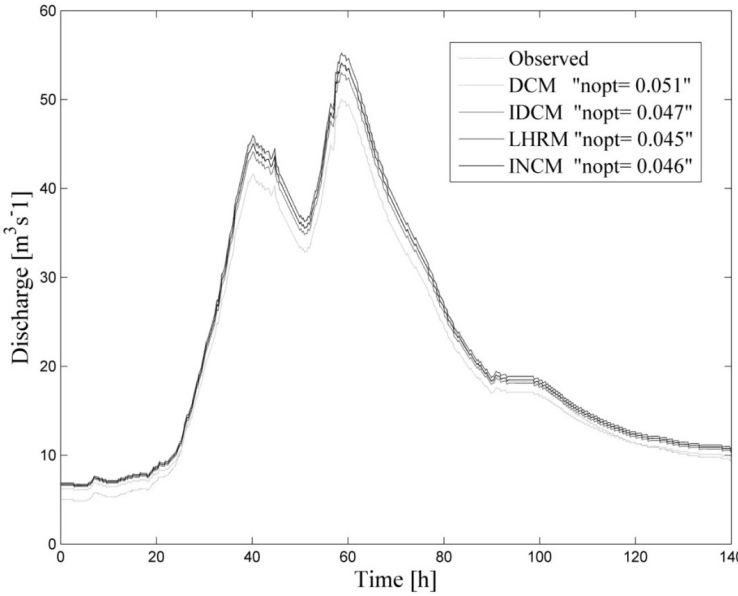

Figure 3.9. Observed and simulated discharge hydrographs at Pfaffenthal gauged site in the event of January 2007.

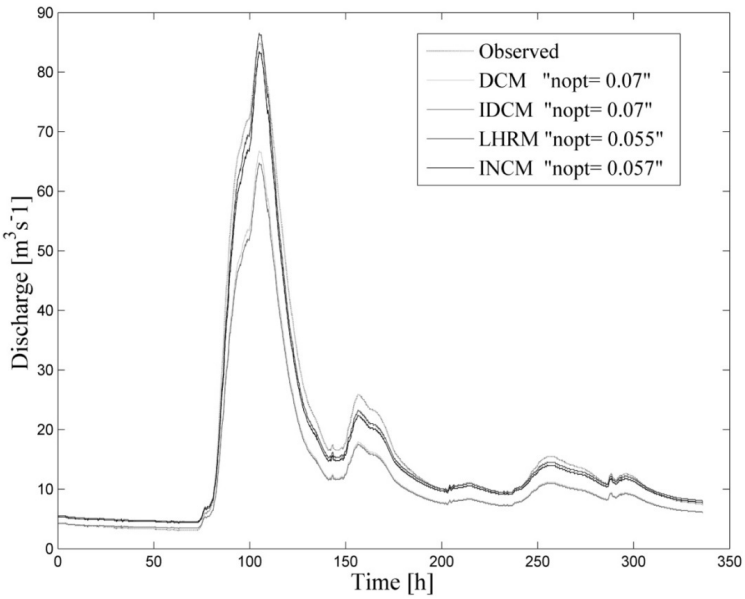

Figure 3.10. Observed and simulated discharge hydrographs at Pfaffenthal gauged site in the event of January 2011.

For all investigated events the Nash Sutcliffe efficiency NS_q is greater than 0.90, as shown in Table 3.6.

Table 3.6. Nash-Sutcliffe efficiency of estimated discharge hydrographs for the analysed flood events.

Event	***DCM*** NS_q **[-]**	***IDCM*** NS_q **[-]**	***INCM*** NS_q **[-]**	***LHRM*** NS_q **[-]**
January 2003	0.977	0.987	0.991	0.989
January 2007	0.983	0.988	0.989	0.992
January 2011	0.898	0.899	0.927	0.93

The error obtained between measured and computed discharges, with all methods, is of the same order of the discharge measurement error. Moreover, this measurement error is well known to be much larger around the peak flow, where the estimation error has a larger impact on the NS coefficient. The NS coefficients computed with the *LHRM* and *INCM* methods are anyway a little better than the other two.

3.6.3 Validation n.3 - Comparison with results of 3D ANSYS CFX solver

The vertically averaged velocities computed using *DCM*, *IDCM*, *INCM* and *LHRM* were compared with the results of the well known ANSYS 3D code, named CFX, which solve the Reynolds-average Navier Stokes (RANS) equations, applied to a prismatic reach with the irregular cross-section measured at the Hunsdorf gauged section of the Alzette river. The length of the reach is about four times the top width of the section.

In the homogeneous multiphase model adopted by CFX, water and air are assumed to share the same dynamic fields of pressure, velocity and turbulence and water is assumed to be incompressible. CFX solves the conservation of mass and momentum equations, coupled with the air pressure-density relationship and the global continuity equation in each node. Call α_l, ρ_l, μ_l and $\mathbf{U}_l$ respectively the volume fraction, the density, the viscosity and the time averaged value of the velocity vector for phase l ($l = w$ (water), a (air)), that is:

$$\rho = \sum_{l=w,a} \alpha_l \rho_l \qquad (3.22a),$$

$$\mu = \sum_{l=w,a} \alpha_l \mu_l \tag{3.22b},$$

where ρ and μ are the density and the viscosity of the "averaged" phase. The air density is assumed to be a function of the pressure p, according to the state equation:

$$\rho_a = \rho_{a,0} e^{\gamma(p-p_o)} \tag{3.22c},$$

where the sub-index 0 marks the reference state values and γ is the air compressibility coefficient.

The governing equations are the following: 1) the mass conservation equation, 2) the Reynolds averaged continuity equation of each phase and 3) the Reynolds averaged momentum equations. Mass conservation implies:

$$\sum_{l=w,a} \alpha_l = 1 \tag{3.23}.$$

The Reynolds averaged continuity equation of each phase l can be written as:

$$\frac{\partial \rho_l}{\partial t} + \nabla \cdot (\rho_l \mathbf{U}) = S_l \tag{3.24},$$

where S_l is an external source term. The momentum equation instead refers to the "averaged" phase and is written as:

$$\frac{\partial (\rho \mathbf{U})}{\partial t} + \nabla \cdot (\rho \mathbf{U} \otimes \mathbf{U}) - \nabla \cdot \left(\mu_{eff} \left(\nabla \mathbf{U} + (\nabla \mathbf{U})^T \right) \right) + \nabla p' = S_M \tag{3.25},$$

where $\otimes$ is the dyadic symbol, S_M is the momentum of the external source term S, and μ_{eff} is the effective viscosity accounting for turbulence and defined as:

$$\mu_{eff} = \mu + \mu_t \tag{3.26}$$

where μ_t is the turbulence viscosity and p' is the modified pressure, equal to:

$$p' = p + \frac{2}{3}\rho k + \frac{2}{3}\mu_{eff}\nabla \cdot \mathbf{U} \tag{3.27}$$

where k is the turbulence kinetic energy, defined as the variance of the velocity fluctuations and p is the pressure. Both phases share the same pressure p and the same velocity $\mathbf{U}$.

To close the set of six scalar equations (Eq.3.23, Eq.324 (two) and Eq.3.25 (three)), we finally apply the k-ε turbulence model implemented in the CFX solver. The implemented turbulence model is a two equation model, including two extra transport equations to represent the turbulent properties of the flow.

Two-equation models account for history effects like convection and diffusion of turbulent energy. The first transported variable is turbulent kinetic energy, k; the second transported variable is the turbulent dissipation, ε. The K-epsilon model has been shown (Jones, 1972; Launder, 1974) to be useful for free-shear layer flows with relatively small pressure gradients. Similarly, for wall-bounded and internal flows, the model gives good results, but only in cases where the mean pressure gradients are small.

The computational domain was divided using both tetrahedral and prismatic elements (Fig. 3.11).

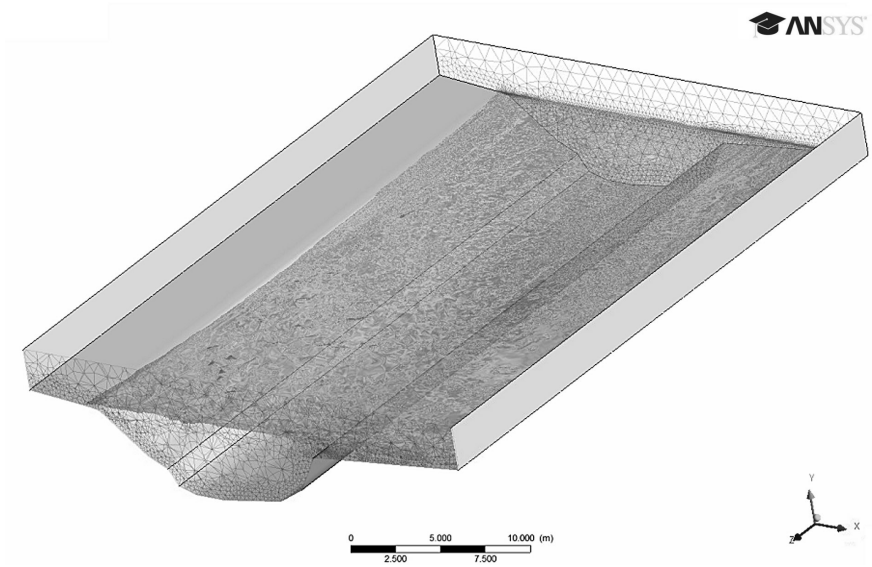

Figure 3.11. Computational domain of the reach of the Alzette river.

The prismatic elements were used to discretize the computational domain in the near-wall region over the river bottom and the boundary surfaces, where a boundary layer is present, while the tetrahedral elements were used to discretize the remaining domain. The number of elements and nodes, in the mesh used for the specific case are of the order respectively $4*10^6$ and $20*10^6$.

A section of the mesh is shown in Fig.3.12.

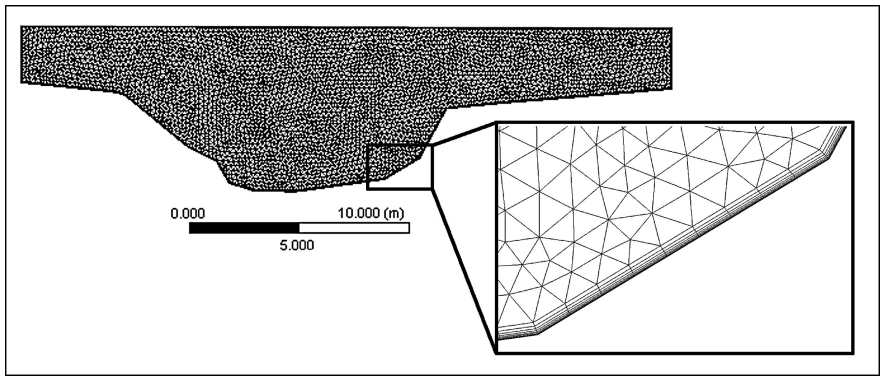

Figure 3.12. A mesh section along the inlet surface.

The quality of the mesh was verified by using a pre-processing procedure by ANSYS® ICEM CFD™ (Ansys inc., 2006).

The six unknowns in each node are the pressure, the velocity components, and the volume fractions of the two phases. At each boundary node three of the first four unknowns have to be specified. In the inlet section a constant velocity, normal to the section, is applied, and the pressure is left unknown. In the outlet section the hydrostatic distribution is given, the velocity is assumed to be still normal to the section and its norm is left unknown. All boundary conditions are reported in Table 3.7.

Table 3.7. Boundary conditions assigned in the CFX simulation.

Geometry Face	Boundary Condition
Inlet	All velocity components
Outlet	Velocity direction and hydrostatic pressure distribution
Side-Walls	Opening
Top	Opening
Bottom	No-slip wall condition, with roughness given by equivalent granular size d_{50}.

The opening condition means that that velocity direction is set normal to the surface, but its norm is left unknown and a negative (entering) flux of both air and water is allowed. Along open boundaries the water volume fraction is set equal to zero. The solution of the problem converges towards two extremes: nodes with zero water fraction, above the water level, and nodes with zero air fraction below the water level.

On the bottom boundary, between the nodes with zero velocity and the turbulent flow a boundary layer exists that would require the modelling of micro scale irregularities. CFX allows the use, inside the boundary layer, of a velocity logarithmic law, according to an equivalent granular size. The relationship between the granular size and the Manning's coefficient, according to Yen (1994), is given by:

$$d_{50} = \left(\frac{n}{0.0474}\right)^6 \qquad (3.28),$$

where d_{50} is the average granular size to be given as the input in the CFX code.

Observe that the assumption of known and constant velocity directions in the inlet and outlet section is a simplification of reality. A more appropriate boundary condition at the outlet section, not available in the CFX code, would have been given by zero velocity and turbulence gradients (Rameshwaran et al. 2013). For this reason, a better reconstruction of the velocity field can be found in an intermediate section, where secondary currents with velocity components normal to the mean flow direction can be easily detected (Peters and Goldberg, 1989; Richardson and Colin, 1996). See in Fig. 3.13 how the intermediate section was divided to compute the vertically averaged velocities in each segment section.

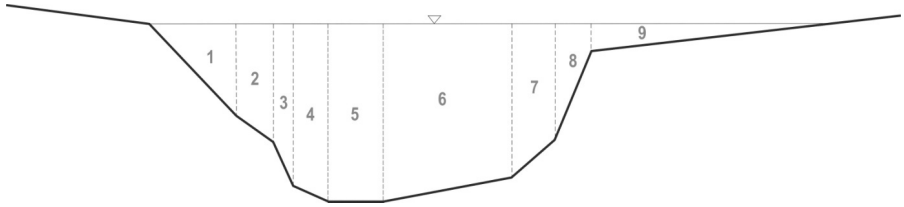

Figure 3.13. Hunsdorf river cross-section: subsections used to compute the vertically averaged velocities.

These 3D numerical simulations confirm that the momentum Γ, proportional to the derivative of the average tangent velocities and equivalent to the left hand side of Eq. 3.2, cannot be set equal to zero, if a rigorous reconstruction of the velocity field is sought after.

To compute the uniform flow discharge, for a given outlet section, CFX code is run iteratively, each time with a different average longitudinal velocity in the inlet section, until the same water depth as in

the outlet section is attained in the inlet section for steady state conditions.Using the velocity distribution computed in the middle section along the steady state computation as upstream boundary condition, transient analysis is carried on until pressure and velocity oscillations become periodic.

In order to test the achievement of the fully developed state within the first half of the modeled length the authors plotted the vertical profiles of the streamwise velocity components for ten verticals, equally spaced along the longitudinal axis of the main channel. See in Fig.3.14 the plot of four of them and their location.

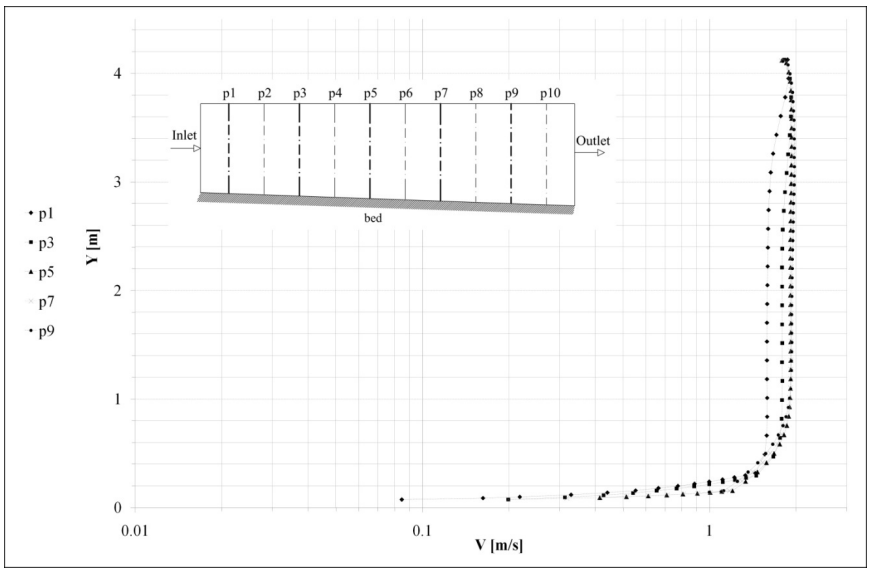

Figure 3.14. Streamwise vertical profile along the longitudinal axis of the mean channel.

The streamwise velocity evolves longitudinally and becomes almost completely self similar starting from the vertical line in the middle section. Stability of the results has been finally checked against the variation of the length of the simulated channel. The dimensionless sensitivity of the discharge with respect to the channel length is equal to 0.2%.

See in Table 3.8 the comparison between the vertically averaged state velocities, computed through the *DCM*, *IDCM*, *INCM*, *LHRM* formulas (u_{DCM}, u_{IDCM}, u_{INCM}, u_{LHRM}) and through the CFX code (u_{CFX}).

Table 3.8. Simulated mean velocities in each segment section using 1D hydraulic models with *DCM*, *IDCM*, *INCM*, *LHRM* and *CFX*, and corresponding differences.

Subsection	u_{CFX} [ms^{-1}]	u_{DCM} [ms^{-1}]	u_{IDCM} [ms^{-1}]	u_{INCM} [ms^{-1}]	u_{LHRM} [ms-1]	Δu_{DCM} [%]	Δu_{IDCM} [%]	Δu_{INCM} [%]	Δu_{LHRM} [%]
1	1.33	1.58	1.47	1.23	1.12	18.79	10.52	-7.52	-15.78
2	1.37	1.42	1.4	1.36	1.38	3.65	2.19	-0.73	0.73
3	1.38	1.53	1.48	1.38	1.4	10.87	7.25	0	1.45
4	1.47	1.64	1.6	1.56	1.57	11.56	8.84	6.13	6.8
5	1.53	1.94	1.8	1.59	1.61	26.79	17.65	3.92	5.23
6	1.57	2.01	1.81	1.6	1.68	28.02	15.29	1.91	7
7	1.46	1.66	1.65	1.49	1.5	13.69	13.01	2.05	2.74
8	1.42	1.48	1.46	1.44	1.43	4.22	2.82	1.4	0.7
9	0.88	0.91	0.9	0.7	0.69	3.4	2.27	-20.45	-21.59

Table 3.8 also shows the relative difference, Δu, evaluated as:

$$\Delta u = \frac{u - u_{CFX}}{u_{CFX}} \times 100 \qquad (3.29).$$

As shown in Table 8, both *INCM* and *LHRM* perform very well in this validation test instead of *DCM*, which clearly overestimates averaged velocities. In the central area of the section the averaged velocities calculated by the *INCM*, *LHRM* and CFX code are quite close with a maximum difference ~7%. By contrast, larger differences are evident close to the river bank, in segments 1 and 9, where *INCM* and *LHRM* underestimate the CFX values. These larger differences show the limit of using a 1D code. Close to the bank the wall resistance is stronger and the velocity field is more sensitive to the turbulent exchange of energy with the central area of the section, where higher kinetic energy occurs.

CHAPTER IV

RIVER FLOW ASSESSMENT THROUGH REVERSE ROUTING MODELING WITH SIGNIFICANT LATERAL INFLOW

4.1 Introduction

The knowledge of river discharge is fundamental for water resources management, water balance evaluation at basin scale, flood design as well as for the calibration and validation of hydrological/hydraulic models. Reliable discharge estimation depends on local hydraulic conditions which are usually defined by recording the water level at hydrometric river sites and then filtering this measure through a rating curve [Herschy, 1999]. To this end, it is required that the river section is equipped with hydrometric sensors for stage measurements, and cableway to carry out velocity measurements by current meter. Overall, the gauge site provides reliable stage observations that, however, may be not sufficient to getting a reliable rating curve if velocity measurements for high flow are not available [Moramarco et al., 2004]. Because of the difficulty to carry out these measurements, at a river site hydraulic information are often absent or limited to low flow. In addition, if unsteady effects are present during a flood, the rating curve, which is a kinematic relationship, is not able to represent the dynamic of flood

anymore and a hysteresis loop occurs [Cunge et al., 1980], whose amplitude depends on how much the inertial and pressure forces influence the flood propagation [Moramarco et al., 2008].

Considering that the conventional techniques of river flow measurements are costly and may be dangerous during high flood events, some routing methods were proposed for the development of the normal rating curves at the two ends of a channel reach, starting from the stages recorded there [e.g. Perumal et al., 2007; Aricò et al., 2009]. However, in the proposed methods the contribution of the intermediate basin subtended by the channel is assumed as negligible. When this condition fails, river discharge may change hydraulic characteristics along the reach mainly due to the lateral contributions of mass. These aspects were investigated by Moramarco et al. [2005a] who developed a simple model named "Rating Curve Model" (*RCM*), refined afterwards by Barbetta et al. [2012], to estimate discharge at a site by relating local stage and hydraulic information recorded at upstream/downstream site, regardless the intermediate basin area. *RCM* is based on three hypotheses: 1) the wave celerity is constant, 2) kinematic approximation holds and 3) the lateral inflow is homogeneous along the reach. Moreover, the model requires that the discharge hydrograph has to be known at one of the channel ends at least.

To circumvent the case of only stages recorded at channel ends with large lateral flow contributions, the estimate of discharge hydrograph can be addressed by two different ways. The first consists to couple hydrologic and hydraulic models [Moramarco et al., 2005b]. In this case, information in terms of rainfall and topographical data of channels are needed and one of the main issues that makes the methodology

particularly poor is the difficulty to represent the rainfall spatial distribution through the available monitoring network [Tarpanelli et al., 2012]. The second way, useful if rainfall data are not available or inconsistent for the rainfall field, is known as the "reverse routing process" able to determine an upstream/downstream discharge hydrograph based upon the knowledge of downstream/upstream stage hydrograph only and the hydraulics characteristics of the river reach [D'Oria et al., 2012; D'Oria et al., 2014]. Das [2010] employed linear and nonlinear Muskingum method for reverse flow routing stressing on the fact that there is a need for separate calibration of Muskingum methods. D'Oria et al. [2012] applied a Bayesian Geostatistical Approach (*BGA*) to evaluate unknown upstream flow hydrographs in multiple reach systems starting from stages recorded at downstream end. In this case, *BGA* is (tightly) coupled with the hydraulic model in which, however, the hydraulic roughness is assumed known [D'Oria et al., 2014], thus driving the assessment of discharge hydrograph. Moreover, the procedure requires hydraulic modelling of the entire river network, including the main channel tributaries. Recently, Zucco et al. [2015] developed a flood reverse routing model based on the continuity equation and Rating Curve Model where parameters are estimated by using a complex genetic algorithm.

Based on the above issues, this work aims to show that using the only information coming from the stage hydrographs recorded at channel ends with a large intermediate basins, it is usually possible to derive the discharge hydrograph in all the river sections downstream of the upstream one, without needing information in terms of rainfall data. To this end, the MAST hydraulic model [Aricò and Tucciarelli, 2007] is used and the

lateral inflow between the hydraulic model boundary sites is assumed concentrated in a small number of confluences where discharge hydrographs are estimated as well. Equipped river reaches along the Tiber River, central Italy, and along the Alzette River, in Luxembourg, are used to test the procedure.

The next chapter r is organized as follows: Section 4.2 provides an overview of the theoretical background of the reverse routing process, when only stage measurements are available at the two ends of the monitored channel. In Section 4.3, the lateral inflow assessment is addressed, while in section 4.4 the same problem is solved when consistent lateral inflow is present along the channel using the MAST hydraulic model, applied assuming upstream water level boundary condition along with head driven lateral inflows at intermediate sections. In Section 4.5, calibration and validation performance criteria of the proposed model will be discussed. Section 4.6 is dedicated to the description of the selected case studies and dataset. Section 4.7 contains the analysis of the results obtained through the application of the proposed approach, while final remarks on its potential usefulness are laid down inthe conclusions of this thesis.

4.2 Reverse routing process: indirect discharge estimation by means of unsteady-state water level data analysis

The Saint–Venant (SV) equations are commonly applied for the simulation of unsteady shallow water flows. The one-dimensional (1D) SV equations can be written in the following form for a non-prismatic river channel:

$$\frac{\partial A}{\partial t} + \frac{\partial q}{\partial x} = p \tag{4.1},$$

$$\frac{\partial q}{\partial t} + \frac{\partial (q^2 / A)}{\partial x} + gA\frac{\partial h}{\partial x} + gA(S_f - S_0) = 0 \tag{4.2},$$

where q is the discharge, A is the cross-section area, h is the water depth, p is the lateral inflow per unit length (assumed normal to the flow direction), S_0 is the bottom bed slope and S_f is the friction slope. Friction slope is estimated according to the uniform flow formulas, that is:

$$S_f = \frac{q^2}{Q^2(h)} \tag{4.3},$$

where $Q(h)$ is the specific discharge in the main river (also called conveyance), estimated according to uniform-flow condition and unit bottom slope. The relationship linking the water depth h to the specific discharge Q is function of one or more parameters, according to the chosen empirical or semi-empirical law. The most popular relationship is the Manning formula [Herschel, 1897], corrected according to Huthoff et al. [2008] or other researchers [Spada et al., 2015].

It is well known that when a natural runoff process occurs along rivers the gravity force component in Eq. (4.2) largely exceeds the inertia force that, therefore, can be neglected leading to the diffusive approach. According to this assumption, Eq. (4.2) reduces to the following relationship:

$$\frac{\partial(h+z)}{\partial x} = -\frac{q^2}{Q^2(h)} \tag{4.4},$$

where derivative of z is the opposite of S_0 (i.e., $S_0 = -\partial z / \partial x$) and the argument inside brackets is the water level $H=(h+z)$. The choice of neglecting inertial terms in Eq. (2) improves quite a lot the robustness of the solution with respect to the input topographic error, as shown in Aricò et al. [2011]. Merging Eq. (4) and Eq. (1), it is possible to get a single second order equation in the H unknown, that is:

$$\frac{\partial H}{\partial t} - \frac{1}{B}\frac{\partial}{\partial x}\left(Q(h)\frac{\partial H}{\partial x}\left|\frac{\partial H}{\partial x}\right|^{-1/2}\right) = p \tag{4.5},$$

where B is the cross section width. A side effect of neglecting the inertial terms in Eq. (4.2) is that the resulting Eq. (4.5) is a nonlinear diffusive equation, where the proper boundary conditions do not depend on the specific Froude number occurring at the two ends of the computational domain. Eq. (4.5) is usually solved for flow routing by setting a known discharge at the upstream boundary and a known water level at the downstream boundary. However, when the upstream discharge hydrograph is unknown, the solution can be obtained by setting the known stage hydrograph as upstream boundary condition and the

upstream discharges are computed as solution of the flow routing problem.

Observe that, by setting the measured stage hydrographs as boundary condition (BC) in both the initial and final sections, it is possible to associate a different discharge upstream hydrograph to any assigned Manning coefficient, even if the shape in space (not in time) of the wave around the downstream boundary section strongly depends on the selected parameter. This probably explains the difficulty of calibrating the Manning coefficient starting from a blind set of water level data, because of the non-uniqueness of the so posed inverse problem. On the other hand, Aricò et al. [2007] and Corato et al. [2011] have shown that the downstream BC has a weak effect on the solution of the flow routing problem in any section since a short distance from the end of the channel. On the opposite, the same solution is strongly affected by the assigned Manning coefficient and by the upstream stage hydrograph. This implies that it is much better, for calibration, to set the river model downstream boundary at a short distance after the downstream gauged section, to approximate somehow the corresponding BC and to use the information contained in the measured downstream stage hydrograph for the calibration of the Manning coefficient. On the basis of this observation, the following strategy is proposed: 1) the computational domain is extended of about $L/3$ after the second gauged section, where L is the distance between the two gauged sections; 2) an approximated boundary condition is assigned to the final section of the computational domain, usually the zero diffusion condition corresponding to zero second order water level spatial derivatives; 3) the Manning coefficient n is selected in order to optimize a similarity criterion between the measured and the

computed water level hydrograph at the downstream gauged section. Water stage solution of the diffusive problem, for given n parameter value, is obtained by applying the MAST numerical solver [Aricò and Tucciarelli, 2007].

The previously described procedure is particularly efficient for the estimation of the peak flow, when extrapolation beyond the actually measured points is needed for the use of rating curves and direct measurements are difficult.

4.3 Lateral inflow estimation

The main limit of the previously described methodology is the assumption of lateral inflows known along the reach bounded by the upstream and the downstream gauged sections. Because the distance between the two gauged sections must be long enough to appreciate the travel time between the two recorded waves, it is very common that lateral contribution due to confluences with tributaries affect the flood formation process along the main channel. If a large number of gauged sections were available along the tributaries and the main channel, it would possible, in principle, to model the entire river network dealing with a more general reverse flow calibration problem. If this is not the case, we shall show in the following that, using as input data only the stage hydrographs measured at the two gauged sections, as well as the tributary bathymetry of the river reach and of each confluence, it is possible to derive the discharge hydrograph at all the reach river sections.

To this end, assume the lateral inflow to be concentrated in a small number of confluences. Call I_1, I_2,…, I_N the corresponding sections along

the main river. Assume to know the topography of the final section T_j of each tributary channel *j*, ending in the confluence section I_j. Finally, assume a one to one relationship between the water depth and the discharge to hold in section T_j and the kinetic energy dissipated at the confluence to be negligible with respect to the water depths of both the main and the tributary channels.

According to the previous hypothesis, as well as to the diffusive approximation in the momentum equations of the tributary channel, discharge of the jth tributary channel at the inlet section, Q_j^T, can be written as:

$$Q_j^T = Q_j^S(H_j)\sqrt{S_j} \tag{4.6},$$

where $Q_j^S(H_j)$ is the corresponding specific discharge, function of the water level inside brackets, computed per unit energy gradient, according to any selected stage – discharge relationship; H_j is the water level common to the main channel section I_j and to the tributary channel section T_j. It is worth noting that the hypothesis of constant water level at the confluence for both the tributary and the main channel is strictly related to the diffusive hypothesis holding also in the main channel. If kinetic energy gradients in both the main and the tributary channels were consistent with respect to the other terms of the momentum equations, this assumption would fail. Eq. (4.6) can be re-written as:

$$Q_j^T = Q_j^K(H_j)K_j \tag{4.7},$$

where $Q_j^K(H_j)$ is equal to the specific discharge Q_j^S, computed assuming unit roughness, is called normalized discharge and K_j (said conveyance)

can be considered as a calibration parameter accounting for both the energy slope, S_j, and the Manning roughness along the tributary. If linearity occurs between the inverse of the average Manning coefficient and the specific discharge, parameter K_j will be a constant. We assume the energy slope to remain constant in time along with the K_j parameter. Clearly, this is an approximation because a backwater effect may likely occur along the tributary during flood, especially if the discharge increase is much higher in one of the two channels (tributary or main river). A constant conveyance K_j is equivalent to a kinematic relationship between water depths and discharges, different from each event to the other ones.

Discharge in the left-hand side of Eq. (4.7) can be thought as the integral of the lateral inflow p in the right-hand side of Eq. (4.5), close to the confluence section, and, hence, Eq. (4.5) can be written as:

$$\frac{\partial H}{\partial t} - \frac{1}{B}\frac{\partial}{\partial x}\left(Q(h)\frac{\partial H}{\partial x}\left|\frac{\partial H}{\partial x}\right|^{-1/2}\right) = \sum_{j=1,M}\int Q_j^K\left(H_j\right)K_j\delta\left(x - x_j\right)dx \qquad (4.8),$$

where M is the number of tributaries, $\delta(x)$ is the Dirac Delta function and the integral is extended over all the 1D computational domain.

4.4 Embedding the tributary flow in the MAST hydraulic model

The MAST hydraulic model [Aricò et al., 2007] splits the solution of the Saint Venant equations along the main channel, for each time step Δt, in two iterations. In the first iteration, a prediction convective problem is solved, where the piezometric gradients are kept constant in time and equal to the values computed at the end of the previous time step. In the second iteration, a corrective diffusive problem is solved. All the forcing functions are discretized in each computational cell of the numerical model only in the prediction problem. Solution of Eq. (4.5) at cell *i* in the prediction problem is given by integration along Δt of the following equation in the H_j unknown, carried out using Runge-Kutta methods with self-adapting time sub-steps:

$$\frac{\partial H_j}{\partial t} A_j(h_j) = \overline{Q}_j^k - Q_j^u(h_j) \frac{H_j^k - H_{j+1}^k}{\sqrt{\Delta x \left| H_j^k - H_{j+1}^k \right|}} + p\Delta x \qquad (4.9),$$

where A_j is the horizontal cross sectional area of cell *j*, h_j is the water depth of the main channel in section *j*, *k* is the index of the last solved time step, $\overline{Q}_j^k$ is the average discharge entering in the computational cell *j* during the time step Δt, $Q_j^u(h_j)$ is the specific discharge in section *j* per unit root of energy slope and Δx is the distance between the two cell centers.

After solution of Eq. (4.9) for cell *j*, the average discharge entering in the computational cell (*j*+1) along time step Δ*t* is computed as:

$$\overline{Q}_{j+1}^{k} = \overline{Q}_{j}^{k} + p\Delta x - \frac{W_j^{k+1/2} - W_j^{k}}{\Delta t} \tag{4.10},$$

where W_j^k and $W_j^{k+1/2}$ are the water volumes in the computational cell j at the beginning and at the end of the prediction problem, respectively, and $W_j^{k+1/2}$ is computed as function of $H_j^{k+1/2}$, solution of Eq. (4.9) at the end of Δt. The tributary flow can be embedded in Eq. (4.9) by setting:

$$\frac{\partial H_j}{\partial t} A_j(h_j) = \overline{Q}_j^k - Q_j^u(h_j) \frac{H_j^k - H_{j+1}^k}{\sqrt{\Delta x \left| H_j^k - H_{j+1}^k \right|}} + Q_j^k(H_j) K_j \tag{4.11},$$

where the last term is the right-hand side of Eq. (4.7). The average discharge entering in the computational cell (j+1) during the time step Δt is computed as:

$$\overline{Q}_{j+1}^{k} = \overline{Q}_{j}^{k} + Q_j^k \left(\frac{H_j^k + H_j^{k+1/2}}{2} \right) - \frac{W_j^{k+1/2} - W_j^{k}}{\Delta t} \tag{4.12}.$$

Assuming the specific discharge relationship $Q_j^u(h_j)$ in Eq. (4.11) to depend on a single calibration parameter, the average Manning coefficient, M+1 calibration parameters have to be determined if M is the number of the tributaries. Specifically, the calibration parameters are the average Manning coefficient of the main river and the K_j coefficients of the tributary flows.

4.5 Performance metrics

4.5.1 Calibration

The calibration procedure aims to estimate the set of parameters values (K and n) able to reproduce most accurately the discharge hydrograph in the upstream section. Assuming the MAST model to be a good approximation of the relationship holding between the discharge hydrograph in the upstream section and the stage hydrograph in the downstream gauged one, the calibration is actually made on the computed downstream stage hydrograph. Almost all the fitness indices available in literature measure the match between the computed and the measured hydrographs as a linear function of the quadratic errors. This leads to the conclusion that, generally, calibration provides a better fitness during the peak region of the stage hydrograph [Legates and Mc Cabe, 1999]. A very popular efficiency measure is the Nash-Suctliffe efficiency coefficient [Nash and Sutcliffe, 1970]:

$$NS_h = \left[1 - \frac{\sum_{i=1,N} (h_{i\_obs} - h_{i\_sim})^2}{\sum_{i=1,N} (h_{i\_obs} - \overline{h}_{obs})^2} \right] \qquad (4.13),$$

where h_{i_obs} is the i^{th} datum of the observed stage hydrograph, h_{i_sim} is the i^{th} datum of the simulated stage hydrograph, $\overline{h}_{obs}$ is the mean observed stage and N is the total number of hydrograph ordinates. NS_h can range from $-\infty$ to 1, with a perfect fit obtained for NS_h=1. The advantage of using the NS_h measure instead of the root mean square error ($RMSE$) is

that it is dimensionless and its optimum value carries useful information about the relative estimation error associated to the optimal solution.

An open issue about parameter calibration concerns the number of observations and the corresponding time period used for the computation of the performance measures. A very large amount of information can be derived during the rising limb, when the high slope guarantees a small sensitivity of both the spatial and temporal water level derivatives with respect to the water level error. On the other hand, it is expected that expanding the observation time period after the peak time can provide a further and consistent decrease of the discharge error also for the remaining part of the hydrograph. The same performance measure can be used for discharge comparison purposes when accurate estimates of the discharge are available at the investigated sections, to carry out a validation of the proposed procedure. Therefore, to evaluate the sensitivity of the performance of the model to the calibration period, different temporal extensions are considered to this end, covering from the beginning of the rising limb up to the time along the recession limb, identified by the stage reduction given as a percentage of the stage peak value, ΔPR.

Maximization of the efficiency indices provides good results when the bias of the measurement error is negligible. This assumption fails when the zero hydrometric value is unknown (or uncertain) in the water level hydrograph of the downstream section. In this case, when lateral inflow is negligible, much better results can be found by computing the parameter set corresponding to a perfect match of the measured and the computed

peak time lag between the upstream and the downstream gauged sections [Aricò et al., 2009].

4.5.2 Validation performances

The performances of proposed procedure are evaluated by means of three criteria applied to the estimated discharge and downstream water level hydrographs. The considered performance metrics are: the relative magnitude peak error, the root mean square error and the Nash Sutcliffe efficient coefficient, and applied to the discharge hydrograph are calculated as follows:

Relative magnitude peak error:

$$\Delta Q_p = \left[\frac{Q_p\big|_{sim}}{Q_p\big|_{obs}} - 1 \right] \times 100 \qquad (4.14a),$$

Root mean square error:

$$RMSE = \sqrt{1 - \frac{\sum_{i=1,N} (Q_{i\_obs} - Q_{i\_sim})^2}{N}} \qquad (4.14b),$$

Nash Sutcliffe efficiency coefficient:

$$NS_q = \left[1 - \frac{\sum_{i=1,N} (Q_{i\_obs} - Q_{i\_sim})^2}{\sum_{i=1,N} (Q_{i\_obs} - \overline{Q}_{obs})^2} \right] \qquad (4.14c),$$

where Q_p and Q_i are the peak value and the i^{th} datum of the discharge hydrograph, N is the number of data in the hydrograph and $\overline{Q}$ is the mean discharge value. Subscript *sim* and *obs* refer to estimated and observed

data, respectively. The same Equations (4.14) are used to evaluate performance of estimated downstream water level hydrograph. In this case, the variable discharge is replaced by the water level.

4.6 Study areas and dataset

Even if the proposed approach could be applied to the case of several tributaries (M > 1 in Eq. 8), the most common case is that of a single confluence between two gauged sections, where it is possible to estimate the tributary discharge as difference between the discharges measured in the two sections. Two study areas of this type are used for testing the proposed approach.

4.6.1 The Tiber River

The first case study is selected in the Tiber River basin, central Italy (see Figure 4.1). The investigated reach is bounded upstream by the hydrometric section of Ponte Felcino (2035 km^2) and downstream by the gauged site of Ponte Nuovo (4145 km^2). The reach is about 20 km long and is characterized by a significant intermediate drainage area (2110 km^2) that is about 50% of the downstream basin. The main tributary along the selected reach is the Chiascio River (1962 km^2) that flows in the main channel about 1.5 km upstream Ponte Nuovo site. The Ponte Rosciano hydrometric station is located along the Chiascio River about 2 km upstream the confluence with the Tiber River (see Figure 4.1).

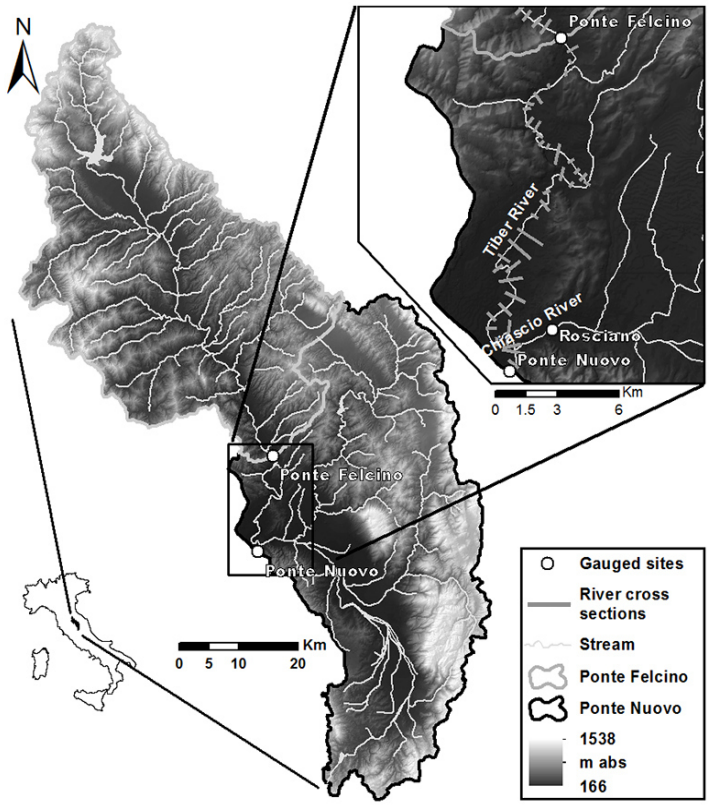

Figure 4.1. Morphology of the Tiber River basin at Ponte Nuovo with the location of the hydrometric gauged sections.

The geometry of 85 river cross sections, including the three gauged sites, is known in the selected study area. Stage and discharge data are available at the three stations, that are provided with ultrasonic stream gauges, recording a continuous series of water levels with a time step of 30 min. In addition, reliable rating curves are available for assessing discharges used as benchmark for performance evaluation. The normalized discharge curves in the last section of the tributary rivers and in all the sections of the main ones have been computed according to the algorithm proposed

by Spada et al. [2015]. Five floods events, whose main characteristic are summarized in Table 4.1, are selected for testing the proposed methodology.

Table 4.1. Tiber River: main properties of the selected flood events in terms of peak discharge, Q_p, peak stage, h_p, time to peak, t_p, and flood event duration, ΔT.

Event	ΔT (h)	Ponte Felcino			Ponte Nuovo		
		Q_p	h_p	t_p	Q_p	h_p	t_p
December 1996	80	341.5	4.22	34.0	728.4	6.43	37.0
December 1998	90	296.4	3.94	34.5	716.8	6.37	38.5
December 1999	140	157.1	2.79	56.5	765.8	5.38	57.5
December 2008	150	522.1	4.98	61.5	925.0	7.29	66.5
November 2012	83.5	671.5	6.03	59.5	1048.4	7.93	58.0

4.6.2 The Alzette River

The second case study is selected in the Alzette River basin (Gran-Duchy of Luxembourg). The investigated reach is bounded by the gauged sections of Pfaffenthal and Mersch (see Figure 4.2).

Here, the river meanders in a relative large and flat plain wide about 300 m and with a mean slope of ~0.08%. The river reach length is about 19 km. The drainage areas at Pfaffenthal and Mersch are 360 km^2 and 707 km^2, respectively. An important confluence with the Mamer and Eisch Rivers is located about 1 km upstream of Mersch.

The overall basin area of the two tributaries is the 72.6% (261 km^2) of the upstream basin. Because of the proximity of their confluence with the Alzette River, the two tributaries have been modeled as a single one, with a normalized discharge curve $Q_j^K(H_j)$ equal to the sum of the curves of the two tributaries. In this area, topographic surveys of 162 river cross sections are available. Three flood events are selected for the analysis, for which stage records are available along the Alzette River at the two gauged stations of Pfaffenthal and Mersch as well as along the tributaries in Hunnebuer (along the Eisch River) and in Schoenfels (along the Mamer River) gauged sections. The hydrometric data are recorded every 15 min. The main characteristics of the selected events are summarized in Table 4.2.

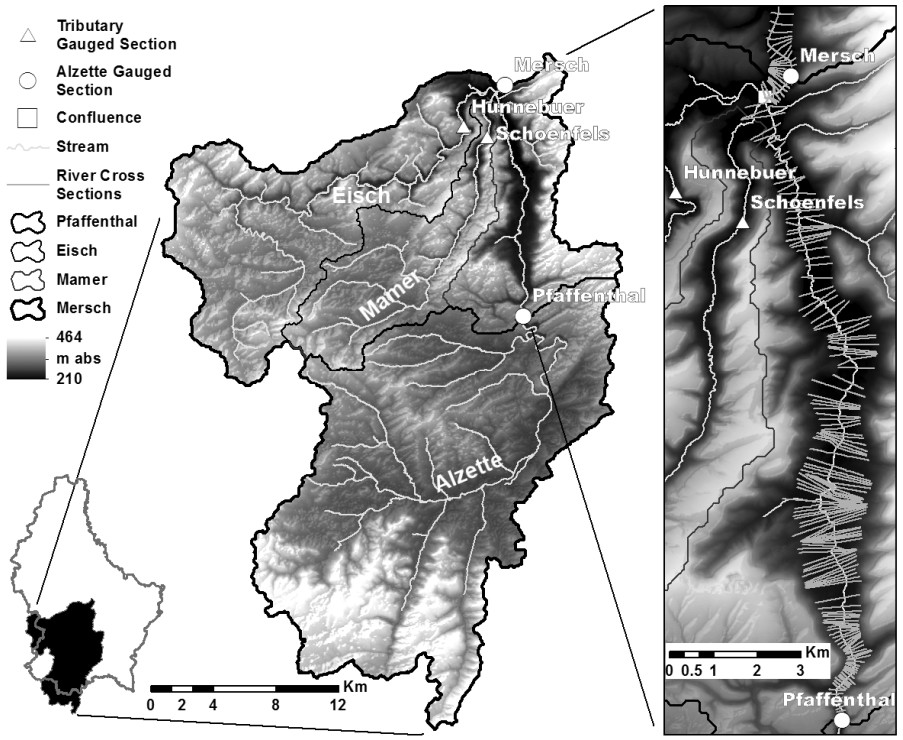

Figure 4.2. Morphology of the Alzette River basin at Mersch with the location of the hydrometric gauged sections.

Table 4.2. As for Table 4.1, but for the Alzette River.

Event	ΔT (h)	Pfaffenthal			Mersch		
		Q_p	h_p	t_p (h)	Q_p	h_p	t_p (h)
January 2003	380	71.0	3.42	203.0	107.4	4.84	214.5
January 2007	140	53.7	2.90	58.5	72.7	3.74	47.0
January 2011	336	84.9	3.81	104.75	107.4	4.84	116.0

4.7 Results and discussion

4.7.1 Tiber River

The case study selected in the Tiber River basin has been modeled assuming a single roughness parameter, n, and one tributary constant K relative to the Chiascio River.

The NS_h measure, computed at Ponte Nuovo section, is plotted as function of the n and K parameters for the first investigated event (December 1996) in Figure 4.3. This result refers to a calibration period, T_{cal}, extended between the beginning of the rising limb at the downstream hydrograph and its peak time.

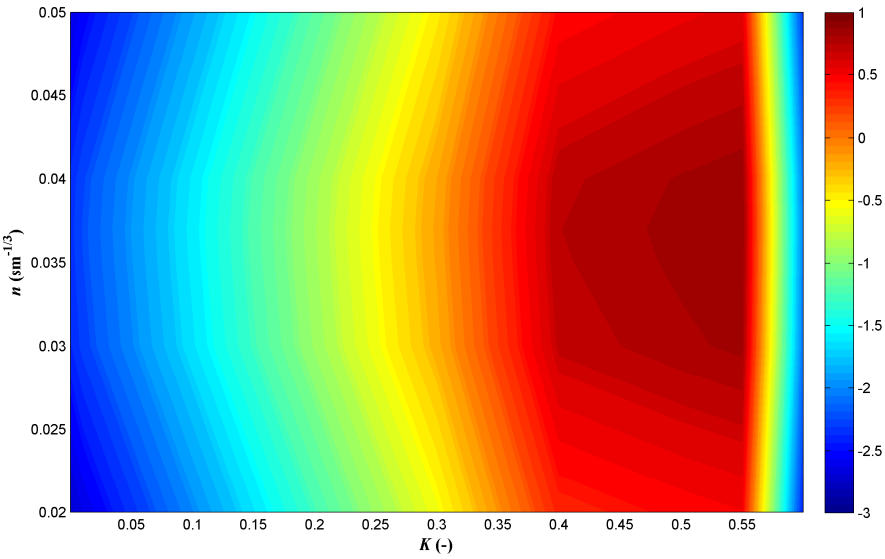

Figure 4.3. Tiber River, Ponte Nuovo section: Nash Sutcliffe, NS_h, versus K-n parameters for the event occurred on December 1996.

The optimal values of the two parameters n and K able to closely reproduce the stage hydrograph observed at Ponte Nuovo section are summarized in Table 4.3 for each investigated event.

Table 4.3. Ponte Nuovo site: optimized parameters values (n=Manning roughness coefficient; K=conveyance parameter) and related calibration performance in terms of Nash-Sutcliffe coefficient, NS_h, calculated over the calibration period, T_{cal}, from the beginning of the rising limb up to the peak time.

Event	n ($sm^{-1/3}$)	K (-)	NS_h	T_{cal} [h]
December	0.037	0.55	0.975	17-38
December	0.037	0.61	0.944	25-39
December	0.038	0.68	0.948	36-59
December	0.037	0.67	0.965	30-75
November	0.036	0.42	0.946	20-65

It is worth noting that the change of the two parameters affects differently the computed hydrographs. Specifically, changing the Manning coefficient, n, leads to a shift of the peak time, but the volume of the computed hydrograph remains almost constant; on the contrary, the value of the tributary constant K mainly affects the volume of the computed hydrographs. This explains the low sensitivity of both performance measures to the Manning coefficient n, even for K values a bit lower or a bit higher than its optimal value. When the volume of the computed hydrograph is very different from the measured one, the performance measure is almost independent from the location of the peak

time, mainly related to the *n* value of the Manning coefficient. This also confirms that matching the peak time location is not sufficient for the calibration of *n*, when consistent lateral inflows are present. By way of example, Figure 4.4 compares for the event of December 1996 the observed stage hydrograph at Ponte Nuovo site with the computed one using optimized parameters and two further simulated hydrographs obtained assuming K=0.02, much smaller than the optimal one equal to 0.55, and 2 different *n* values.

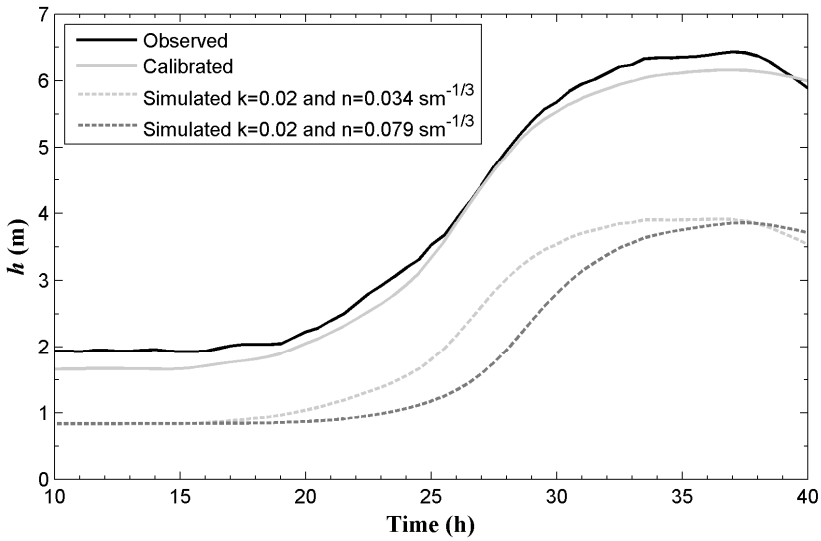

Figure 4.4. Tiber River, Ponte Nuovo section (December 1996 flood): comparison between observed water level hydrograph and simulated ones with different parameter sets.

The dependency of the NS_h performance measure on the duration of the sampling period can be seen in Figures 4.5. The parameter ΔPR of each line represents the stage reduction given as a percentage of the peak

value allowing identifying along the recession limb the end of the sampling time extension. Specifically, Figure 4.5a and 4.5b show for the event of December 1996 the effect of sampling period extension used for calibration on *NS*, for different *n* Manning coefficients and for the optimal *K* value (Figure 4.5a), as well as for the optimal *n* coefficient and for different *K* values (Figure 4.5b). All the sampling periods start from the beginning of the rising limb, identified by its maximum curvature. The best *NS* value curve is always the one computed for an extension equal to the peak time and *NS* values drop, for given *n* value, along with the extension of the observation period.

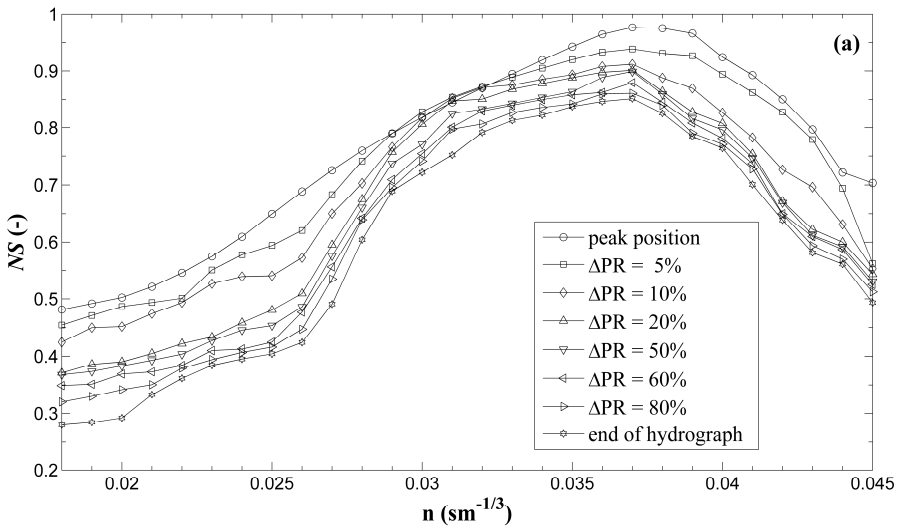

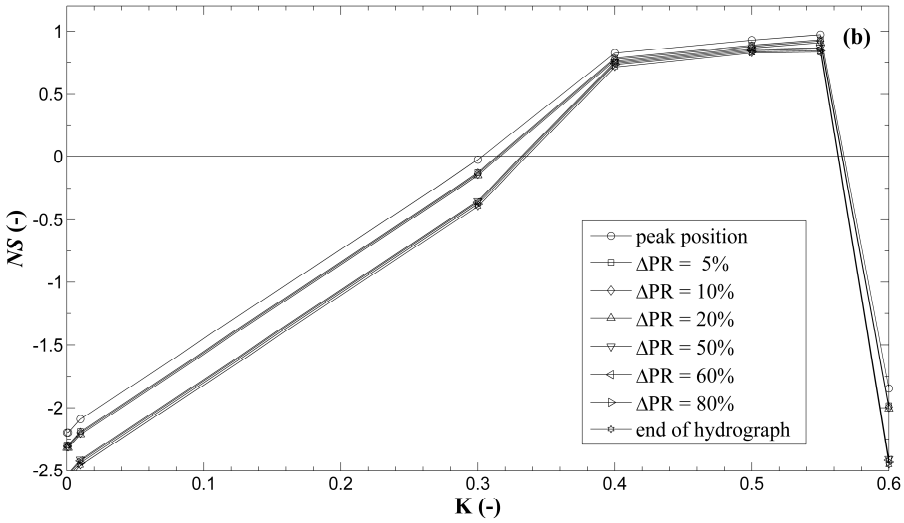

Figure 4.5. Tiber River, Ponte Nuovo section (December 1996 flood): *NS* for (a) constant conveyance parameter, K = 0.55, and variable Manning coefficient, *n*, and (b) for n=0.037 $sm^{-1/3}$ and variable K. Δ*PR* represents the peak stage reduction to identify the calibration period.

Figs. 4.6, 4.7 and 4.8 show for the five investigated events the comparison between the hydrographs computed using the optimal *n* and *K* parameter values and the observed ones. Specifically, the stage hydrographs are compared at Ponte Nuovo gauged site, while the comparison is carried out for the discharge hydrographs for both channel ends, i.e. Ponte Felcino and Ponte Nuovo sections, as well as for the investigated tributary that is Ponte Rosciano hydrometric site. The calibration window used for optimal parameter values estimate is shown in the figures as shaded areas.

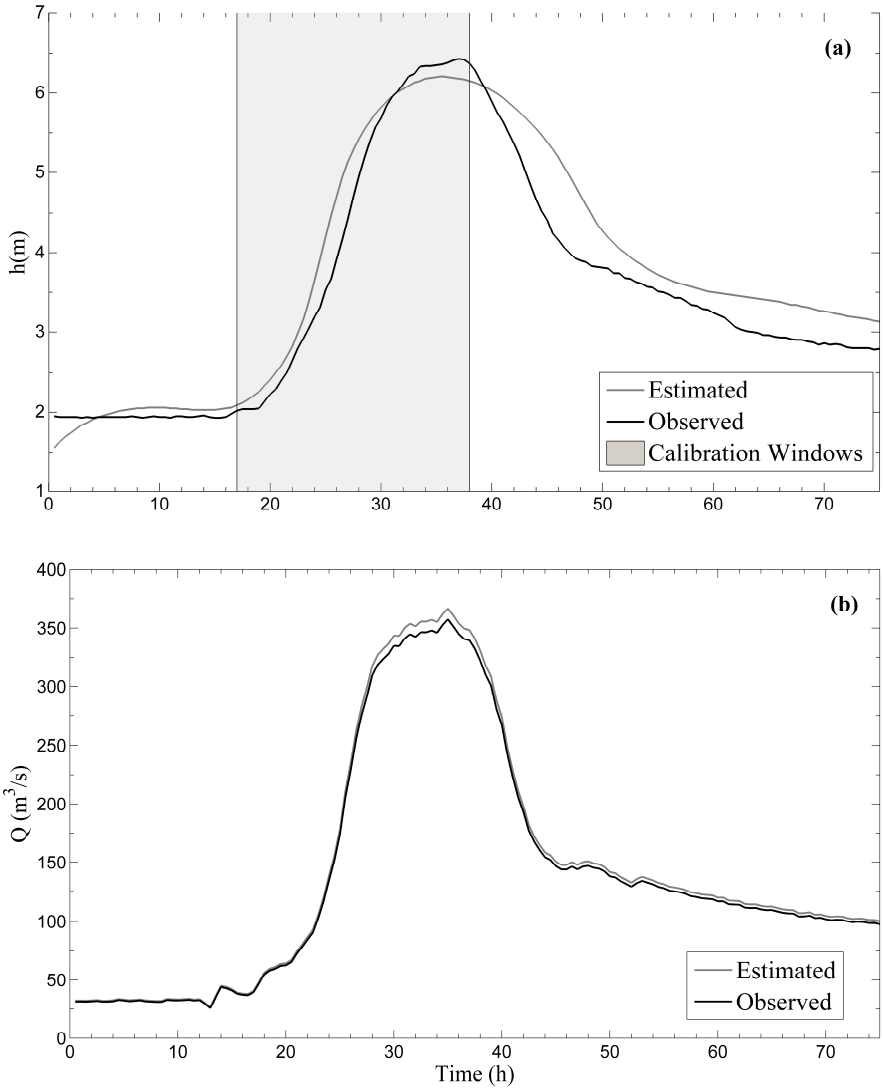
(a)
h(m)
Estimated
Observed
Calibration Windows
(b)
Q (m3/s)
Estimated
Observed
Time (h)

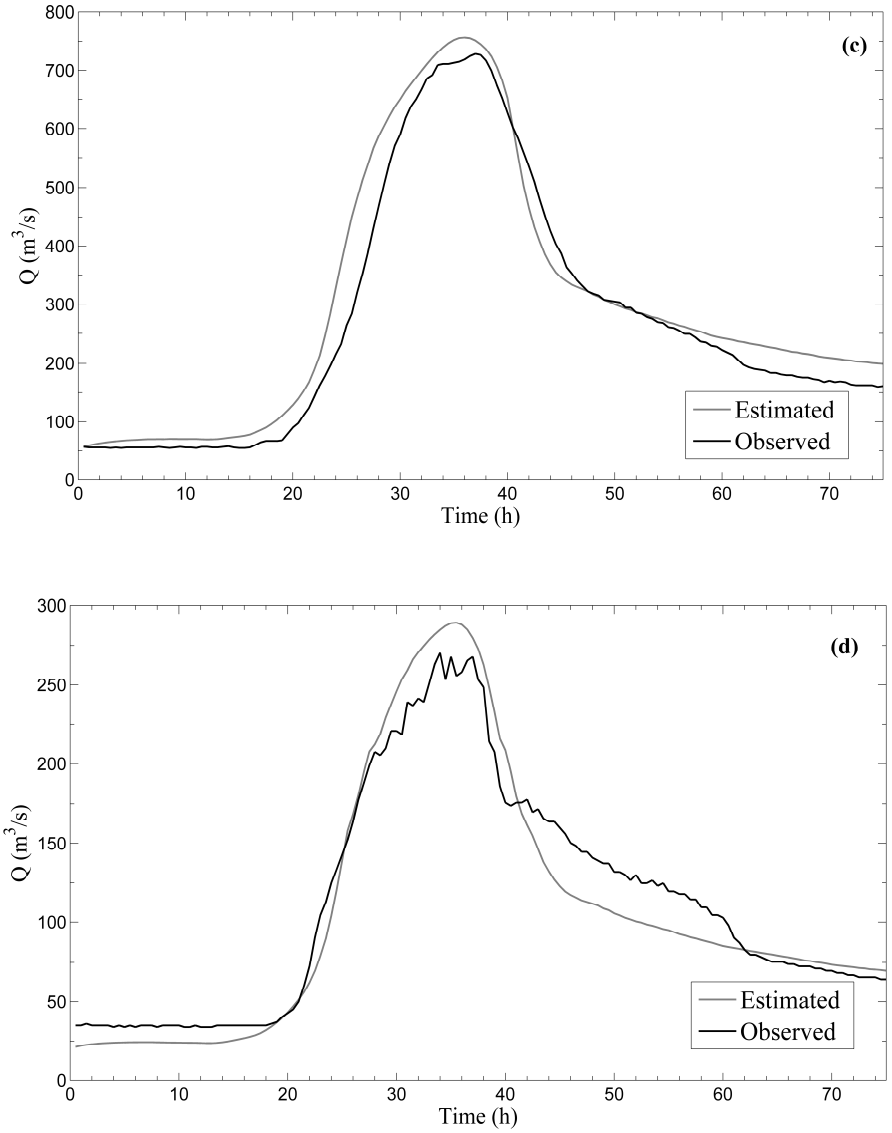

Figure 4.6. Tiber River, December 1996 flood: comparison between observed and computed water level hydrographs at Ponte Nuovo site (a); comparison between observed and computed discharge hydrographs at Ponte Felcino site (b), at Ponte Nuovo section (c) and for the tributary (d).

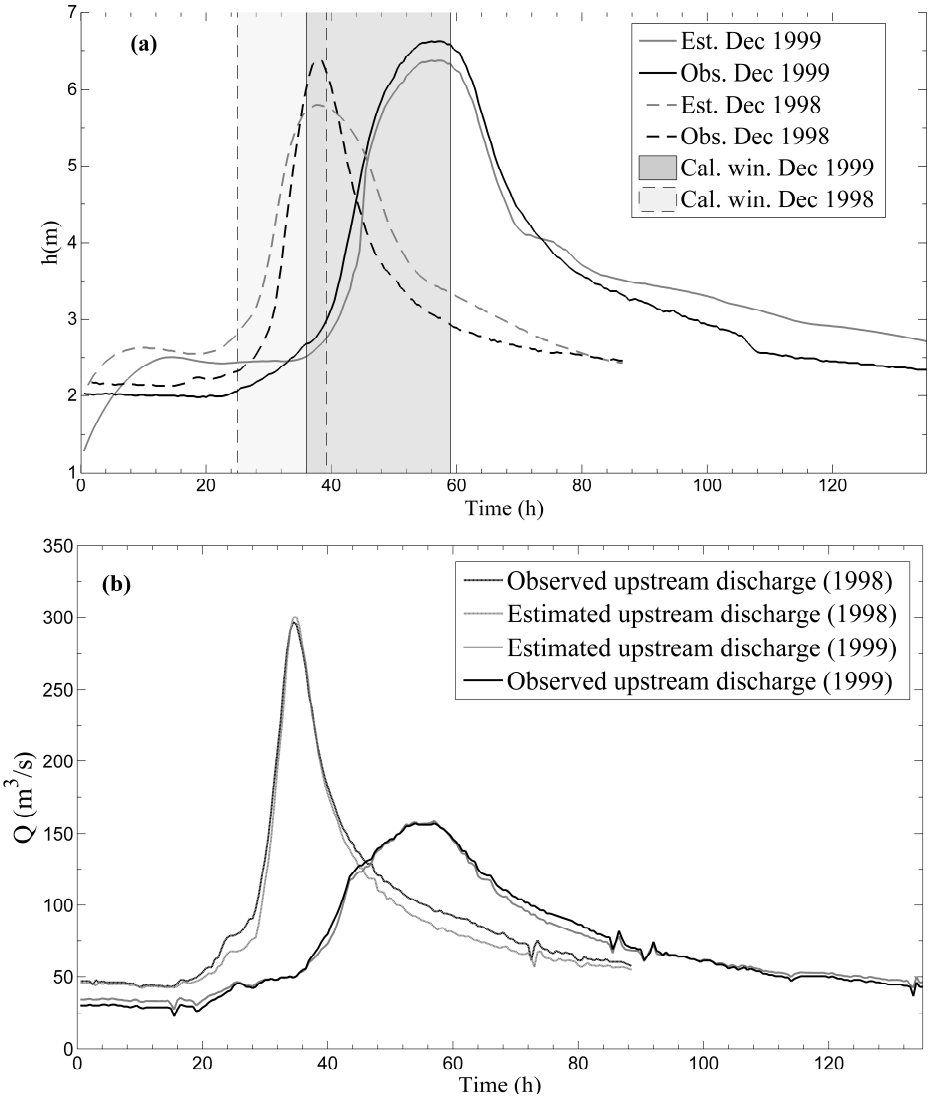
(a)
Est. Dec 1999
Obs. Dec 1999
Est. Dec 1998
Obs. Dec 1998
Cal. win. Dec 1999
Cal. win. Dec 1998
h(m)
Time (h)
(b)
Observed upstream discharge (1998)
Estimated upstream discharge (1998)
Estimated upstream discharge (1999)
Observed upstream discharge (1999)
Q (m3/s)
Time (h)

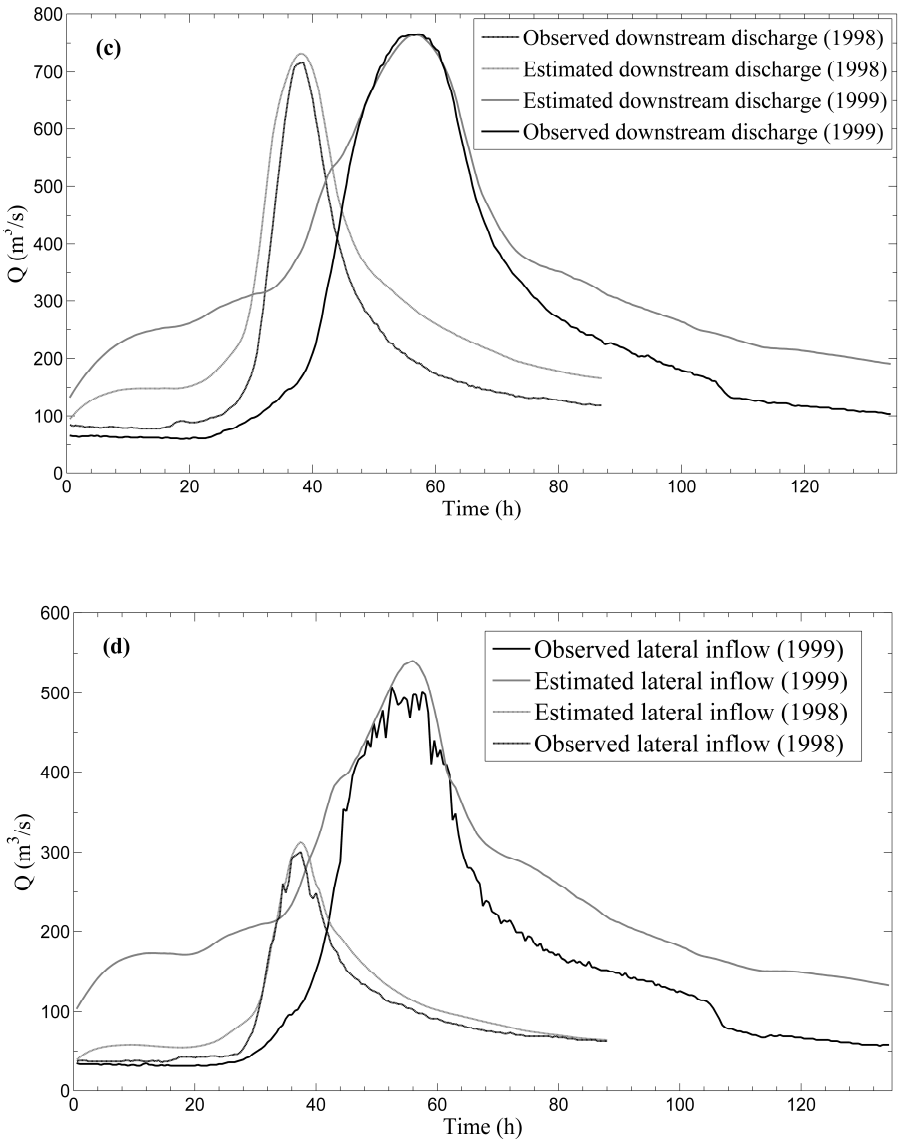

Figure 4.7. As figure 4.6 but for the events of December 1998 and December 1999.

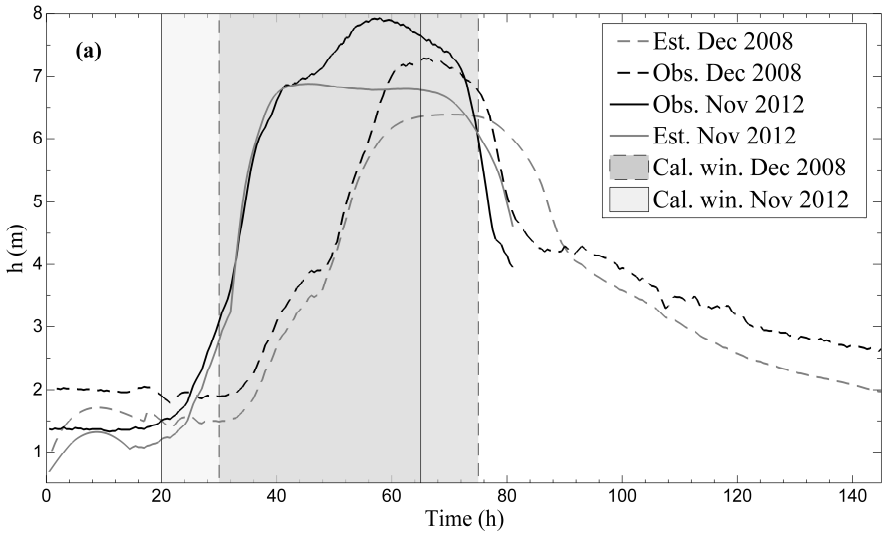
(a)
Est. Dec 2008
Obs. Dec 2008
Obs. Nov 2012
Est. Nov 2012
Cal. win. Dec 2008
Cal. win. Nov 2012
h (m)
Time (h)

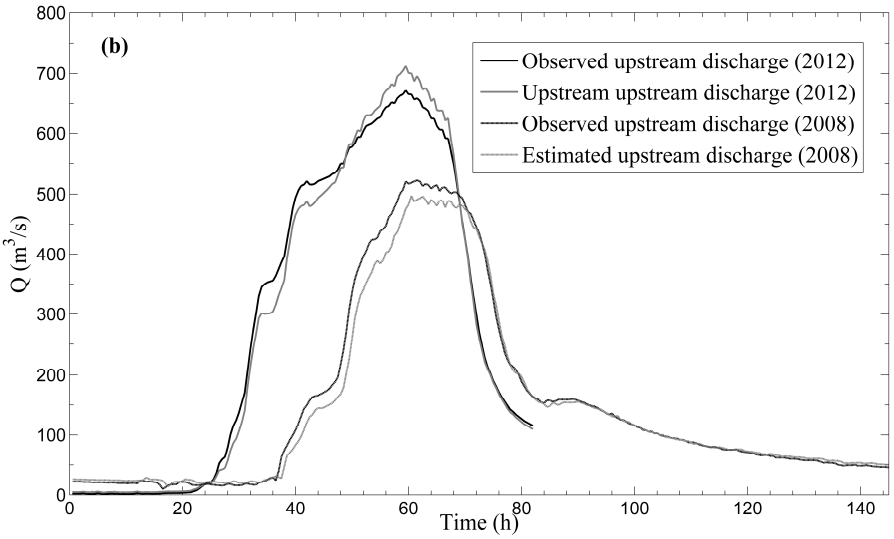
(b)
Observed upstream discharge (2012)
Upstream upstream discharge (2012)
Observed upstream discharge (2008)
Estimated upstream discharge (2008)
Q (m3/s)
Time (h)

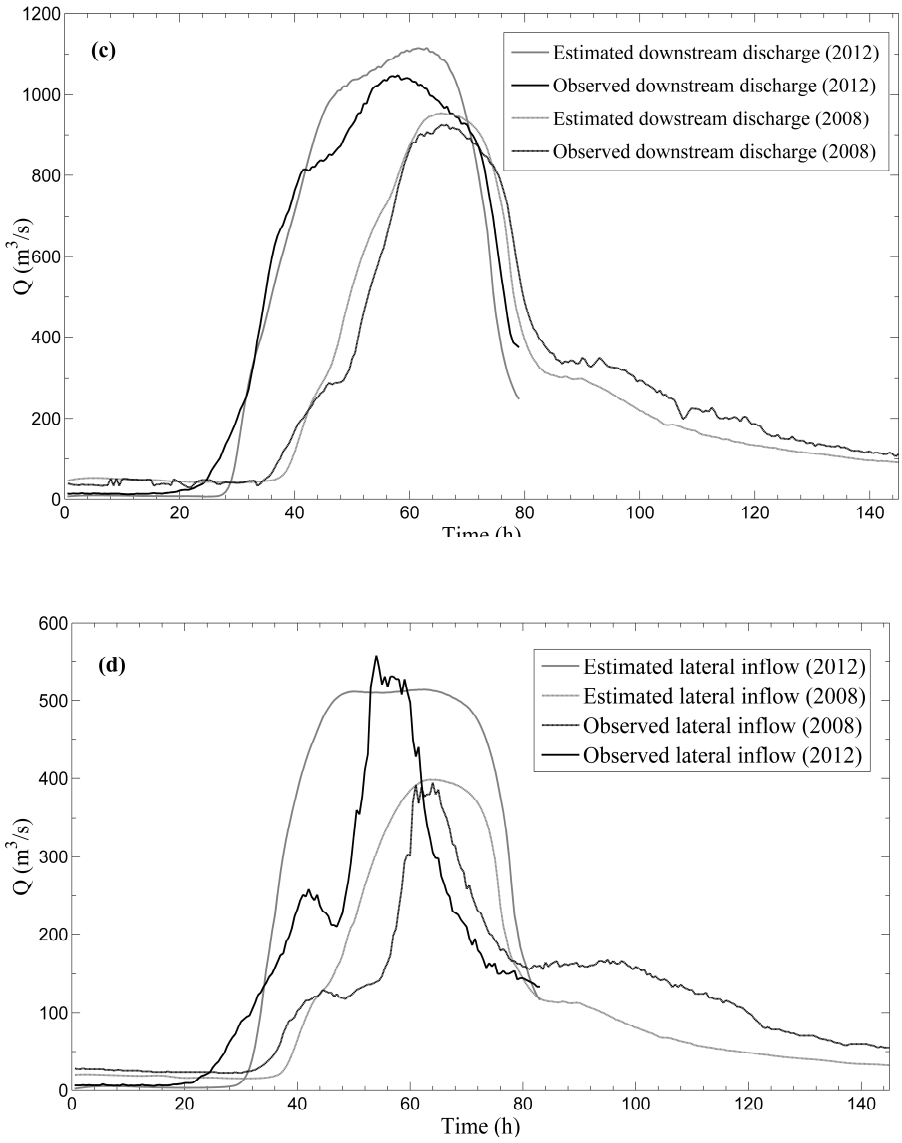

Figure 4.8. As figure 4.6 but for events of December 2008 and November 2012.

The related performances are reported in Table 4.4. As expected, the best match between the observed and the computed hydrographs is

obtained for all the events for the upstream discharge because the computed values are strongly affected by the water depth values measured in the same section and used in Eq. (4.7) for the computation of the normalized discharge. The resulting NS_q indices computed for the entire flood events duration are very high and the difference between the computed and the observed values is smaller than the error on the assessment of the rating curve used for comparison with the computed hydrograph. The performance measures assessed at the Ponte Nuovo downstream site are very satisfactory with an error in peak discharge lower than 6.5% and a NS_q average value, computed for the entire flood duration, equal to 0.86. This result suggests a satisfactory estimation of the lateral inflow that is characterized by a mean error on peak discharge value not exceeding 8% and a mean NS_q equal to 0.60. This result is of considerable interest for the hydrological practice considering that no rainfall-runoff transformation is carried out for the intermediate basin and no rainfall data are used.

The estimated entering volume is found slightly larger than the real one in three flood events , i.e., event 1999, 2008 and 2012. This is likely compensated by a small overestimation of the actual optimum n coefficient, assumed constant also in the sampling period, with water depth values smaller than the higher ones and it is also consistent with the location of the tributary gauged section. This location is 2 km upstream from the confluence and the measured discharge is likely to be a bitter smaller than the discharge occurring at the tributary junction. Finally, we can observe that n optimal parameter remains very similar from one event to the other one, as expected in a relatively short time period, but K has a

larger variation because it is affected by the average piezometric gradient occurring during each specific event.

Table 4.4. Tiber River, performances in terms of Nash Sutcliffe index, NS_q and NS_h, *RMSE*, relative magnitude peak error, ΔQ_p and Δh_p. NS_h is computed for the calibration period, while all other performances are calculated over the entire flood hydrograph.

Event	Ponte Felcino, discharge			Ponte Nuovo, water level			Ponte Nuovo, discharge		
	NSq	RMSE (m^3s^{-1})	ΔQ_p (%)	NS_h	*RMSE* (m)	Δh_p (%)	NS_q	*RMSE* (m^3s^{-1})	ΔQ_p (%)
Dec 1996	0.998	4.46	2.62	0.975	0.39	-3.42	0.948	48.26	3.84
Dec 1998	0.980	8.35	1.31	0.944	0.46	-8.95	0.782	76.87	2.16
Dec 1999	0.991	3.53	1.09	0.948	0.36	-3.78	0.650	124.8	-0.1
Dec 2008	0.985	19.05	-4.7	0.965	0.56	-12.39	0.959	54.48	3.15
Nov 2012	0.993	21.52	6.07	0.946	0.58	-13.24	0.965	77.05	6.47

4.7.2 Alzette River

The case study of the Alzette River has been also modeled considering a unique roughness parameter, n, and one constant K relative to the Mamer and Eisch tributaries. The *NS* analysis results are shown in Figure 4.9 for the first investigated flood event (January 2003). As for the Tiber River case study, the calibration period, T_{cal}, is between the beginning of the rising limb up to the time to peak.

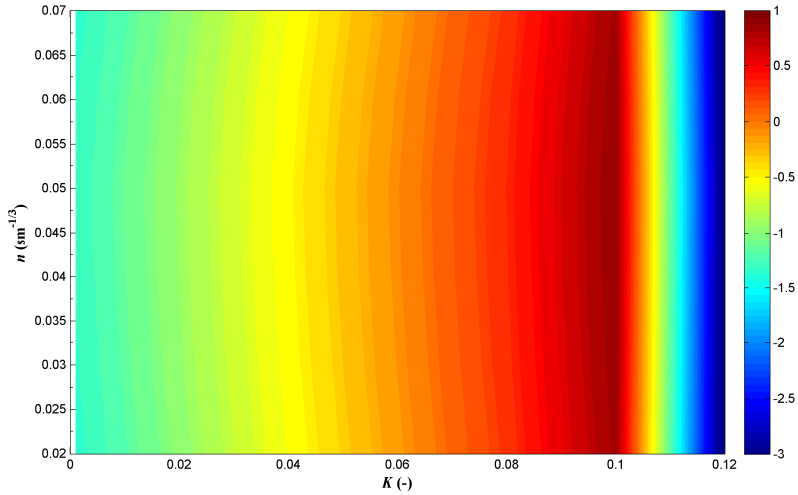

Figure 4.9. Alzette River, Mersch section: Nash-Sutcliffe, NS_h, versus K-n parameters for the event occurred on January 2003.

As shown in the Figure 4.9, the shape of the calibration metric NS_h versus the parameter set (K, n) is similar to the one obtained for the Tiber River. In this case, NS_h is even less sensitive to n than in the previous Tiber basin as shown in Table 4.5 for Mersch site. This smaller sensitivity is likely due to the smaller bed slope of the main river with respect to the

previous study case. The optimal values of *K,* related to the specific event, changes between 0.1 and 0.16.

Table 4.5. As for Table 4.3, but for the Alzette River at Mersch gage site.

Event	n ($sm^{-1/3}$)	K (-)	NS_h	T_{cal} (h)
January 2003	0.05	0.10	0.914	185-222
January 2007	0.04	0.13	0.912	0-52
January 2011	0.049	0.16	0.934	70-120

In Fig. 4.10, for the event January 2003 NS_h is plotted as a function of the n parameter, for different observation period lengths and for the optimal K value (Figure 4.10a), as well as for the optimal n coefficient and for different K values (Figure 4.10b).

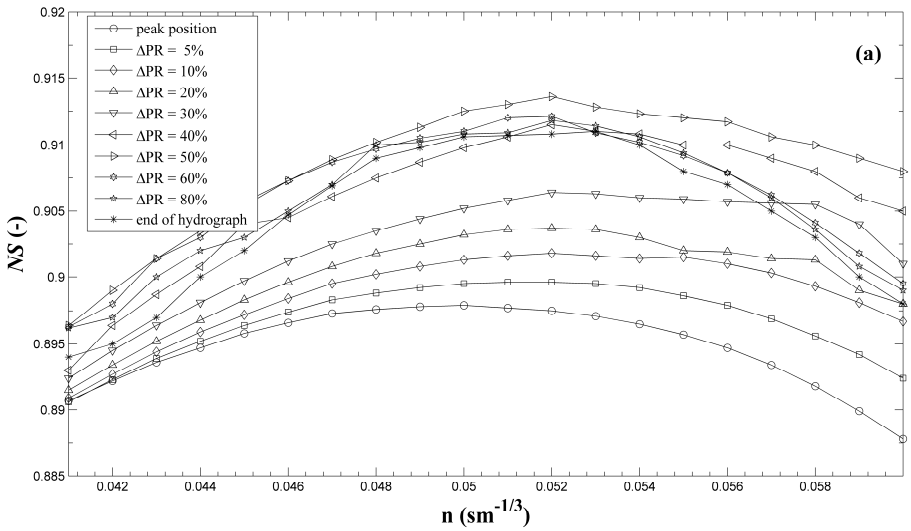

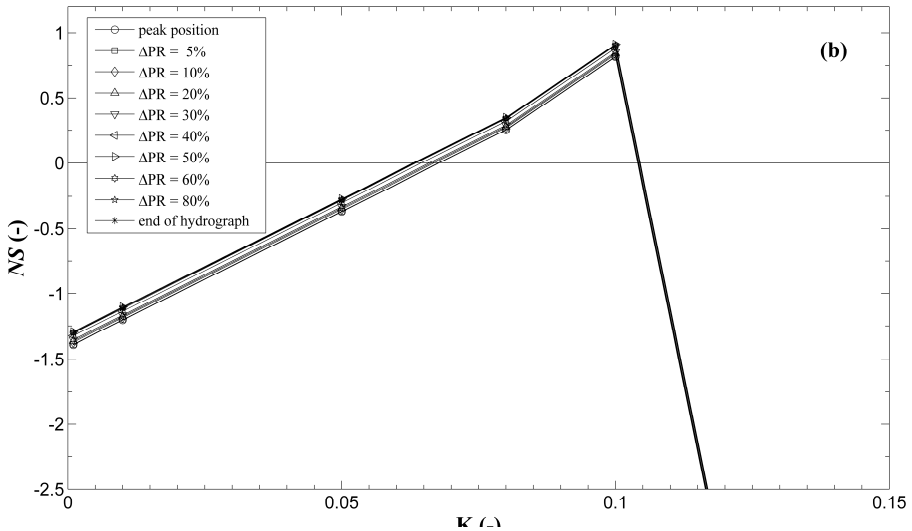

Figure 4.10. Alzette River, Mersch section (January 2003 flood): *NS* for (a) constant conveyance parameter, K = 0.1, and variable Manning coefficient, n, and (b) for n=0.05 $sm^{-1/3}$ and variable K. ΔPR represents the peak stage reduction to identify the calibration period.

A different dependency of the evaluation measure on the duration of the sampling period extension, with respect to the previous case, can be observed. In this case, the optimal extension is larger than the time to peak and is found equal to the time corresponding in the recession limb of the hydrograph to the 50% of the peak discharge value.

Figures 4.11 and 4.12 and Table 4.6 show for all the three investigated floods the comparison between the observed and the computed hydrographs, similarly as shown for the Tiber River. The upstream discharge is simulated with an average NS_q value of 0.992, while the lateral flow is estimated with a mean error on peak discharge equal to 17%. However, a not negligible overestimation on lateral volume is

observed (mean value=50%) and, in this case, the distance between the tributary junctions and the hydrometric sections in the tributary rivers, equal to 3.8 (Mamer) and 5 (Eisch) kilometers, could partially justify the larger estimated lateral inflow.

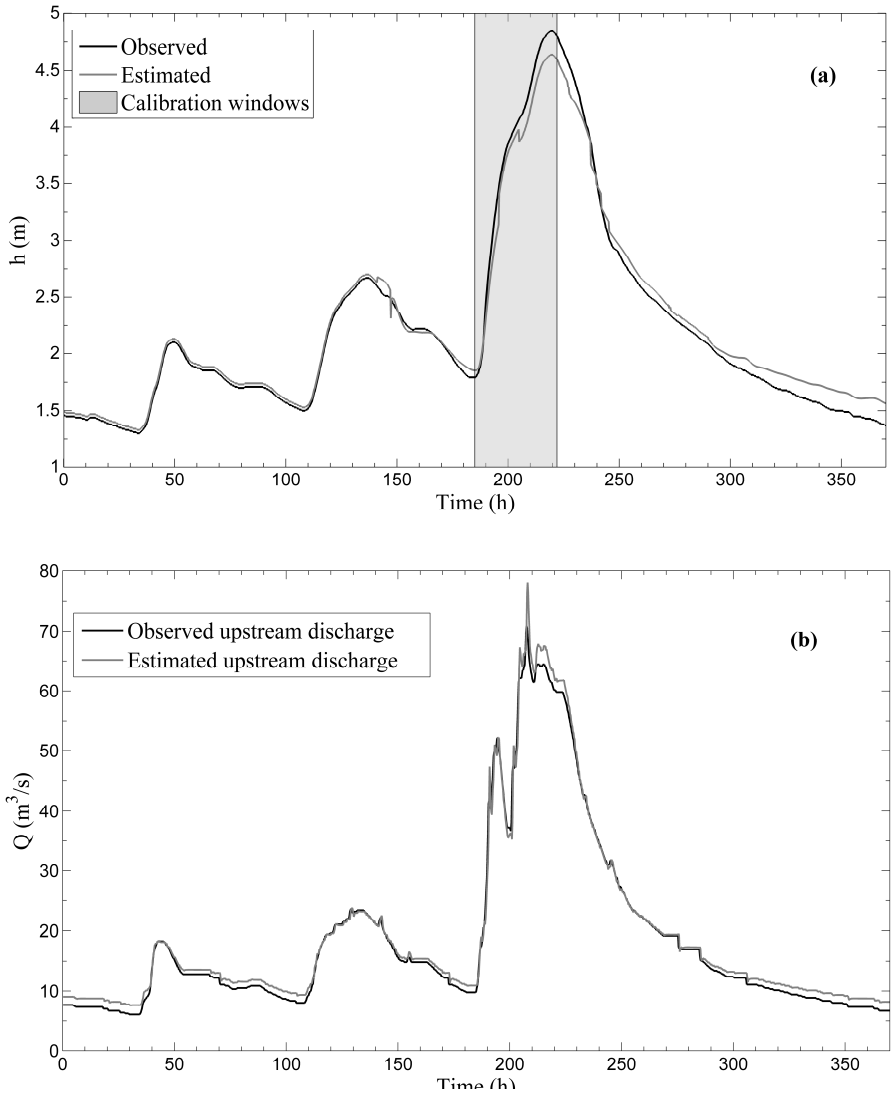

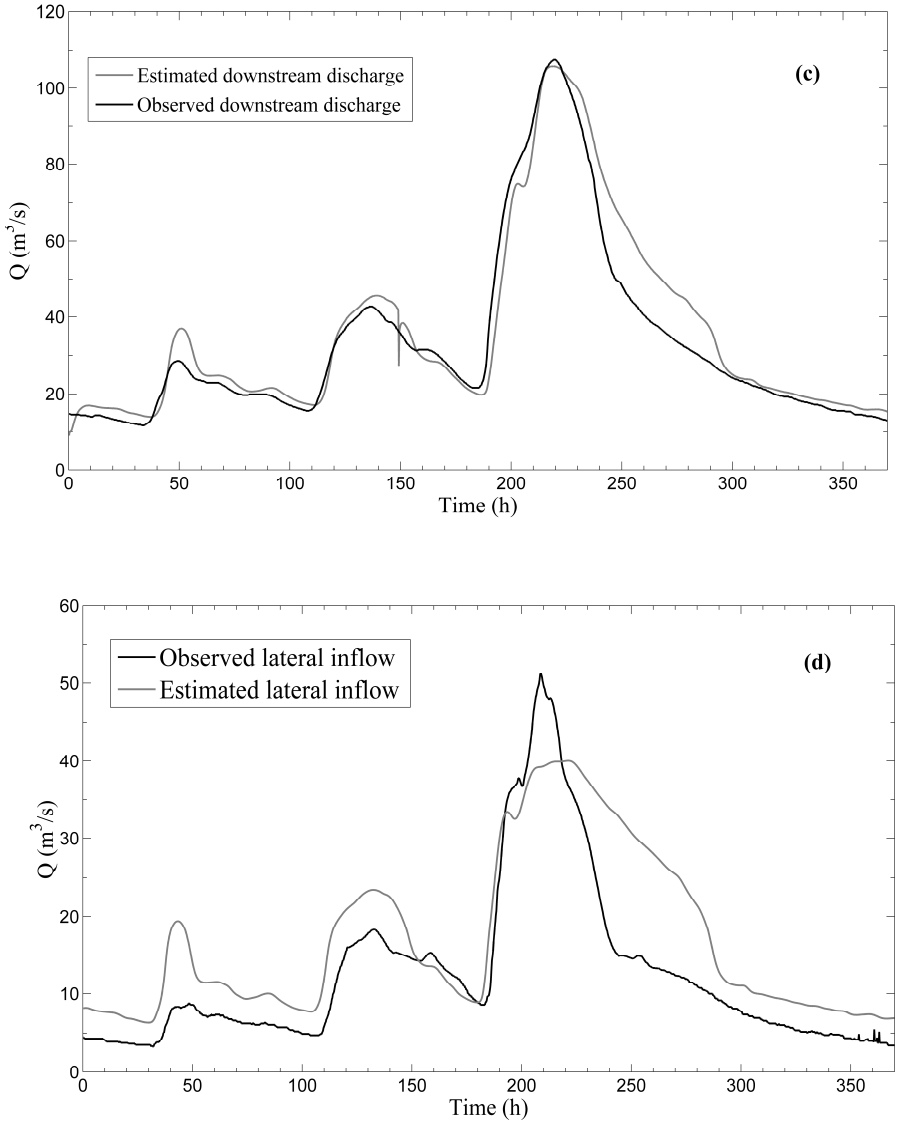

Figure 4.11. Alzette River, January 2003: comparison between observed and computed stage hydrograph at Mersh site (a); comparison between observed and computed discharge hydrograph at Pfaffenthal site (b), at Mersh section (c) and for the tributary (d).

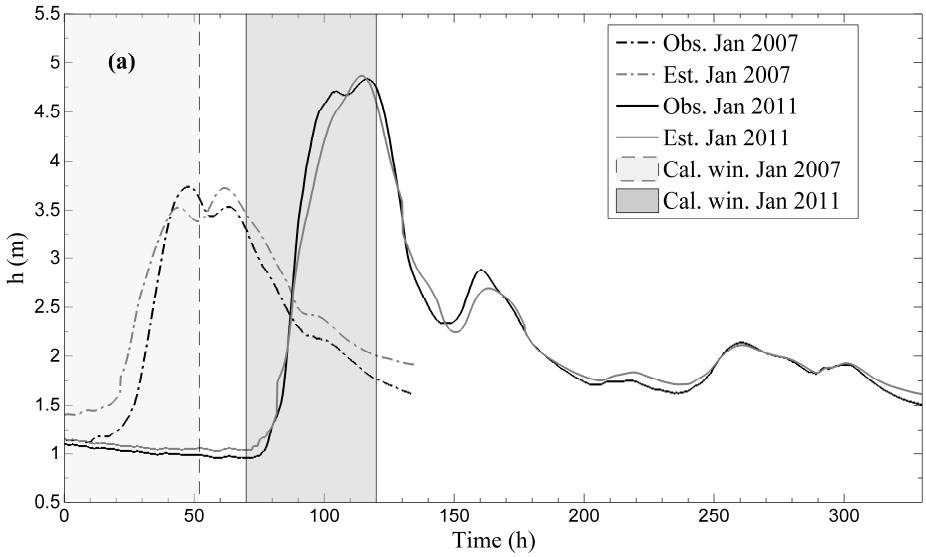
(a)
Obs. Jan 2007
Est. Jan 2007
Obs. Jan 2011
Est. Jan 2011
Cal. win. Jan 2007
Cal. win. Jan 2011
h (m)
Time (h)

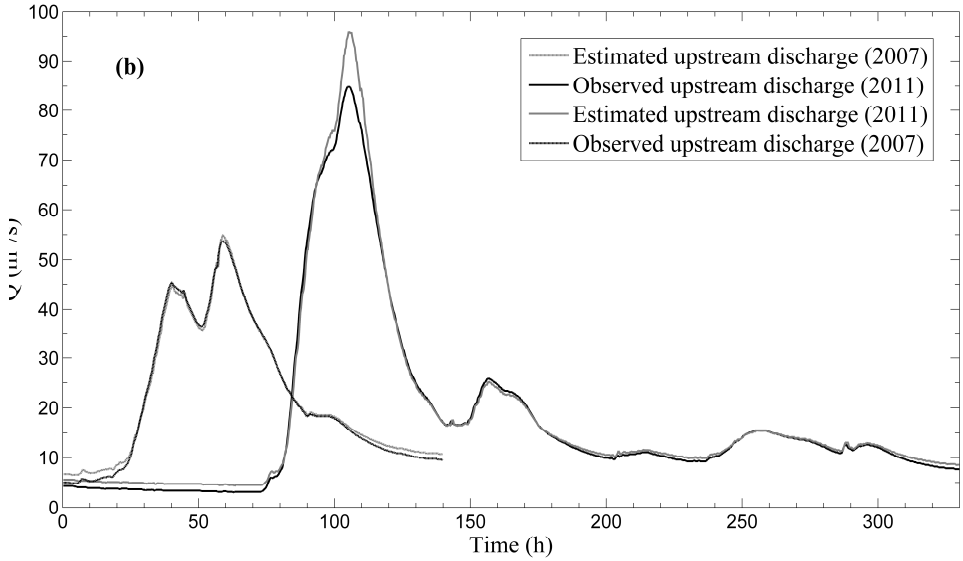
(b)
Estimated upstream discharge (2007)
Observed upstream discharge (2011)
Estimated upstream discharge (2011)
Observed upstream discharge (2007)
Time (h)

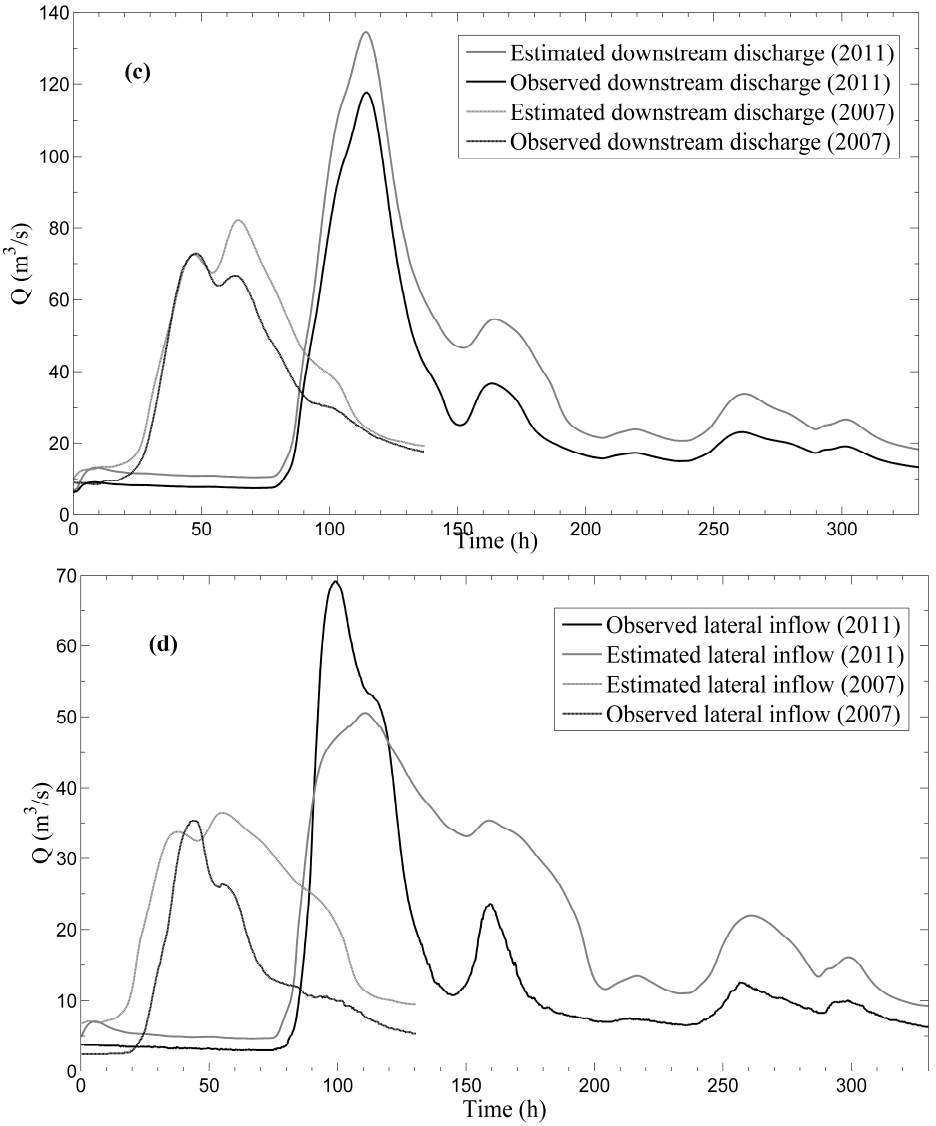

Figure 4.12. As Fig. 4.11 but for the events of January 2007 and 2011.

Table 4.6. As for Table 4.4, but for the Alzette River.

Event	Pfaffenthal, discharge			Mersch, water level			Mersch, discharge		
	NS_q	$RMSE$ (m^3s^{-1})	ΔQ_p (%)	NS_h	$RMSE$ (m)	Δh_p (%)	NS_q	$RMSE$ (m^3s^{-1})	ΔQ_p (%)
Jan 2003	0.99	1.31	9.85	0.91	0.1	-4.13	0.92	6.55	-1.6
Jan 2007	1	0.96	2.42	0.91	0.32	-0.32	0.84	8.38	13
Jan 2011	0.99	1.87	11.1	0.93	0.13	0.63	0.81	10.91	14.2

CONCLUSIONS

In the first part of this thesis, new methods for uniform flow discharge along irregular sections have been presented. The first method, named *INCM*, develops from the original *IDCM* method and it is shown to perform better than the previous one, with the exception of lab tests with very small discharge values. The second one, named *LHRM*, has empirical bases, and gives up the ambition of estimating turbulent stresses, but has the following important advantages:

1. It relies on the use of only two parameters: the friction factor f (or the corresponding Manning's coefficient n) and a second parameter β which on the basis of the available laboratory data was estimated to be equal to 9.

2. The β coefficient has a simple and clear physical meaning: the correlation distance, measured in water depth units, of the vertically averaged velocities between two different verticals of the river cross-section.

3. The sensitivity of the results with respect to the model β parameter was shown to be very low, and a one digit approximation is sufficient to get a discharge variability less than 2%. A fully positive validation of the method was carried out using lab experimental data, as well as field discharge and roughness data obtained by using the unsteady-state level analysis proposed by Aricò et al. (Aricò et al., 2009) and applied to the Alzette river, in the grand Duchy of Luxembourg.

4. Comparison between the results of the CFX 3D turbulence model and the *LHRM* model shows a very good match between the two computed total discharges, although the vertically averaged velocities computed by the two models are quite different near to the banks of the river.

Moreover, the estimation of the velocity profiles in each of the considered sub-sections could be used in order to evaluate the vertical average velocity and so the shear stresses at the boundary of the whole cross section. In fact, it is well-known that bed load transport is directly related to the bed shear stress and that this is proportional in each point of the section to the second power of the vertically averaged velocity, according to Darcy Weisbach (Ferguson, 2007):

$$\tau_0 = \rho U^2 \frac{f}{8} \tag{1}$$

All the bed load formulas available in literature compute the solid flux per unit width. For example, the popular Schoklisch formula (Gyr et al., 2006) is:

$$q_s = \frac{2.5}{\rho_s / \rho} S^{\frac{3}{2}} (q - q_c) \tag{2}$$

where q and q_s are respectively the liquid and the solid discharge per unit width. This implies that the information given by the mean velocity and by the cross section geometry is not sufficient for a good estimation of the bed load in irregular sections. If Eq.(2) holds, the error in the bed load estimation is proportional to the error in the volumetric discharge, discussed in the previous sections.

In the second part of this thesis the indirect method for discharge estimation based on reverse routing modeling along a river reach bounded

by two gauged sections is extended to take into account significant lateral contribution. The proposed methodology quantifies the lateral inflow through the assessment of a specific discharge for each tributary between the two gauged sites. The procedure requires the calibration of few parameters: a mean Manning roughness coefficient for the main channel and one parameter for each tributary located along the selected reach.

The results obtained for two case studies, selected in central Italy and in Luxemburg, indicate that the proposed methodology for indirect discharge estimation in sites with significant lateral inflows is able to provide reliable estimates of the upstream and lateral discharge and to accurately reconstruct the downstream stage hydrograph, used as benchmark for the parameters calibration. Specifically, the average *NSq* value obtained in the tested events for the upstream discharge hydrographs is equal to 0.99 with a minimum value equal to 0.980 obtained in the event of December 1998 at the Tiber River. Results are found satisfactory for the two downstream gage sites as well, with a mean NS_q values equal to 0.86 for both. More accurate field validation is almost impossible, due to the consistent error expected in the rating curve at the peak value during floods. Sensitivity analysis has been also carried out showing that the parameter calibration based only on the match between the computed and the measured peak time is possible only if the lateral inflow is missing or previously known. No general conclusion can be drawn about the optimal extension of the sampling period, also because in practice it depends on the sought after hydrograph parameter (e.g. the peak or the mean values). In the two study cases, good performances have been obtained using for calibration the time period

between the beginning of the rising limb and the peak time, where the hydrograph slope attains the maximum values.

REFERENCES

Abril, J. B., and Knight, D. W. (2004). Stage-discharge prediction for rivers in flood applying a depth-averaged model. *J. Hydraul. Res*., 42(6), 616–629.

Ansys Inc., Canonsburg. (2006). ANSYS CFX Reference guide.

Ackers, P. (1993). Flow formulae for straight two-stage channels. *J. Hydraul. Res.*, 31(4), 509–531.

Aricò, C. and Tucciarelli, T. (2007). A Marching in Space and Time (MAST) solver of the shallow water equations. Part I: the 1D model. Advances in Water Resources, 30(5), 1236-1252.

Aricò, C., Nasello, C. and Tucciarelli, T. (2009). Using unsteady water level data to estimate channel roughness and discharge hydrograph, *Advances in Water Resources*; 32(8), 1223-1240.

Aricò, C., Sinagra, M., Begnudelly, L., Tucciarelli, T. (2011). MAST-2D diffusive model for flood prediction on domains with triangular Delaunay unstructured meshes. *Advances in Water Resources*, 34(11), 1427-1449, doi: 10.1016/j.advwatres.2011.08.002.

Aster, C., Borchers, B., Clifford, H. (2012). Parameter Estimation and

Inverse Problems. Elsevier, ISBN: 978-0-12-385048-5.

Barbetta, S., Franchini, M., Melone, F., and Moramarco, T. (2012). Enhancement and comprehensive evaluation of the Rating Curve Model for different river sites. *J. Hydrol.*, 464-465, 376-387 (http://dx.doi.org/10.1016/j.jhydrol.2012.07.027.

Bousmar, D., and Zech, Y. (1999). Momentum transfer for practical flow computation in compound channels. *J. Hydraul. Eng.*; 696–706.

Cao, Z., Meng, J., Pender, G., & Wallis, S. (2006). Flow resistance and momentum flux in compound open channels. *J. Hydraul. Eng.*; 1272–1282.

Chow, V. T. (1959). Open channel hydraulics. New York: McGraw-Hill.

Corato, G., Moramarco, T., and Tucciarelli, T. (2011). Discharge estimation combining flow routing and occasional measurements of velocity, *Hydrol. Earth Syst. Sci.*,15, pp. 2979-2994.

Cunge, J. A., Holly, F. M., and Verwey, A. (1980). Practical aspects of computational river hydraulics. Pitman, London.

Das, A. (2010). Discussion of “Applying Particle Swarm Optimization to Parameter Estimation of the Nonlinear Muskingum Model” by H.-J.

Chu and L.-C. Chang. *Journal of Hydrologic Engineering*, 10.1061/(ASCE)HE.1943-5584.0000224,946-949.

Dey, M., and Lambert, M. F. (2006). Discharge prediction in compound channels by end depth method. *J. Hydraul. Res.,*44(6), 767–776.

D'Oria, M., Mignosa, P., and Tanda, M. G. (2012). Reverse level pool routing: comparison between a deterministic and a stochastic approach. *J Hydrol*., 470(1), 28–35 http://dx.doi.org/10.1016/j.jhydrol.2012.07.045

D'Oria, M., Mignosa, P., and Tanda, M. G. (2014). Bayesian estimation of inflow hydrographs in ungaiged sites of multiple reach systems. *Advances in Water Resources*, 63(1), 143-151.

Ferguson, R. (2007) Flow resistance equations for gravel and boulder-bed streams. *Water resources research*, 43, W05427.

Gyr, A, and Hoyer k. (2006), Sediment Transport A geophysical Phenomenon, Springer, 30-31.

Herschel, C. (1897). On the origin of the Chezy formula, *J. Assoc. of Engineering Soc.* 18, 363-368.

Hu, C., Ji, Z., and Guo, Q. (2010). Flow movement and sediment transport in compound channels. *J. Hydraul. Res*., 48(1), 23–32.

Huthoff, F., Roos, P. C., Augustijn, D. C. M., and Hulscher, S. J. M. H. (2008). Interacting divided channel method for compound channel flow. *J. Hydraul. Eng*., 1158–1165.

Herschy, R. W. (1999). Hydrometry: Principles and Practice, 2nd Edn., John Wiley and Sons, New York, NY, p. 376.

Jones, W. P., and Launder, B. E. (1972). The Prediction of Laminarization with a Two-Equation Model of Turbulence*, International Journal of Heat and Mass Transfer*; vol. 15, pp. 301-314.

Kejun Yang, Xingnian Liu; ShuyouCao and Er Huang. (2013). Stage-Discharge Prediction in Compound Channels, *J. Hydraul. Eng.*

Knight, D. W., and Abril, B. (1996).Refined calibration of a depth averaged model for turbulent flow in a compound channel. *Proc. ICE Water Maritime Energy*; 118(3), 151–159.

Knight, D.W., and Demetriou, J. D. (1983). Flood plain and main channel flow interaction, *J. Hydraul. Eng.*, 1073–1092.

Knight, D. W., and Hamed, M. E. (1984).Boundary shear in symmetrical compound channels, *J. Hydraul. Eng.*, 1412–1430.

Knight, D. W., McGahey, C., Lamb, R., and Samuels, P. G. (2010).Practical channel hydraulics: Roughness, conveyance and afflux. CRC Press/Taylor and Francis, Leiden, The Netherlands, 1–354.

Knight, D. W., and Sellin, R. H. J. (1987). The SERC flood channel facility. *J. Inst. Water Environ.* Manage, 1(2), 198–204.

Knight, D. W., and Shiono, K. (1996). River channel and floodplain hydraulics. Chapter 5, Floodplain processes, M. G. Anderson,D. E. Walling, and P. D. Bates, eds., Wiley, New York, 139–181.

Knight, D. W., Shiono, K., and Pirt, J. (1989).Prediction of depth mean velocity and discharge in natural rivers with overbank flow. Proc., Int. Conf. on Hydraulic and Environmental Modelling of Coastal, Estuarine and River Waters, R. A. Falconer, P. Goodwin and R. G. S. Matthew, eds., Gower Technical, Univ. of Bradford, U.K., 419–428.

Lambert, M. F., and Sellin, R. H. J. (1996). Discharge prediction in straight compound channels using the mixing length concept. *J.Hydraul. Res.*,34(3), 381–394.

Launder, B. E., and Sharma, B. I. (1974). Application of the Energy Dissipation Model of Turbulence to the Calculation of Flow Near a Spinning Disc. Letters in Heat and Mass Transfer; vol. 1, no. 2, pp. 131-138.

Legates, D. R., and McCabe, G. J. Jr. (1999). Evaluating the use of "goodnessof-fit" measures in hydrologic and hydroclimatic model validation. *Water Resources Research*, 35(1): 233–241

Liao, H., and Knight, D. W. (2007). Analytic stage-discharge formulas for flow in straight prismatic channels. *J. Hydraul. Eng.*, 1111–1122.

Lyness, J. F., Myers, W. R. C., Cassells, J. B. C., and O'Sullivan, J. J. (2001). The influence of planform on flow resistance in mobile bed compound channels *Proc., ICE Water Maritime Eng.*; 148(1), 5–14.

McGahey, C. (2006). A practical approach to estimating the flow capacity of rivers. Ph.D. thesis, The Open Univ., Milton Keynes, U.K,. (British Library).

McGahey, C., Knight, D. W., and Samuels, P. G. (2009). Advice, methods and tools for estimating channel roughness. *Proc. ICE Water Manage,* 162(6), 353–362.

Moreta, P. J. M., and Martin-Vide, J. P. (2010). Apparent friction coefficient in straight compound channels. *J. Hydraul. Res.*, 48(2), 169–177.

Myers,W. R. C., & Brennan, E. K. (1990). Flow resistance in compound channels. *J. Hydraul. Res.*, 28(2), 141–155.

Moramarco, T., Saltalippi, C. and Singh, V.P. (2004). Estimation of mean velocity in natural channels based on Chiu's velocity distribution equation, *J. Hydrologic Engrg*., 9(1), 42-50, doi:10.1061/(ASCE)1084-0699(2004)9:1(42), 2004.

Moramarco T., Barbetta S., Melone, F., Singh V.P. (2005a). Relating local stage and remote discharge with significant lateral inflow. *Journal of Hydrologic Engineering*, 10(1), 58-69.

Moramarco T., Melone F., Singh V.P. (2005b). Assessment of flooding in urbanized ungauged basins: a case study in the Upper Tiber area, Italy. *Hydrol. Proc*., 19, 1909-1924.

Moramarco T., Pandolfo C., Singh V.P. (2008). Accuracy of kinematic wave and diffusion wave approximations for flood routing, *J. Hydrologic Engrg*., 13 (11), 1078-1088, doi:10.1061/(ASCE)1084-0699(2008)13:11(1089).

Nash J.E., Sutcliffe J.V. (1970). River flow forecasting through conceptual models, part 1: a discussion of principles, *J. Hydr.* , 10:282-90.

Omran, M., and Knight, D. W. (2010). Modelling secondary cells and sediment transport in rectangular channels. *J. Hydraul. Res.*, 48(2), 205–212.

Peters J.J. and Goldberg A. (1989). Flow data in large alluvial channels in Maksimovic, C. &Radojkovic, M. (eds) Computational Modeling and Experimental methods in Hydraulics; Elsevier, London, 77-86.

Perumal, M., Moramarco, T., Shaboo, B. , Barbetta S. (2007). A methodology for discharge estimation and rating curve development at ungauged sites, *Water Resour. Res*., 43, W02412, doi:10.1029/2005WR004609.

Rameshwaran, P. and Shiono, K. (2007). Quasi two-dimensional model for straight overbank flows through emergent vegetation on floodplains. . *J. Hydraul. Res. 45(3), 302-315.*

Rameshwaran, Ponnambalam; Naden, Pamela; Wilson, Catherine A.M.E.; Malki, Rami; Shukla, Deepak R.; Shiono, Koji. (2013). Inter-comparison and validation of computational fluid dynamics codes in two-stage meandering channel flows. *Applied Mathematical Modelling*, 37 (20-21). 8652-8672.

Rhodes, D. G., and Knight, D. W. (1994). Velocity and boundary shear in a wide compound duct. *J. Hydraul. Res.,*32(5), 743–764.

Richardson R. W. and Colin R. Thorne. (1998). Secondary Currents around Braid Bar inBrahmaputra River, Bangladesh. *J. Hydraul. Eng.*, 124(3), 325–328.

Sahu M., Khatua K.K., Mahapatra S.S. (2011). A neural network approach for prediction of discharge in straight compound open channel flow. *Flow Measurement and Instrumentation*, 22, 438-446.

Schlichting, H. (1960). Boundary layer theory, 4th Ed., McGraw-Hill,NewYork.

Sellin, R. H. J. (1964). A laboratory investigation into the interaction between the flow in the channel of a river and that over its flood plain. La Houille Blanche, 7, 793–801.

Shiono, K., Al-Romaih, J. S., and Knight, D. W. (1999). Stage-discharge assessment in compound meandering channels. *J. Hydraul. Eng.*, 66–77.

Shiono, K., and Knight, D. W. (1991). Turbulent open-channel flows with variable depth across the channel. *J. Fluid Mech.*,222, 617–646.

Spada, E., Sinagra M., Tucciarelli T., Sammartano V., Corato G. (2015): Computation of vertically averaged velocities in irregular sections of straight channels, *Hydrol. Earth Syst. Sci.*, 19, 3857-3873

Stephenson, D., andKolovopoulos, P. (1990). Effects of momentum transfer in compound channels. *J. Hydraul. Eng.*, 1512–1522.

Tang, X., and Knight, D. W. (2008). Lateral depth-averaged velocity distributions and bed shear in rectangular compound channels. *J. Hydraul. Eng.*, 1337–1342.

Van Prooijen, B. C., Battjes, J. A., andUijttewaal, W. S. J. (2005). Momentum exchange in straight uniform compound channel flow. *J. Hydraul. Eng.*, 175–183.

Zucco, G., Tayfur, G. and Moramarco, T. (2015). Reverse flood routing in natural channels using genetic algorithm. Water Resources Management, in Press, doi:10.1007/s11269-015-1058-z.

Wormleaton, P. R., Allen, J., andHadjipanos, P. (1982). Discharge assessment in compound channel flow. *J. Hydraul. Div.*, 108(9), 975–994.

Wormleaton, P. R., &Hadjipanos, P. (1985). Flow distribution in compound channels. *J. Hydraul. Eng.*, 357–361.

Yen, B.C. (1992).The Manning formula in context. Channel Flow Resistance: Centennial of Manning's Formula,. Editor Water Resources Publications, Littleton, Colorado, USA, p. 41.

MIKE11, A Modelling System for Rivers and Channels, Reference Manual, DHI 2009

HEC-RAS, River Analysis System, Hydraulic Reference Manual, US Army Corps of Engineers 2010.